ABSTRACT

O'TOOLE, CONOR. Stabilizing Ore Mine Tailings with Microbial Induced Carbonate Precipitation and Assessing the Implications of Design Practices on the Resiliency of Hydraulic Infrastructure. (Under the direction of Dr. Brina M. Montoya).

Mine tailings are by-products of ore mine processing and are disposed of in dam impoundments and tailings ponds. Mine tailings storage facilities are crucial infrastructure to the mining industry. As more ore material is processed, gradual deposition of these mine tailings can produce excessive shear stresses and lead to internal and external structural weaknesses. Embankments formed by fills of coarse waste and tailings from mining operations, the lack of regulations on specific design criteria, and lack of dam stability requirements and monitoring during construction are also contributing factors to the susceptibility of these structures. Static or seismic induced liquefaction is a phenomenon that occurs in loose, saturated cohesionless soils such as silty sands and sandy materials, in which the materials act as a liquid under induced stress. Liquefiable soils require soil improvement techniques in order to reduce and mitigate the effects of liquefaction.

Microbial induced carbonate precipitation (MICP) is a bio-mediated cementation process that uses biological activity to improve the geotechnical properties of granular soils. MICP, or more generally bio-cementation, has the potential to improve the resilience of fine-grained and granular materials to prevent phenomena such as static liquefaction and erosion. Bio-cementation processes have also been previously used to stabilize byproduct materials such as coal ash and mature fine tailings. Mine tailing sediments tend to form weak and vulnerable layers which can negatively affect the overall performance of tailings impoundments and dams, and have previously contributed to catastrophic failures of these structures.

Work in this thesis is focused on evaluating the effect of MICP treatment on two ore mine tailings, one from an iron and one from a gold mine. Additionally, two sets of materials from each mine, a fine-grained "slime", and a coarser-grained sandy silt, were assessed. The effect of MICP on the engineering and physical properties of the mine tailings materials is investigated through monotonic direct simple shear tests and fall cone testing. Fall cone testing of the untreated and treated slimes fraction indicated increased strength improvement via MICP, and was confirmed with calcium carbonate content measurements and analytical testing methods (SEM, XRD, etc.)

Untreated and treated samples of the coarser fraction of the mine tailings were treated at two different levels of cementation and tested at 100 kPa confining pressure. Shear wave velocity measurements throughout treatment allowed for direct non-destructive monitoring of improvement in the treated materials. Results indicated significant improvement in the monotonic shear response of both silt materials at both levels of cementation. Confirmation of calcium carbonate was completed via acid washing, and signified that MICP successfully increased the shear strength of the mine tailings materials

In addition, analysis of NCDOT hydraulic design practices of roadway infrastructure was investigated to identify and evaluate specific design features or elements that contributed to increased resilience during extreme weather events. Specifically, analysis was completed comparing the damages and design decisions made following Hurricanes Matthew and Florence, two extreme storms that caused a large amount and high degree of damage throughout the state. A review and analysis of hydraulic guidelines was completed, and the state of practice for NCDOT design procedures is described within.

Stabilizing Ore Mine Tailings with Microbial Induced Carbonate Precipitation and Assessing the Implications of Design Practices on the Resiliency of Hydraulic Infrastructure

by
Conor O'Toole

A thesis submitted to the Graduate Faculty of
North Carolina State University
in partial fulfillment of the
requirements for the degree of
Master of Science

Civil Engineering

Raleigh, North Carolina
2022

APPROVED BY:

_____	_____
Dr. Brina Montoya Committee Chair	Dr. Mohammed Gabr
_____	
Dr. Shane Underwood	

DEDICATION

To my wonderful and supportive wife, Zita, who is my best friend and my companion. You have always encouraged and picked me up when I need it. To all the exciting times and many adventures we have ahead of us.

BIOGRAPHY

Conor O'Toole was born on May 11th, 1992 in San Marino, California. In 2014, he earned a B.A. degree from Bowdoin College, in Brunswick, Maine, majoring in Geology with a minor in Physics. From 2014 to 2016, he completed an M.S. program in Petroleum Engineering with a focus in Geoscience Technologies at University of Southern California, after which he worked as a professional engineer in the energy industry until 2019. In January 2020, he moved to Raleigh and enrolled at North Carolina State University to pursue his Master's degree in Civil Engineering under the direction of Dr. Brina Montoya.

ACKNOWLEDGMENTS

I would like sincerely thank my advisor, Dr. Brina M Montoya, whose support and guidance have allowed me to succeed throughout my research and time at NC State. I could not have asked for a more patient and encouraging advisor and mentor. I also would like to thank my committee members, Dr. Mohammed Gabr and Dr. Shane Underwood, who have guided and supported me throughout my program and studies. Additionally, this work could not have been done without the support from NSF, NewFields Engineering, and the North Carolina Department of Transportation, their support is greatly appreciated.

I also want to express my sincere appreciation to Qianwen Liu, who mentored me and helped me countless times in my research and lab work. I would also like to thank my other colleagues, who I have had the pleasure of interacting with through my work in the lab and in courses: Marlee, Thomas, Pegah, Azmayeen, Nancy, Cassie, Cristina, Faria, Zahra, Sarah, Hannah, Kelly, and Sophia.

Lastly, to my loving wife, Zita, who has been my rock, I would not be who I am or where I am today without you.

TABLE OF CONTENTS

LIST OF TABLES xi

LIST OF FIGURES xiii

Chapter 1: Introduction 1

1.1 Background 1

1.2 Objectives and Layout of Thesis 3

1.2.1 Objectives 3

1.2.2 Layout 3

References 5

Chapter 2: Description of Mine Tailings and Tailings Operations 6

2.1 Description of Mine Tailings 6

2.1.1 Physical and Engineering characteristics 6

2.1.2 Geo-chemical and Chemical Characteristics 7

2.2 General Overview of Mining Operations 9

2.3 Tailings Facility Construction 10

2.3.1 Typical Dam Construction Methods 10

2.3.2 Working Conditions of Studied Mine Tailings Facility 10

References 12

Chapter 3: The Effect of Microbial Induced Carbonate Precipitation on Fine-Grained Mine Tailings 19

3.1 Introduction 19

3.2 Testing Methods 20

3.2.1 Microbial Cultivation 20

3.2.2 Proof of Concept Column Test 20
3.2.3 Fall Cone Test 21
3.2.4 Mass of Calcium Carbonate Acid Wash 22
3.3 Results 22
3.3.1 Self Weight Consolidation Results- Particle Sedimentation 22
3.3.2 Fall Cone Test Results 23
3.3.3 Mass of Carbonate Test Results 24
3.3.4 XRD Results 24
3.3.5 Acid Dissolution 25
3.4 Discussion 25
3.4.1 Water Content 25
3.4.2 Fall Cone Testing 26
3.4.3 Acid Dissolution 27
3.5 Conclusions 27
References 29
Chapter 4: The Ability of Microbial Induced Carbonate Precipitation to Stabilize High Water-Content Tailings 38
4.1 Objectives 38
4.2 Materials and Methods 38
4.2.1 Coarse Grained Materials 38
4.2.2 Methods of High Water Content Testing 39
4.3 Results 40
4.3.1 Sedimentation and Precipitation Results 40

4.3.2 Fall Cone Testing 42
4.3.3 Mass of Calcium Carbonate 43
4.4 Conclusions and Limitations 44
References 45
Chapter 5: The Effect of Microbial Induced Carbonate Precipitation on the Undrained Shear Strength of Silty Mine Tailings 52
5.1 Introduction 52
5.2 Methods 53
5.2.1 Direct Simple Shear 53
5.2.2 Sample Apparatus and Preparation Method 53
5.2.3 Sample Preparation Method 53
5.2.4 MICP Treatment Method 54
5.2.5 Shear Wave Velocity Measurements 56
5.2.6 Mass of Calcium Carbonate Acid Washing 57
5.3 Results and Discussion 57
5.3.1 General Instability 57
5.3.2 Undrained Shear Response of Untreated Silts 58
5.3.3 Undrained Shear Behavior of MICP Treated Silts 59
5.4 Conclusions 63
References 64
Chapter 6: The Impact of Hydraulic Design Practices on Resiliency of Infrastructure 75
6.1 Introduction 75
6.2 Overview of Hydraulic Design Practice 77

6.2.1 Resources for Estimating Probability of Annual Exceedance 78
6.2.2 Uncertainty and Extreme Events Consideration in Current Guidelines 79
6.2.3 Effects of Non-Stationarity and Climate Change in Hydraulic Design 80
6.3 National, State, and Regional Hydraulic Design Practices 83
6.3.1 Current State of Practice in North Carolina 84
6.3.1.1 Hydrologic Methods Used by the North Carolina DOT 84
6.3.1.1.1 Flood Insurance Study (FIS) Method 84
6.3.1.1.2 Rational Method 85
6.3.1.1.3 NCDOT Highway Hydrologic Charts (1973) Method 85
6.3.1.1.4 USGS Methods 86
6.3.1.1.5 Natural Resources Conservation Service (NRCS) Method 87
6.3.1.2 Design Frequency 88
6.3.2 State of Practice from Nearby State Highway Agencies 88
6.3.2.1 Virginia (2002, revised 2021) 88
6.3.2.2 Tennessee (2012) 89
6.3.2.3 South Carolina (2009) 89
6.3.2.4 Georgia (2020) 90
6.3.2.5 Florida (2012) 90
6.3.3 Hydraulic Design Procedures 91
6.3.3.1 HDS-5 91
6.3.3.2 HY-8 92
6.3.3.2.1 Discharge Data 93
6.3.3.2.2 Tailwater Data 93

6.3.3.2.3 Roadway Data 94
6.3.3.2.4 Culvert Data 95
6.3.3.2.5 Site Data 96
6.3.3.2.6 Output- Analyze Crossing 96
6.4 Case Studies and Variances of Q25 vs Florence and Matthew Flow Conditions 97
6.4.1 Precipitation Intensity Analysis 98
6.4.1.1 Adjusted Peak Discharge 99
6.4.2 Comparing HDS-5 and HY-8 99
6.4.3 HDS-5 Analysis 100
6.4.4 HY-8 Analysis 100
6.4.5 Comparison of Base Discharge Results 102
6.4.6 Comparison of Adjusted Discharge Results 103
6.5 Analysis of Decision Making from Different Hydrologic Methods 104
6.5.1 Key Updates to Hydraulic Design Guidelines 104
6.5.2 Timing of Matthew and Florence Storms 105
6.5.3 Practice vs Guidelines 106
6.5.3.1 USGS Methods 107
6.5.3.2 NCDOT Highway Hydrologic Charts 107
6.5.3.3 NRCS Method 108
6.5.3.4 Hydraulic Reports 108
6.6 Summary and Conclusions 108
References 110

Chapter 7 Contributions and Future Work 125

7.1 Contributions 125

7.2 Future Work 125

LIST OF TABLES

Table 2.1 Physical Properties of Slime and Silt Samples 14

Table 2.2 Elemental Analysis of Slimes 1 and 2 14

Table 3.1 a) MICP recipes and b) target water contents for fall cone test of slimes 31

Table 3.2 FCT results of untreated slimes with variable water contents 31

Table 3.3 FCT results for MICP treated Slimes 1 and 2 with different recipes and corresponding initial water contents (wi) and final water contents (wf)..... 31

Table 3.4 Mass of CaCO3 (wt.%) results for baseline untreated and MICP treated samples 31

Table 3.5 Remaining CaCO3 Mass % at varying pH solutions for Slime 1..... 32

Table 3.6 Remaining CaCO3 Mass % at varying pH solutions for Slime 2..... 32

Table 3.7 Remaining % of initial CaCO3 Mass at varying pH solutions for Slime 1 32

Table 3.8 Remaining % of initial CaCO3 Mass at varying pH solutions for Slime 2 32

Table 4.1 Physical Properties of Slime and Silt Samples 46

Table 4.2 Soil column height for modified high water content FCT-sedimentation tests..... 46

Table 4.3 Calcium Carbonate content for high water content tests, including control value 47

Table 5.1 Chemical Recipe for MICP treatment of Silts 1 and 2 66

Table 5.2 Naming convention for samples of Silt 1 and 2 and their cementation levels..... 66

Table 5.3 Planned injection volumes for treatment of Low and Moderate cementation..... 66

Table 5.4 Actual injection volumes for treatment of Low and Moderate cementation 67

Table 5.5 Effect of MICP on shear strength behavior of Silts..... 67

Table 5.6 Effect of MICP on the maximum normalized shear strength at yield and residual of Silts.....68

Table 6.1 Hydrologic Methods Utilized by NCDOT from NCDOT Guidelines for Drainage Studies and Hydraulic Design, 2016. 112
Table 6.2. Typical Runoff Coefficients to be used in Rational Method Calculations 112
Table 6.3 Storm Design Frequency for NCDOT Structures from NCDOT Guidelines for Drainage Studies and Hydraulic Design, 2016..... 112
Table 6.4 Culvert Data Shape and Material choices in HY-8 software..... 113
Table 6.5 Maximum 24 hours rainfall intensity data for selected case studies..... 113
Table 6.6 Adjusted Peak Discharge Values based on precipitation ratios..... 113
Table 6.7 Results of analysis completed utilizing HDS-5 and HY-8 for base peak discharge in identified sites in Robeson County (red cells have calculated HW/D > 1.25 and green cells have calculated HW/D ≤ 1.25)..... 114
Table 6.8 Results of analysis completed utilizing HDS-5 and HY-8 for peak discharge values adjusted using Ratios 1 and 2..... 114
Table 6.9 NCDOT Hydraulic Guidelines 1999 in determining appropriate hydrologic method to use in estimating peak discharge. 114
Table 6.10 NCDOT Hydraulic Guidelines 2016 in determining appropriate hydrologic method to use in estimating peak discharge. 114
Table 6.11 Comparison of Peak Discharge using 1999 vs 2016 NCDOT Guidelines 115

LIST OF FIGURES

Figure 2.1 Grain size distribution for Slimes 1 and 2 and Silts 1 and 2 15

Figure 2.2 XRD Mineral Identification for Slimes 1 and 2 15

Figure 2.3 SEM images from Cryo-SEM for Slime 1 at 500x and 1000x magnification 16

Figure 2.4 SEM images from Cryo-SEM for Slime 2 at 500x and 1000x magnification 17

Figure 2.5 Schematic illustrations of (a) upstream, (b) downstream, and (c) center-line sequentially raised tailings dams. The starter dike is represented by the darkest prism and successively lighter elements represent newer raises, after Vick (1990).. 18

Figure 2.6 Illustration of representative dam construction, a variation of upstream-style construction known as the "drained stack" method, with typical location of vertical and bottom drainage systems (Morgenstern, Vick et al 2016) 18

Figure 3.1 from DeJong et al, 2010- An overview of bio-mediated calcium carbonate precipitation and the relevant chemical reactions 33

Figure 3.2 a) Gasometric testing apparatus and b) gas volume to CaCO3 mass calibration 33

Figure 3.3 Pictures of self-consolidation column tests from beginning of trial (day 0) to end of trial (day 7). *S.*p. in the figure refers to *S.* pasteurii. 34

Figure 3.4 FCT Sur results normalized for water content of Slimes 1 (a) and 2 (b) with error bars..... 35

Figure 3.5 XRD results of treated slime samples indicating calcite for both Slime 1 and 2 36

Figure 3.6 Remaining % of original CaCO3 Mass for Slime 1 samples, including average..... 37

Figure 3.7 Remaining % of original CaCO3 Mass for Slime 2 37

Figure 4.1 Grain size distribution for all 4 materials- Slimes 1 and 2 & Silts 1 and 2 48

Figure 4.2 Modified high water content testing container to allow visualization of sedimentation behavior and periodic fall cone testing measurements once consolidation is complete. 48
Figure 4.3 Pictures of modified self-consolidation-fall cone column tests from beginning of trial (day 0, left) to end of trial (day 7, right). Photos were also taken on days 2 and 5 49
Figure 4.4 MICP treated samples in modified column-FCT tests that developed stiff upper layer that inhibited consolidation and dewatering 49
Figure 4.5 Untreated undrained shear strength estimates from Fall Cone Tests for both Slimes and both Silts at varying water contents 50
Figure 4.6 Top down view of FCT measurement of modified column test with stiff upper layer present, showing impact crater where cone broke through precipitate into soft soil. 50
Figure 4.7 Undrained shear strength behavior from FCT for MICP treated Silts via modified column testing 51
Figure 5.1 Sample preparation tools used in assembly of DSS specimens 69
Figure 5.2 Photo and illustration of bottom-up injection setup for gravity drainage MICP treatment undergoing MICP treatment at 10 kPa confining pressure 69
Figure 5.3 DSS end cap with bender element for shear wave velocity measurements 70
Figure 5.4 Example of specimen in DSS device during shearing with distinct failure plane developed along weakest plane of sample 70
Figure 5.5 a) Stress–strain plots, b) change in pore water pressure, c) and stress paths of constant-volume DSS tests on moist-tamped, untreated Silt 1 and 2 specimens..... 71

Figure 5.6 Increases of VS after application of Low and Moderate levels of MICP treatment over the course 9 and 18 injections, respectively, for Silt 1 and 2 as measured by bender elements 71

Figure 5.7 a) Stress–strain plots, b) change in pore water pressure, c) and stress paths of constant-volume DSS tests on moist-tamped, MICP-treated Silt 1 72

Figure 5.8 a) Stress–strain plots, b) change in pore water pressure, c) and stress paths of constant-volume DSS tests on moist-tamped, MICP-treated Silt 2 73

Figure 5.9 Early shear-strain behavior indicating higher mobilization of shear strength up to peak stress in MICP treated samples over untreated samples of Silt 1 74

Figure 6.1 Linear trend of 1-day annual maximum from rainfall stations with minimum of 50 years data, NOAA Atlas 14 Vol 2 116

Figure 6.2 Variance of 1-day annual maximum from rainfall stations with minimum of 50 years data, NOAA Atlas 14 Vol 2 116

Figure 6.3 Hydrologic contour map for North Carolina utilized in the NCDOT Method 117

Figure 6.4 a) Runoff Chart with relevant frequency correction factors, b) drainage area cover factor chart, and c) shape correction factor chart used in NCDOT Method (1973) 117

Figure 6.5 Regional flood-frequency equations for un-gaged urban and small, rural streams in Georgia, South Carolina, and North Carolina, from USGS, 2014 118

Figure 6.6 Solution for runoff equation to be used in NRCS Method 118

Figure 6.7 Example of digitized HDS-5 nomographs used in hydraulic design of culverts 119

Figure 6.8 Computerized program version of HDS-5 Nomographs 119

Figure 6.9 Inputs window in HY-8 software used to build sites and pipe cross sections: Red- Discharge Data; Green- Tailwater Data; Orange- Roadway Data; Blue- Culvert Data; Black- Site Data 120
Figure 6.10 Discharge Data input windows for HY-8: (a) Minimum, Design, Maximum; (b) User Defined; and (c) Recurrence Interval 120
Figure 6.11 Tailwater Data input window where user defines Bottom Width, Channel Slope, Manning's Number, Channel Invert Elevation, and Rating Curve. Additionally to the right, the drop down where user defines channel type 121
Figure 6.12 Roadway Data input window in HY-8, where user defines roadway elevation data including Crest Length, Crest Elevation and Top Width. Drop down list includes choices for Constant Roadway Elevation and Irregular 121
Figure 6.13 Visual of HY-8 software inputs to build cross section along; (a) the roadway direction and (b) along the pipe/flow direction, along with labeled features of analysis and site data 122
Figure 6.14 Outputs of HY-8 Analyze Crossing window showing the results of calculations completed based on inputs previously defined for a given site 123
Figure 6.15 Matrix of failure criterion for case study identification 123
Figure 6.16 Cumulative precipitation for Hurricanes Matthew (a) and Florence (b) for their respective durations 124
Figure 6.17 Using failure criterion matrix, map of identified a) potential case studies in Robeson County, Division 6, and b) chosen case studies. Blue dots are damaged in only Florence, red triangles are only in Matthew, and Green are damaged in both 124

Figure 6.18 Timeline of relevant events including examples of damage from storm events 124

Chapter 1 Introduction

1.1 Background

Mine tailings are by-products generated once the valuable minerals or materials have been extracted. The State of World Mine Tailings (Bowker, 2020) estimates that nearly 534 billion m^3 of cumulative mine tailings were stored in facilities around the world, and that an additional 40-50 billion m^3 of waste will be generated in the next 5 years. Once generated, these by-products need to be stored, most often in on-site tailings storage facilities. These tailings are often transported to the on-site storage facilities as a slurry, and are retained behind dams raised in stages built with the coarser fraction of the mine tailings waste, or "silts". The fine mine tailing sediments, or "slimes", are typically weakened layers that negatively affect the overall performance of tailings impoundments and dams, and have previously contributed to catastrophic failures of these structures. Improper storage and management of these structures can lead to devastating consequences and cause great harm to the environment and communities (Hudson-Edwards et al 2003). The high cost of maintenance and monitoring of tailings dams during operations of the mine is considered to be an attributing factor to these structures susceptibility to failures (Rico et al., 2008). Stability issues for tailings storage facilities tend to increase with age, height, volume, and seismic hazard, and are also dependent on construction method and governance (Franks et al. 2021).

Tailings dam failures account for nearly three-fourths of major mining related environmental disasters in the world, and an estimated 3 of the world's mine tailings dams experience failure every year (Schoenberger, 2016). For example, after the collapse of the Fundão dam on November 5th, 2015, 43 million m^3 of iron ore tailings were released, flooding the town and killing at least 17 people (Carmo et al., 2017). The January 25th, 2019 failure at the

Córrego de Feijão mine released 12 million m^3 of tailings, killing at least 259 people (Santamarina et al., 2019). These failures are considered to be some of the largest environmental disasters in tailing dam failure history and illustrate the devastating effects that these failures can have on the surrounding communities. In order to mitigate these instabilities, soil improvement techniques are required to increase strength and resilience against static liquefaction.

Soil improvement techniques look to mitigate the hazards in an economic and sustainable method. Researchers have made efforts to utilize biopolymers like xanthan and guar gum to bond particles together (Chen et al, 2013). Other common approaches in soil improvement practice are to inject synthetic materials such as cement and epoxies into the pore spaces to bind soil particles (Anagnostopoulos, 2015). More recently, bio-mediated soil improvement methods have been developed to sustainably enhance soil properties to mitigate potential hazards. Microbial induced calcium carbonate precipitation (MICP) is a sustainable biological soil improvement technique that can provide cohesive bonds between soil particles through microbial metabolism (DeJong et al, 2010). MICP, or more generally bio-cementation, has the potential to improve the resilience of granular materials to prevent phenomena such as liquefaction and erosion. The primary properties of the soil that can be changed significantly during MICP treatments include permeability, stiffness, compressibility, shear strength, and volumetric behavior (DeJong et al. 2010). Previous studies have used MICP for coal ash and mature fine tailings (Montoya et al, 2019; Safavizadeh et al, 2019; Liu and Montoya, 2020) indicating the potential advantages of using MICP for byproduct stabilization.

MICP is a novel approach to soil improvement of mine tailings by using a natural, biological process to cement the particles together. MICP has the potential to increase the

strength of the mine tailings and prevent particle migration while maintaining the permeability of the sediment to allow for drainage, which is an additional factor in mine tailings management.

1.2 Objectives and Layout of Thesis

1.2.1 Objectives

There are two primary objectives of this research 1) to evaluate the effect of MICP treatment on ore mine tailings materials; 2) to analyze the state of design practice for NCDOT highway infrastructure in order to determine key elements that contributed to improved performance during extreme weather events.

1.2.2 Layout

To understand the response of the mine tailings in varying conditions, characterization of the physical and chemical properties of the mine tailings is required. Two sets of mine tailings materials from each of the iron and gold mines- named “Slimes” and “Silts”- were examined in this study. In Chapter 2, “Description of Mine Tailings and Tailings Operations”, the results of various characterization tests of physical properties and chemical compositions are presented. In addition, an overview of the mining operations and working conditions of the mine where the mine tailings materials originated is described in detail.

In Chapter 3, “The Effect of Microbial Induced Carbonate Precipitation on Fine-Grained Mine Tailings”, proof of concept testing procedures are detailed, where MICP treatment via ex-situ mixing technique was evaluated on the Slimes to determine the effect on the fabric and undrained shear strength.

A novel approach to stabilizing both Slimes and Silts mine tailings materials at high water contents was examined. In Chapter 4 “The Ability of Microbial Induced Carbonate Precipitation

to Stabilize High Water-Content Tailings", self-weight consolidation in glass cylinders was combined with fall cone testing (FCT) to observe the influence that MICP treatment had on dewatering and strengthening of these materials at field conditions (e.g.- high water contents).

The impact of MICP treatment on the engineering properties of these materials had not previously been studied. In Chapter 5, "The Effect of Microbial Induced Carbonate Precipitation on the Shear Strength of Mine Tailings", monotonic direct simple shear tests were completed on untreated and treated Silt mine tailings materials to characterize the shear strength behavior of the Silts. Two cementation levels were used, and the shear wave velocity was directly monitored during the treatment proess.

In Chapter 6, "The Effect of Hydraulic Design Practices on the Resiliency of Infrastructure", analysis of NCDOT hydraulic design practices of roadway infrastructure was investigated to identify and evaluate specific design features or elements that contributed to increased resilience during extreme weather events.

Finally, in Chapter 7, "Summary, Contribution, and Future work", the conducted work is summarized, the contributions from the work are explicitly discussed, and the future work of each chapter are presented.

References

Anagnostopoulos, C. A. (2015). “Strength properties of an epoxy resin and cement-stabilized silty clay soil.” Applied Clay Science, 114, 517–529.

Bowker, L. (2020). “World Mine Tailings Failures-from 1915.” World Mine Tailings Failures from 1915, <https://worldminetailingsfailures.org/>; (Jun. 3, 2021).

Chen, R., Zhang, L., and Budhu, M. (2013). “Biopolymer Stabilization of Mine Tailings.” Journal of Geotechnical and Geoenvironmental Engineering, 139(10), 1802–1807.

DeJong, J. T., Mortensen, B. M., Martinez, B. C., and Nelson, D. C. (2010). “Bio-mediated soil improvement.” Ecological Engineering, 36(2), 197–210.

Franks, D.M., Stringer, M., Torres-Cruz, L.A., Baker, E., Valenta, R., Thygesen, K., Matthews, A., Howchin, J., Barrie, S. (2021). “Tailings facility disclosures reveal stability risks.” *Scientific Reports*, 11, 5353.

Hudson-Edwards, K. A., Macklin, M. G., Jamieson, H. E., Brewer, P. A., Coulthard, T. J., Howard, A. J., and Turner, J. N. (2003). “The impact of tailings dam spills and clean-up operations on sediment and water quality in river systems: the Rios Agrio–Guadiamar, Aznalcóllar, Spain.” Applied Geochemistry, 18(2), 221–239.

Liu, Q., and Montoya, B. M. (2020). “Experimental Study of Consolidation Behavior of Mature Fine Tailings Treated with Microbial Induced Calcium Carbonate Precipitation.” Geo-Congress 2020.

Montoya, B. M., Safavizadeh, S., and Gabr, M. A. (2019). “Enhancement of Coal Ash Compressibility Parameters Using Microbial-Induced Carbonate Precipitation.” Journal of Geotechnical and Geoenvironmental Engineering, 145(5), 04019018.

Rico, M., Benito, G., Salgueiro, A. R., Díez-Herrero, A., and Pereira, H. G. (2008). “Reported tailings dam failures.” Journal of Hazardous Materials, 152(2), 846–852.

Safavizadeh, S., Montoya, B. M., and Gabr, M. A. (2019). “Microbial induced calcium carbonate precipitation in coal ash.” Géotechnique, 69(8), 727–740.

Santamarina, J. C., Torres-Cruz, L. A., and Bachus, R. C. (2019). “Why coal ash and tailings dam disasters occur.” Science, 364(6440), 526–528.

Schoenberger, E. (2016). “Environmentally sustainable mining: The case of tailings storage facilities.” Resources Policy, 49, 119–128.

Chapter 2 Description of Mine Tailings and Tailings Operations

2.1 Description of Mine Tailings

Ore mine tailings were received from an iron and a gold mine (Slime 1 / Silt 1, and Slime 2 / Silt 2, respectively) from a mine in South America. For each mine, the tailings were separated as slimes and silts. The physical and chemical characteristics of the tailings are described below.

2.1.1 Physical and Engineering characteristics

The physical properties of the mine tailings are outlined below and were determined using the appropriate testing method. Table ***2.1*** outlines geotechnical tests that are generally conducted when analyzing soils. Water contents (ASTM D2216) of the natural tailing samples were tested upon arrival. Particle size distribution, Atterberg limits, specific gravity, and pH were tested for the tailing materials using sieve analysis (ASTM D6913) and hydrometer analysis (ASTM D7928), the Casagrande cup method (ASTM D4318), water pycnometer (ASTM D854), and pH strips (Fisherbrand), respectively.

Scanning electron cryo-microscopy (Cryo-SEM) is a form of electron microscopy where a hydrated but cryogenically fixed sample is imaged on a scanning electron microscope's cold stage in a cryogenic chamber. Cryo-SEM was utilized in place of conventional SEM to preserve the fabric of the natural soil, as samples that contain moisture are known to be damaged or show artifacts during drying (Nègre et al., 2004). Freeze-drying is considered less disruptive than air drying because it minimizes the sample distortion. Tailings were plunged frozen in liquid nitrogen slush, transferred under vacuum to the Alto-2500 preparation chamber and cryo-fractured. The fractured specimens were etched at -90°C under 4×10^{-6} mbar vacuum for 10 min to reveal the microstructure. After etching, the specimens were cooled down to -120°C and

coated with 5 nm thickness Au/Pd. The fabric of the specimens was obtained under cryo-temperature at 8 mm working distance.

A summary of the results of the tests are presented in Table ***2.1***, Figure **2.1** and Figure ***2.2***. The slimes are largely fine-grained particles (<0.075 mm) as shown in the grain size distribution chart of Figure **2.1**. The natural water contents of Slimes 1 and 2 were 26.24 and 26.23%, respectively. Specific gravity of the samples was 3.46 and 2.61 (Slimes 1 and 2, respectively).

Examples of Cryo-SEM images can be seen in Figure ***2.3*** and Figure ***2.4***. Slime 1 SEM images show definite card-house structure indicative of flocculated without aggregation (edge-to-face particle contacts) fabric, while Slime 2 SEM images indicates less definitive structure as compared to Slime 1, with some flocculated particles.

2.1.2 Geo-chemical and Chemical Characteristics

Chemical analysis conducted by the operators of the mine where the samples originated from indicated that Slimes 1 and 2 contain trace metals as indicated in Table ***2.2***. Heavy metals identified include mercury, arsenic, barium, copper, lead, vanadium, and zinc, however the concentrations of those trace metals are lower than USEPA regulations for inhalation or ingestion hazards (USEPA, 1996). Appropriate PPE, including N95 facemask and nitrile gloves, was worn at all times while handling samples.

Both gold and iron ore mine tailings did not contain sulfide minerals and can therefore be classified as non-acid-generating. Sulfides and other heavy metal elements show a limited solubility and are easily trapped and adsorbed by phyllosilicate minerals; they are thus preferentially partitioned in the fine fraction of sediments (Bianchini et al, 2000). Trace amounts of heavy metals are universal within rocks, soils, surface, and ground water, and it is important to

compare heavy metal concentrations against the natural background concentrations, which can vary from location to location. The mining industry and the extraction of metal ores make up a significant source of environmental contamination by heavy metals, and mining activities that affect sulfide minerals usually result in the excavation of a huge amount of anoxic subsoil rock which can be exposed to the surface oxygen rich environment (Khelfaoui et al., 2020). The exposition of waste rock to water, oxygen, and bacteria may cause metal leaching and the formation of acid mine drainage (AMD). Metal sulfide oxidation is a complex process that includes several redox reactions, which are controlled by the geology, microbiology, and climate of each area. These redox reactions occur in parallel and last as long as there is access to air and water. Runoff from tailings piles and waste rocks can carry large amounts of metal as precipitation infiltrates the piles and promotes geochemical weathering of primary containing metals.

Acid generation associated with this process can be neutralized in the presence of carbonate minerals to maintain circumneutral pH conditions. However, consumption of carbonate minerals due to ongoing sulfide-mineral oxidation often precedes a transition to acidic pH conditions (Lindsay et al., 2015). The resulting pH strongly influences concentrations and mobility of metals released during sulfide mineral oxidation. Levels of pH can affect the preferential precipitation or dissolution of carbonate materials, which can be of beneficial use in soil improvement projects.

The main elements detected in the tailing samples were silica and iron oxides. X-Ray Diffraction (XRD) analysis of the baseline untreated samples was conducted to identify the mineral phases and crystallinity in each sample. XRD results for the minerals present in Slimes 1 and 2 are depicted in Figure ***2.2***. Results indicate that Slimes 1 and 2 consist predominantly of

quartz. Secondary amounts of Hematite (Fe_2O_3), and Goethite ($Fe^{+3}O(OH)$), Birnessite ($(Na,Ca)_{0.5}(Mn^{4+},Mn^{3+})_2O_4 \cdot 1.5H_2O$) were in Slime 1, while Slime 2 had secondary amounts of muscovite ($KAl_3Si_3O_{10}(OH)_2$), birnessite ($(Na,Ca)_{0.5}(Mn^{4+},Mn^{3+})_2O_4 \cdot 1.5H_2O$ and albite ($NaAlSi_3O_8$). These iron and aluminum oxide minerals have crystalline structures and are stable and undergo slow weathering in non-acidic conditions (Bowen, 1929). Therefore, these tailings have a low potential for mobilizing metals, including iron, under circum-neutral pH conditions.

2.2 General Overview of Mining Operations

The mine tailings samples were obtained from iron and gold mines (Slime 1 / Silt 1, and Slime 2 / Silt 2, respectively). The processing from these mines follows standard ore processing of froth flotation. First, ore is ground into an extremely fine powder. The powder is mixed with water to create a slurry, which is mixed with surfactants to increase the desire material hydrophobic behavior, and is added to a water tank referred to as a flotation cell. Air is injected into the tank to create a thick, bubbly froth, capable of selectively attaching itself to the surface of the desired mineral particles, which float to the surface while the undesired minerals are allowed to sink. This process is referred to as “direct” flotation, while “reverse” flotation works by causing the desired mineral to sink using collector solutions that have anionic behaviors (Vidyadhar and Singh, 2007). Sodium hydroxide (NaOH) is added throughout the milling and flotation stages for the purpose of pH adjustment. Coagulants and flocculants are added to the generated waste and flotation circuits to promote the separation of fines. The desired mineral froth is mechanically scooped off the surface and collected. The concentrate may be recycled into the flotation cell and recollected after additional flotation, thus increasing the quality of the concentrated material. The final concentrate is processed for final metal recovery, while the remaining material, the sandy and fine particles, are deposited in a mine tailings pond, where they are stored for a number of

years before further processing to recycle water and extract additional ore or other precious metals.

2.3 Tailings Facility Construction

2.3.1 Typical Dam Construction Methods

There are three types of dam construction methods that are outlined in Figure ***2.5***: upstream, downstream and centerline. These methods designations are named relative to the position of the constructed crest of the dam to the previous crest or starter dike, and the design chosen for a given site will depend upon various factors including topography, geology, climate, the type of tailings, and cost.

An upstream tailings dam consists of placing new material on top of the crest but within the impoundment, moving the crest further upstream (Martin, T.E & McRoberts, E.C., 1999). The downstream design refers to the successive raising of the embankment that positions the fill and crest further downstream. A center-lined dam has sequential embankment dams constructed directly on top of another while fill is placed on the downstream side for support with deposited slurry on the upstream side. Of the construction methods outlined, upstream construction is the cheapest, as less material is required for successive raising of the impoundment crest (Soares et al, 2000). However, there are a number of disadvantages to this method in management, including phreatic surface control, water storage capacity, and seismic and static liquefaction susceptibility (Vick, 1990).

2.3.2 Working Conditions of Studied Mine Tailings Facility

Working conditions were obtained for one of the mines where the examined tailings originated. During the stage of processing where fines and sandy particles are separated and disposed of, it is estimated that around 650 tons of sand tailings and 400 tons of slime tailings are produced per

hour. In-situ testing at the mine indicated that water content of the slime tailings was upwards of 150%, with sand and silt tailings moisture content values around 80%. The tailings are stored for 10 years before further processing to extract additional ore and other precious metals. As previously mentioned, the remaining sandy and fine particles are deposited in tailings ponds, constructed similarly as shown in Figure **2.6**, where they are stored for a minimum of 10 years. Deposition based on grain size preserves the integrity of the dam by placing the coarser, more porous material within the structure; in addition, this methodology also results in the finer fraction forming an impermeable barrier, which reduces the potential for piping or seepage through the dam structure (Kossoff et al., 2014).

The tailings pond constructed for the facility where the mine tailings originated from utilized a variation of the upstream dam construction method. This alternative method, the drained stack concept, aims to progressively stack the sands behind a starter dam, with the slimes or fine materials retained behind the sand stack. The starter dam is subsequently raised on top of the sands as the sandy and fine mine tailings material is disposed of during processing. The critical construction and management condition of this design method is to maintain adequate drainage within the loose, uncompacted sands of the sand stack and start dam, such that the sands remained unsaturated and stable (Morgenstern et al., 2016). Drainage methods typically utilized are high-capacity drainage system beneath the starter dam, concrete galleries (or conduits) beneath the dam abutments to convey upstream surface water downstream of the dam, and separation of the fine grained slimes from the sands during deposition by maintaining a sand beach width from the dam crest (Figure **2.6**).

References

ASTM. (2010). “D2216 Standard Test Methods for Laboratory Determination of Water (Moisture) Content of Soil and Rock by Mass”. ASTM International, West Conshohocken, PA.

ASTM. (2014). “D854 Standard Test Methods for Specific Gravity of Soil Solids by Water Pycnometer”. ASTM International, West Conshohocken, PA.

ASTM (2017a). “D4318 Standard Test Methods for Liquid Limit, Plastic Limit, and Plasticity Index of Soils”. ASTM International, West Conshohocken, PA.

ASTM (2014). “D4373 Standard Test Method for Rapid Determination of Carbonate Content of Soils”. ASTM International, West Conshohocken, PA.

ASTM (2017b.) “D6913 Standard Test Methods for Particle-Size Distribution (Gradation) of Soils Using Sieve Analysis”. ASTM International, West Conshohocken, PA.

ASTM (2017c). “D7928 Standard Test Method for Particle-Size Distribution (Gradation) of Fine-Grained Soils Using the Sedimentation (Hydrometer) Analysis”. ASTM International, West Conshohocken, PA

Bianchini, G., Laviano, R., Lovo, S., and Vaccaro, C. (2000). “Chemical–mineralogical characterisation of clay sediments around Ferrara (Italy): a tool for an environmental analysis.” Applied Clay Science 21 (2002) 165– 176

Bowen, N. L. (1929). The Evolution of the Igneous Rocks. Nature, 124(3126). https://doi.org/10.1038/124474a0

Khelfaoui, M., Medjram, M. S., Kabir, A., Zouied, D., Mehri, K., Chikha, O., & Trabelsi, M. A. (2020). Chemical and mineralogical characterization of weathering products in mine wastes, soil, and sediment from the abandoned Pb/Zn mine in Skikda, Algeria. Environmental Earth Sciences, 79(12). https://doi.org/10.1007/s12665-020-09043-x

Kossoff, D., Dubbin, W. E., Alfredsson, M., Edwards, S. J., Macklin, M. G., & Hudson-Edwards, K. A. (2014). Mine tailings dams: Characteristics, failure, environmental impacts, and remediation. Applied Geochemistry, 51. https://doi.org/10.1016/j.apgeochem.2014.09.010

Lindsay, M. B. J., Moncur, M. C., Bain, J. G., Jambor, J. L., Ptacek, C. J., & Blowes, D. W. (2015). Geochemical and mineralogical aspects of sulfide mine tailings. Applied Geochemistry, 57. https://doi.org/10.1016/j.apgeochem.2015.01.009

Morgenstern, N. R., Vick, S. G., Viotti, C. B., & Watts, B. D. (2016). Report on the Immediate Causes of the Failure of the Fundão Dam.

Nègre, M., Leone, P., Trichet, J., Défarge, C., Boero, V., & Gennari, M. (2004). Characterization of model soil colloids by cryo-scanning electron microscopy. Geoderma, 121(1–2). https://doi.org/10.1016/j.geoderma.2003.09.011

Soares, L., Arnez, F. I., & Hennies, W. T. (2000). Major causes of accidents in tailing dam due to geological and geotechnical factors. In Mine Planning and Equipment Selection– International Symposium (pp. 371-376

T.E. Martin, & E.C. McRoberts. (1999). Some considerations in the stability analysis of upstream tailings dams. In Proceedings of the Sixth International Conference on Tailings and Mine Waste, 99, 287–302.

USEPA. 1996. Soil Screening Guidance: User's Guide Second Edition, 20460, Washington, DC, USA: EPA EPA540/R-96/018. Office of Emergency and Remedial Response

Vick, S. G. (1990). Planning, Design and Analysis of Tailings Dams. John Wiley and Sons, Inc., New York, N.Y.

Vidyadhar, A and Singh, Ratnakar. 2007. "Froth Flotation and its Application to Concentration of Low Grade Iron Ores." In Processing Iron Ore, by A Vidyadhar and R Singh, 103-114.

Table 2.1 Physical Properties of Slime and Silt Samples.

Property	Test Results			
	Slime 1	Slime 2	Silt 1	Silt 2
Water Content (%)	26.24	26.23	8.7	14.3
Liquid Limit (%)	26.8	27.8	25.5	40
Specific Gravity	3.46	2.61	2.85	2.69
Sand Content (%)	42.5	20.6	36.7	36.6
Silt Content (%)	52.7	77.3	62.2	62.2
Clay Content (%)	4.8	2.1	1.1	1.2
D50 (mm)	0.07	0.04	0.05	0.05
C_c	1.08	4.62	1.10	1.60
C_u	26.33	10	7.4	14.4

Table 2.2 Elemental Analysis of Slimes 1 and 2 from iron and gold mine, respectively.

Analyte	Slime 1	Slime 2
Aluminum (mg/Kg)	3,800.0	2,000.0
Arsenic (mg/Kg)	23.0	1,100.0
Barium (mg/Kg)	32.0	17.0
Cadmium (mg/Kg)	2.1	0.7
Calcium (mg/Kg)	1,500.0	3,100.0
Chromium (mg/Kg)	18.0	10.0
Cobalt (mg/Kg)	4.2	7.8
Copper (mg/Kg)	8.9	5.0
Iron (mg/Kg)	330,000.0	27,000.0
Lead (mg/Kg)	24.0	17.0
Magnesium (mg/Kg)	210.0	3,400.0
Manganese (mg/Kg)	990.0	390.0
Mercury (mg/Kg)	0.1	0.0
Nickel (mg/Kg)	17.0	16.0
Phosphorus (mg/L)	640.0	500.0
Silver (mg/Kg)	4.2	1.0
Sodium (mg/Kg)	830.0	190.0
Tin (mg/Kg)	42.0	9.5
Vanadium (mg/Kg)	13.0	2.0
Zinc (mg/Kg)	11.0	69.0

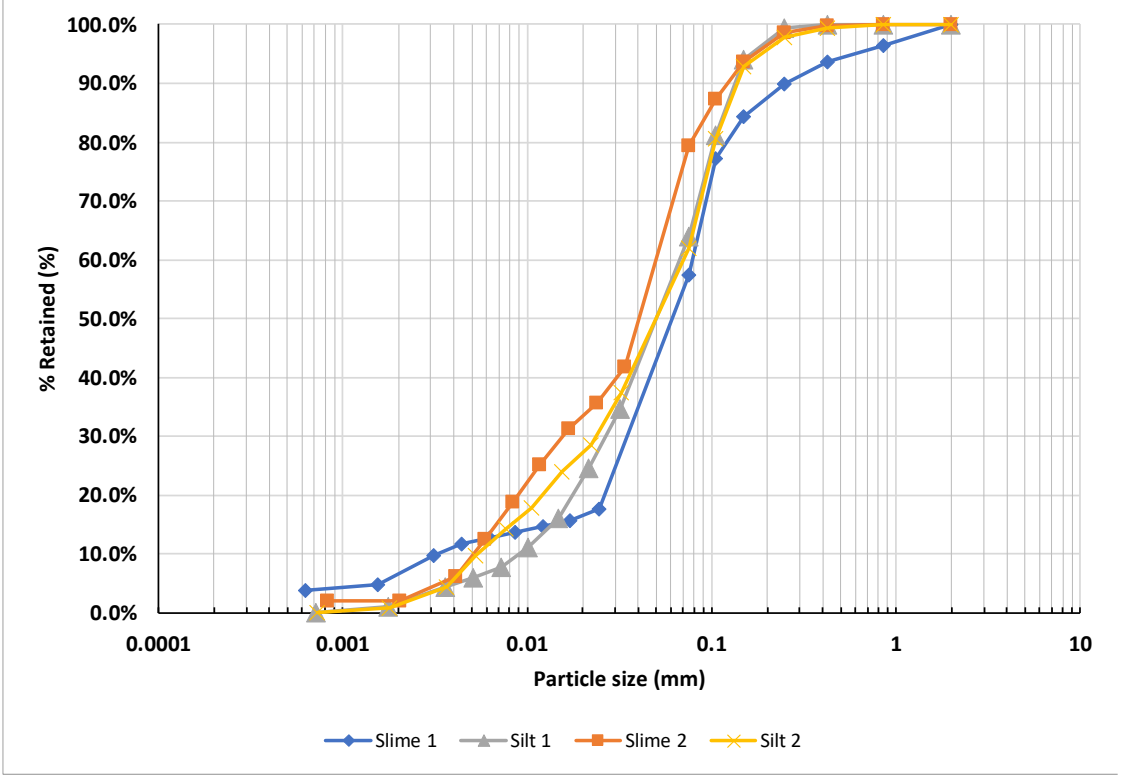

Figure 2.1 Grain size distribution for Slimes 1 and 2 and Silts 1 and 2.

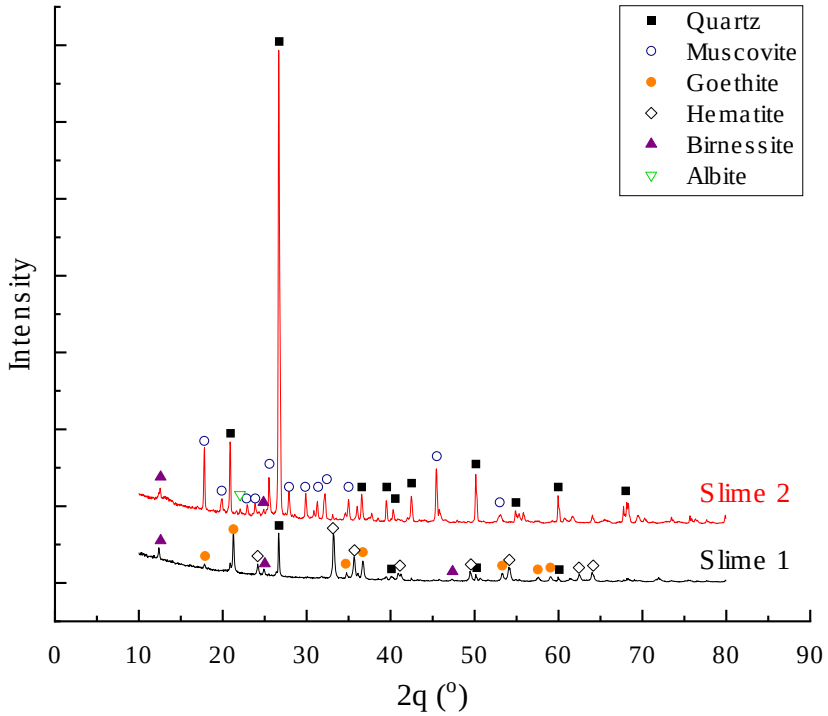

Figure 2.2 XRD Mineral Identification for Slimes 1 and 2.

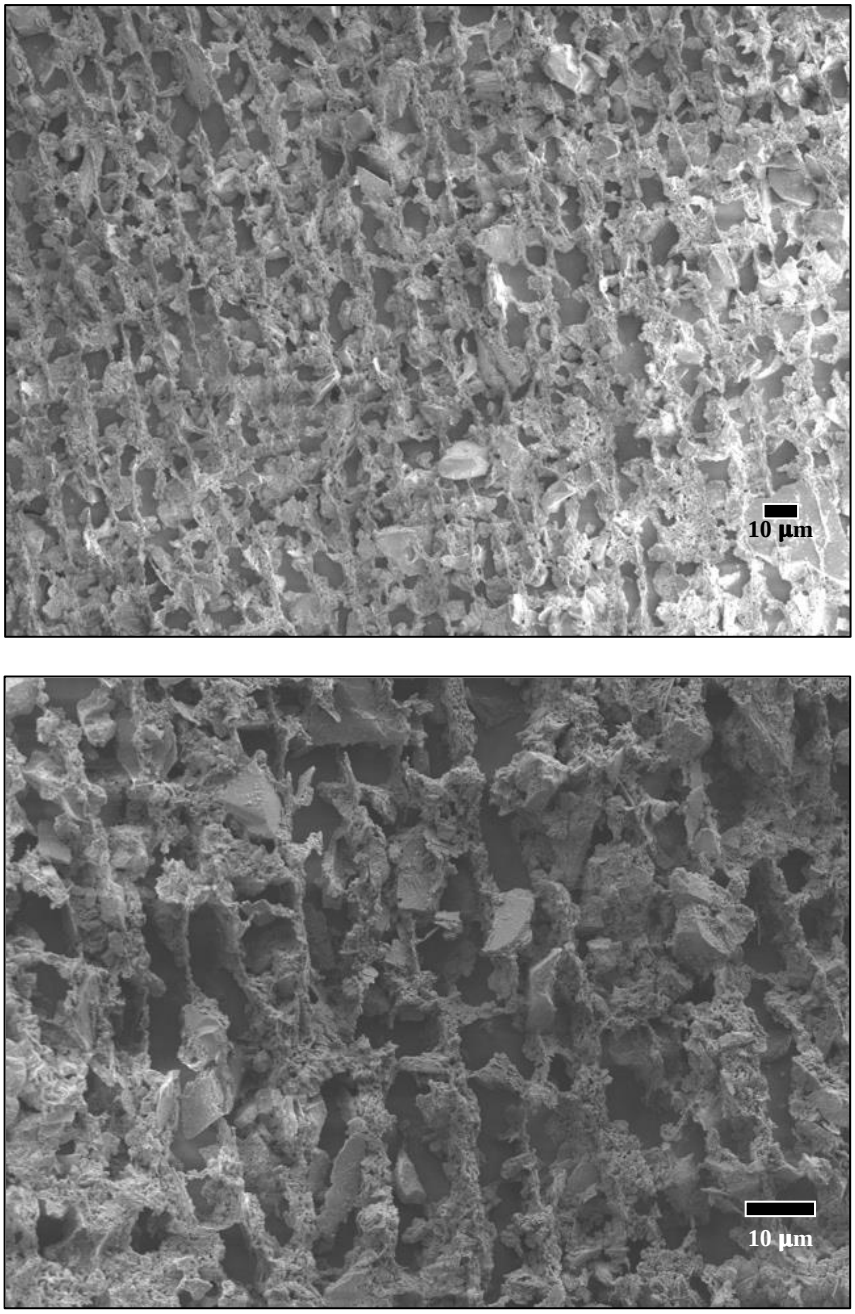

Figure 2.3 SEM images from Cryo-SEM for Slime 1 at 500x and 1000x magnification.

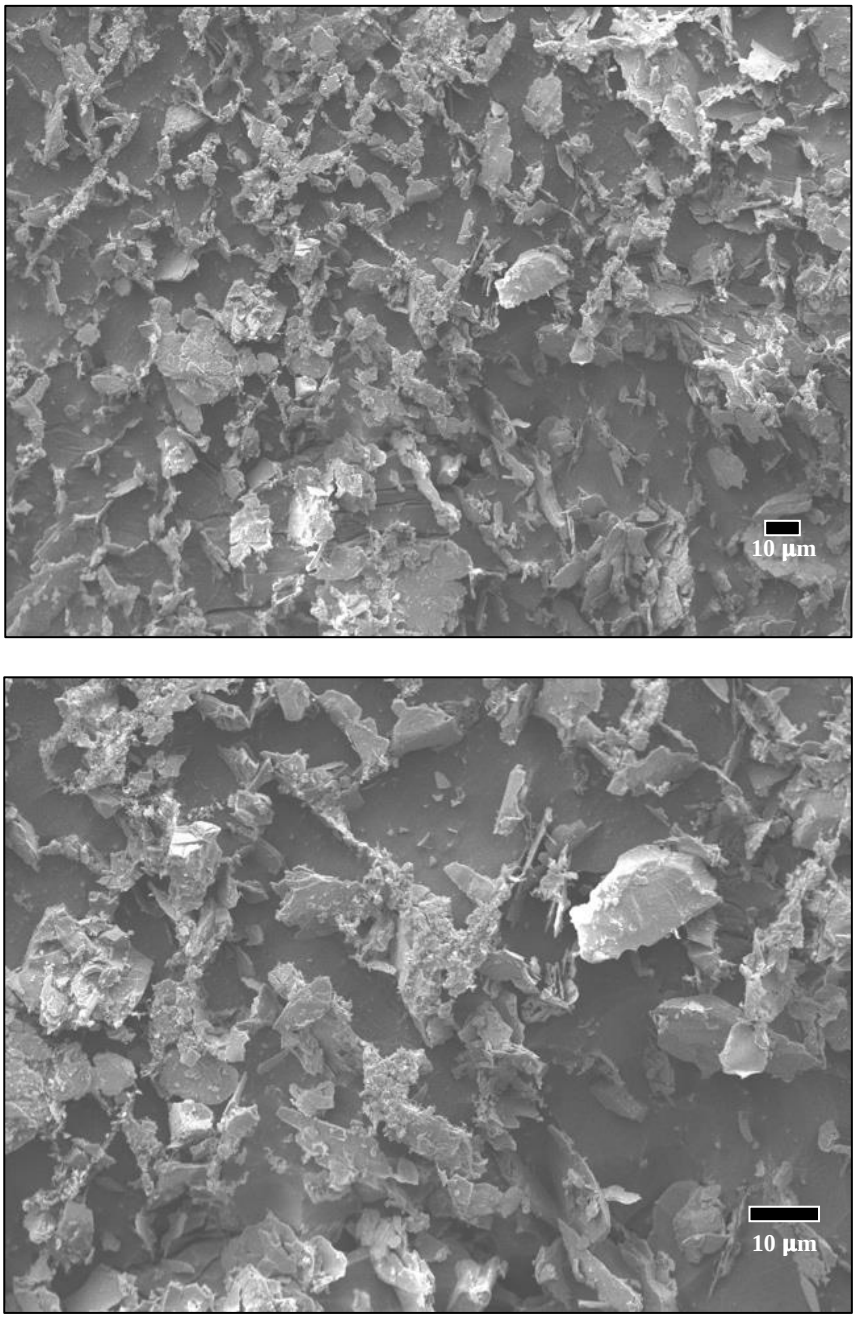

Figure 2.4 SEM images from Cryo-SEM for Slime 2 at 500x and 1000x magnification.

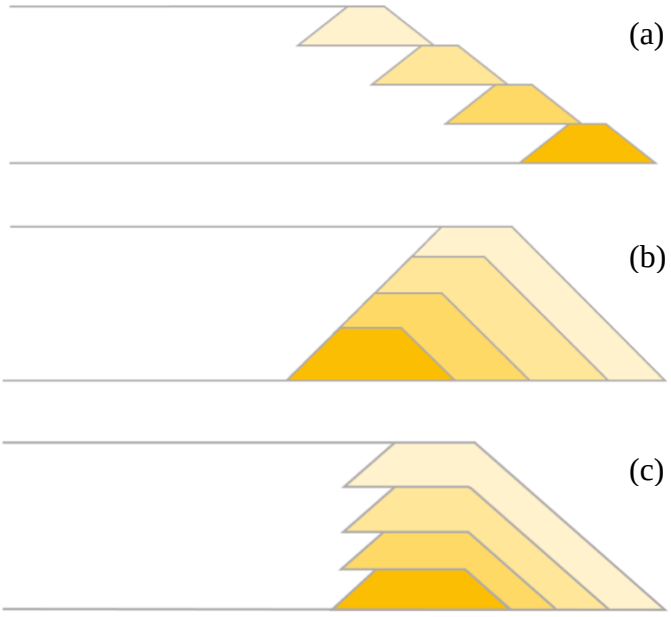

Figure 2.5 Schematic illustrations of (a) upstream, (b) downstream, and (c) center-line sequentially raised tailings dams. The starter dike is represented by the darkest prism and successively lighter elements represent newer raises, after Vick (1990).

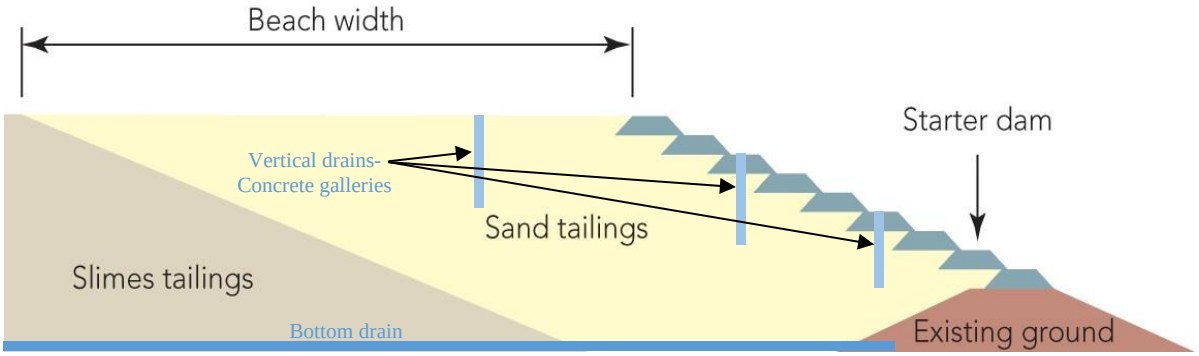

Figure 2.6 Illustration of representative dam construction, a variation of upstream-style construction known as the "drained stack" method, with typical location of vertical and bottom drainage systems (Morgenstern, Vick et al 2016).

Chapter 3 : The Effect of Microbial Induced Carbonate Precipitation on Fine-Grained Mine Tailings

A version of this chapter is published as a Geotechnical Special Publication (GSP) from Geo-Congress 2022: O'Toole, C., Liu, Q., Montoya, B.M., Kananizadeh, N., Odle, W. (2022). "The Effect of Microbial Induced Carbonate Precipitation on Fine-Grained Mine Tailings." Proceedings from ASCE Geo-Congress 2022, Charlotte, NC, ASCE Geotechnical Special Publication (GSP) 331.

3.1 Introduction

As introduced in Chapter 2, the iron and gold ore mine tailings were subjected to tests to further characterize and quantify the effect of MICP on changes in shear strength and fabric of the soils. The bio-cementation process of MICP is utilized in geotechnical engineering to enhance soil characteristics to improve strength and stiffness. This is done by introducing various ingredients including $CaCl_2$ (calcium chloride), urea, and bacteria (i.e.- *Sporosarcina pasteurii*). *Sporosarcina pasteurrii* is an alkalophilic soil bacterium with a highly active urease enzyme. MICP relies upon microbial induced urea hydrolysis, which produces carbonate (CO_3^{-2}), bicarbonate (HCO_3^-), carbonic acid (H_2CO_3), ammonia (NH_3), and ammonium (NH_4^+), as shown in the enzymatic reactions in Figure **3.1**. The precipitation of carbonate occurs because the equilibrium of calcium carbonate ($CaCO_3$) precipitation-dissolution shifts toward precipitation, also shown in the chemical reactions depicted in Figure **3.1** (DeJong et al, 2010). The precipitated calcium carbonate coats soil particles, cements soil matrix at the particle-particle contacts, and fills the soil void space, increasing the soils strength, stiffness, and dilatancy (Lin et al, 2016; Feng et al. 2016; Nafisi et al. 2020; among many others). Mujah and Cheng (2017) theorized that increased calcium carbonate precipitation in the region of particle to particle

contacts is the result of the greater concentration of microbes, mostly due to the reduced shear stresses and availability of nutrients at the grain contacts.

In this chapter, a proof of concept self-weight consolidation column test was utilized as a benchmark to confirm that MICP would occur in the ore tailings slime samples. This test served 2 functions: to observe the flocculation or suspension behavior of the slimes in a slurry, and to determine if calcium carbonate would precipitate via MICP. Once MICP was confirmed via mass of carbonate acid wash, a more robust testing procedure was conducted to quantify the effect MICP had on the shear strength of the slime samples. Additionally, the susceptibility of MICP-treated tailings to acidic conditions were evaluated.

3.2 Testing Methods

3.2.1 Microbial Cultivation

S. pasteurii (ATCC 11859) was used to induce urea hydrolysis in the experiments herein. The suspension and incubation of the growth media followed previous studies (Liu and Montoya 2020). The value of optical density at a wavelength of 600 nm (OD_{600}) of the bacterial solution was ~0.9 (i.e., ~10^7 cells/mL). Urea and calcium chloride were purchased from Alfa Aesar and Fisher, respectively.

3.2.2 Proof of Concept Column Test

For the self-weight consolidation column test, three sets of sample environments were prepared for each slime: 1) mixed with deionized (DI) water (Set 1), 2) mixed with DI water and 75 g/L Urea + 15 g/L CaCl2 (Set 2), and 3) mixed with DI water and 75 g/L Urea + 15 g/L CaCl2 + 50 mL S. pasteurii (Set 3). Each column contained 50 ± 0.05g of mine tailings that was mixed with their sample environments utilizing an agitator similar to the apparatus outlined in ASTM D7928. Transferring the contents to a glass graduated cylinder, DI water was added to the

suspension to reach 1000 mL. Once the total suspension volume was added to the column, the suspension was mixed again by repeatedly turning the apparatus upside down 10 times to ensure proper mixing. Calcium carbonate was observed to have precipitated on the walls of the graduated cylinder, and a thick, stiff upper layer of calcium carbonate was observed at the water-soil column partition. Acid wash confirmed that the stiff upper layer was calcium carbonate, and the researchers continued to the next phase of Fall Cone Testing.

3.2.3 Fall Cone Test

Fall cone testing was used in order to evaluate the effects of MICP on the undrained shear strength of the mine tailings. Traditional testing methods such as triaxial testing (TX) or direct simple shear (DSS) were not utilized due to the high fine fraction of the mine tailings. Lower permeability associated with the finer grained soils would hinder the ability for adequate drainage and flow through the sample, significantly increasing the amount of time to conduct these tests.

Mine tailings samples were oven dried overnight at 110˚C. Once fully dried, test samples were prepared to a range of target water contents; baseline samples were mixed with DI water and MICP-treated samples were mixed with the appropriate recipe and water content (Table **3.1**). Samples were labeled according to their respective recipes and target water contents. For example, a sample of Slime 1 with MICP recipe 1 (R1) and target water content 1 (W1) has been denoted as S1R1W1. Treated samples were subjected to periodic FCT measurements over 15 days; baseline samples were tested immediately after preparation, as there would not be an increase in strength over time. In between FCT, MICP-treated samples were covered with parafilm to prevent excess evaporation and stored in an incubator at 30°C to promote microbial activity. Following International Organization of Standards (ISO) standard 17892-6:2017,

samples of Slimes 1 and 2 were subjected to FCT to obtain depth of penetration values. The average of 5 penetration values for each sample are then used to estimate the undrained shear strength (S_{ur}), using Eq. 3 (ISO 17892-17)

$$S_{ur} = cg\frac{m}{i^2} \quad (3)$$

Where c= 0.80 for cones with 30° tip, g= acceleration due to gravity (m/s^2), m= mass of cone tip (g) , and i=measured penetration (mm).

3.2.4 Mass of Calcium Carbonate Acid Wash

To confirm calcium carbonate precipitation and the level at which MICP contributed to calcium carbonate precipitation, a quantitative gasometric method was implemented. The method in this paper is designed based on ASTM D4373 method. A simpler apparatus using glass serum bottles, sealed with a rubber stoppers and crimped with metal tops, and 10-mL and 50-mL Fisher syringes was designed for this process. An image of this apparatus can be seen in Figure **3.2**a. Assuming ideal gas law and utilizing known amounts of pure calcium carbonate (Fisher), a calibration between gas volume (GV) measured in the syringes (with volume of 1M HCl acid subtracted) and $CaCO_3$ mass was derived with high correlation (R^2=0.9996), which can be seen in Figure **3.2**b. With this relationship, samples of slimes can be tested to determine their $CaCO_3$ mass, for both untreated samples as a control group and for treated samples to determine the increase due to MICP.

3.3 Results

3.3.1 Self Weight Consolidation Results- Particle Sedimentation

From pictures taken throughout the test, as seen in Figure **3.3**, it was determined that the column of Set 1, where the slimes are suspended in DI water, showed eventual settlement of a majority of particles near the end of the 7 days, but there was evidence along the inside of the column that

particles were adhering to the glass walls. Assuming the Guoy-Chapman theory for the diffuse double layer (DDL) is true, particles suspended in the DI water have the highest DDL thickness of those studied herein, and therefore, will have less attraction in particle-particle interactions (Mitchell and Soga, 2005). For Set 2, which consists of the slimes suspended with MICP ingredients (namely $CaCl_2$), introducing a solution with electrolyte of cation valence 2 from the Set 2 sedimentation columns agree with this, which showed decreased soil thickness (i.e., more consolidated) as compared with Set 1. Set 3 columns with MICP ingredients + *S. pasteurii* showed increasing levels of flocculation and evidence of calcium carbonate precipitation, compared to Sets 1 and 2. As expected, calcium carbonate was not identified in Sets 1 and 2 due to lack of ureolytic activity to drive the MICP process. The introduction of electrolytes to solution (e.g., $CaCl_2$) and confirmed calcite (from XRD analysis) occupied more void space in the soil fabric, expelling water and decreasing the soil thickness.

3.3.2 Fall Cone Test Results

Values for the baseline shear strength evaluated from FCT for the untreated slime samples at varying water contents were gathered and can be seen compiled in Table **3.2**. The undrained shear strength investigated via FCT reveals that the shear strength decreases with increasing water content. Initial FCT results indicate Slime 1 has a lower overall strength as compared to Slime 2; however, Slime 2 had higher sensitivity to varying water contents (Table **3.2**). From the corresponding SEM images in Figure ***2.3***, we can infer that for Slime 1, which indicated the "card-house" structure of flocculated particles along the edge-to-face contacts, the increased water content has less effect on the shear strength than for the dispersed fabric of Slime 2. Although covered by parafilm, water contents of treated samples declined 2-4% after 15 days of incubation and their S_{ur} values over the test period can be found summarized in Table **3.3**.

Comparison between the treated and untreated samples' S_{ur} values indicated increases in strength for both slime samples as visualized in Figure **3.4** with accompanying error bars during measurement. Slime 2 showed increased strength improvement over Slime 1, as indicated 1.02-4.5 times increase in S_{ur}, as compared to 1.5-3.0 in Slime 1. S1W2R1 had no discernible strength increase despite having low indications of calcium carbonate present in the sample. Additionally, a thin layer of water was evident on the surface of the S2W2R2 sample, which may have influenced the FCT measurement. The apparent lack of change in the S_{ur} for these 2 samples in the presence of CaCO3 precipitation (as seen in Table **3.4**) warrants further investigation.

3.3.3 Mass of Carbonate Test Results

Results from the gasometric test, as presented in Table **3.4**, indicated that calcium carbonate precipitated for all MICP treated samples as compared to the baseline untreated slimes. Slime 1 $CaCO_3$ mass, reported in wt.% of total soil mass, increased ranging from 9.06 to 10.54 times the baseline value, and Slime 2 increased ranging from 6.05 to 6.91 times the baseline value.

3.3.4 XRD Results

X-Ray Diffraction (XRD) analysis of the baseline untreated samples was conducted to identify the mineral phases and crystallinity in each sample. XRD qualitatively identifies the crystalline phases of the mine tailings sample. Samples were oven dried and crushed to a fine powder. XRD uses electrons that hit the solid samples and x-rays are emitted. When x-rays hit a soil particle or crystal structure, x-rays diffract based on this crystal structure, but other x-rays penetrate further into the sample until colliding into another crystal. The machine reads the different angles that are diffracted throughout the measured sample, and the scattered x-rays and their intensities create a pattern. Analysis was performed for 2θ range from 0 to 80º with a scanning step of 0.05º and a speed of 3º/min. XRD patterns results of analysis conducted on the MICP-treated Slime 1

and 2 samples are shown in Figure **3.5**. As compared to XRD results of untreated samples in Figure ***2.2***, treated samples of Slimes 1 and 2 show matching to calcite peak intensities in all 4 sample numbers of recipes and water contents.

3.3.5 Acid Dissolution

The susceptibility of the precipitated calcium carbonate was examined under varying pH conditions to simulate acid rain dissolution. At the increments of increasing pH, samples of Slime 1 and 2 from original ex-situ mixing and Fall Cone Tests were tested. The samples were dissolved in HCl acid solutions at measured pH as seen in Table **3.5**. Using the known initial $CaCO_3$ mass % of each Slime as seen in Table **3.4**, the remaining % relative to the initial % mass- i.e.- at a 3.5 pH solution, 40% of the CaCO3 mass will remain. The results can be found in both Table **3.5** and Figure **3.6** for Slime 1 and Table **3.6** and Figure **3.7** for Slime 2.

Slime 2 presented issues during this iteration of acid wash testing. Additionally, due to heavier cementation that resulted in higher % Mass of $CaCO_3$, Slime 2 in particular showed resilience to the acid solutions. Compared to Slime 1, less than 20% of the $CaCO_3$ in Slime 2 samples dissolved at 3 pH, whereas almost 80% dissolved in Slime 1. For S2W2R1 samples, several duplicate samples at different pH solutions resulted in “negative” values utilizing the modified gasometric method. For example, 30 mL of HCl acid was added to the system and the resulting syringe showed 28 mL of gas produced.

3.4 Discussion

3.4.1 Water Content

The final water contents for the treated samples were below the initial water contents calculated at the beginning of the test. Two proposed reasons for this discrepancy are: 1) evaporation, and 2) dewatering from urea hydrolysis. While performing the FCT, the covering for each sample

was removed, and a small amount of evaporation could occur at this time. Dewatering of the slimes was evident by a thin layer of water observed on the surface of at least one sample. Assuming urea was completely hydrolyzed during the MICP process, and using equations presented in DeJong et al., 2010, an estimate of 12 g (or mL) of water would be utilized, and extruded, from the soil system to create calcium carbonate. However, more research is required to better quantify the dewatering of fine-grained soils due to MICP.

3.4.2 Fall Cone Testing

There is no consensus as to the comparability of S_{ur} from FCT with strength estimates from other tests, such as Unconfined Compression Test (UCT) or Direct Shear Test (DST). Results from Canelas et al (2018) showed good correlation to results from DST. However, Tanaka et al. (2012) concluded that FCT and UCT were not comparable based on tested soils. For our purposes, the FCT results offer value in comparison of relative strength increase between the control and treated slimes.

In regard to the FCT results, a few explanations for the observed slimes' behaviors are proposed: 1) Increases in strength over time for each sample are more likely due to continued microbial processing and precipitation of calcium carbonate, and not exclusively associated with changes from initial to final water contents; 2) Higher increases in shear strength of Slime 2 samples may be attributed to the affinity for aggregation within the soil matrix based on the SEM results. With a higher fine fraction than Slime 1, there are more particle-to-particle interactions within the soil matrix that may lead to more effective bonding of the $CaCO_3$ precipitates; 3) Chemical analysis conducted on the untreated samples indicated that Slime 1 had lower natural [Ca^+] than Slime 2. The increased number of available or exchangeable Ca^+ ions could potentially contribute to increased precipitation.

Multiple treatment cycles have been shown to increase the shear strength improvement when the soils treated with MICP are granular and allow for adequate flow of bacteria and urea. MICP treated sands have indicated increased cohesion and shear strength, as well as resilience to freeze-thaw cycles and acid rain (Nafisi et al, 2020; Liu et al, 2019). However, with fine-grained soil and hand-mixing utilized, it is likely that the cemented bonds between particles created during MICP would be broken during mixing, negating potential shear strength increases while indicating higher calcium carbonate content.

3.4.3 Acid Dissolution

The lack of dissolution of calcium carbonate identified in Slime 2 samples is believed to related to the available H+ ions in a given volume of moderate pH HCl solution. At these diluted acid solutions, there are not enough available H^+ ions to dissolve all the $CaCO_3$ present. When the volume of acid was increased, the resulting gas volume measured did not correspond with higher dissolution of CaCO3. This also may be due to the low number of available H^+ ions, and their inability in a larger volume solution to dissolve the available CaCO3. It is not clear why the "negative" dissolution values seen in S2W2R1 occurred for Slime 2 samples and was not seen in Slime 1 samples.

3.5 Conclusions

Shear strength increases of up to 450% have been shown in the MICP treated samples compared to the untreated controls. Fall cone testing indicated that MICP provided significant strength increase from apparent CaCO3 precipitation. While promising results, these increases are only indicative of 1 cycle of treatment, and if subjected to the multiple treatments, higher shear strength may be achieved. This study was a novel application of MICP on fine grained mine

tailings, and additional work in the next chapters expanded upon the results of these experiments to include other granular materials from the same mines.

References

ASTM. (2010). “D2216 Standard Test Methods for Laboratory Determination of Water (Moisture) Content of Soil and Rock by Mass”. ASTM International, West Conshohocken, PA.

ASTM. (2014). “D854 Standard Test Methods for Specific Gravity of Soil Solids by Water Pycnometer”. ASTM International, West Conshohocken, PA.

ASTM (2017a). “D4318 Standard Test Methods for Liquid Limit, Plastic Limit, and Plasticity Index of Soils”. ASTM International, West Conshohocken, PA.

ASTM (2014). “D4373 Standard Test Method for Rapid Determination of Carbonate Content of Soils”. ASTM International, West Conshohocken, PA.

ASTM (2017b.) “D6913 Standard Test Methods for Particle-Size Distribution (Gradation) of Soils Using Sieve Analysis”. ASTM International, West Conshohocken, PA.

ASTM (2017c). “D7928 Standard Test Method for Particle-Size Distribution (Gradation) of Fine-Grained Soils Using the Sedimentation (Hydrometer) Analysis”. ASTM International, West Conshohocken, PA

DeJong, J. T., Mortensen, B. M., Martinez, B. C., and Nelson, D. C. (2010). “Bio-mediated soil improvement.” Ecological Engineering, 36(2), 197–210.

Feng, K., Montoya, B.M. (2016). “Influence of Confinement and Cementation Level on the Behavior of Microbial Induced Calcite Precipitated Sands under Monotonic Drained Loading.” *ASCE Journal of Geotechnical and Geoenvironmental Engineering*, 142(1).

Lin, H., Suleiman, M. T., Brown, D. G., and Kavazanjian, E. (2016). “Mechanical Behavior of Sands Treated by Microbially Induced Carbonate Precipitation.” Journal of Geotechnical and Geoenvironmental Engineering, 142(2), 04015066.

Liu, Q., and Montoya, B. M. (2020). “Experimental Study of Consolidation Behavior of Mature Fine Tailings Treated with Microbial Induced Calcium Carbonate Precipitation.” Geo-Congress 2020.

Liu, S., Wen, K., Armwood, C., Bu, C., Li, C., Amini, F., Li, L. (2019). Enhancement of MICP-Treated sandy SOILS against environmental deterioration. Journal of Materials in Civil Engineering, 31(12), 04019294.

Mitchell, J. K., and Soga, K. (2005). *Fundamentals of soil behavior, 3rd ed*. Wiley, Hoboken, NJ.

Montoya, B. M., Safavizadeh, S., and Gabr, M. A. (2019). “Enhancement of Coal Ash Compressibility Parameters Using Microbial-Induced Carbonate Precipitation.” Journal of Geotechnical and Geoenvironmental Engineering, 145(5), 04019018.

Nafisi, A., Montoya, B. M., and Evans, T. M. (2020). “Shear Strength Envelopes of Biocemented Sands with Varying Particle Size and Cementation Level.” Journal of Geotechnical and Geoenvironmental Engineering, 146(3), 04020002.

Safavizadeh, S., Montoya, B. M., and Gabr, M. A. (2019). “Microbial induced calcium carbonate precipitation in coal ash.” Géotechnique, 69(8), 727–740.

Santamarina, J. C., Torres-Cruz, L. A., and Bachus, R. C. (2019). “Why coal ash and tailings dam disasters occur.” Science, 364(6440), 526–528.

Tanaka, H., Hirabayashi, H., Matsuoka, T., and Kaneko, H. (2012). “Use of fall cone test as measurement of shear strength for soft clay materials.” Soils and Foundations, 52(4), 590–599.

DeJong JT, Mortensen BM, Martinez BC, Nelson DC. 2010. Bio-mediated soil improvement. Ecol Eng 36(2):197–210

Lin, H., Suleiman, M., Brown, D., and Kavazanjian, E. (2016). “Mechanical behavior of sands treated by microbially induced carbonate precipitation.” J. Geotech. Geoenviron. Eng., 10.1061/(ASCE)GT.1943-5606.0001383, 04015066

Mujah D., Shahin MA, Cheng L. State-of-the-art review of biocementation by microbially induced calcite precipitation (MICP) for soil stabilization. Geomicrobiol J 2017; 34:524-37

Table 3.1 a) MICP recipes and b) target water contents for fall cone test of slimes.

(a) #	Cementation solution		Bacterial solution	(b) #	Target Water Content
	Urea (mM)	$CaCl_2$ (mM)	Bacteria (mL)		
R1	333	100	40	W1	27
R2	333	300	40	W2	30

Table 3.2 FCT results of untreated slimes with variable water contents.

	Slime 1				Slime 2				
S_{ur} (kPa)	3.52	3.23	1.45	1.22	10.56	6.69	4.96	3.71	2.53
w (%)	24.5%	24.9%	29.1%	30.3%	23.6%	25.7%	26.7%	27.1%	28.4%

Table 3.3 FCT results for MICP treated Slimes 1 and 2 with different recipes and corresponding initial water contents (w_i) and final water contents (w_f).

#	MICP Treated Slime 1						MICP Treated Slime 2					
Day	0	3	8	10	13	15	0	3	8	10	13	15
S_{ur} Estimate (kPa)	S1W1R1, w_i=25.2%, w_f=21.9%						S2W1R1, w_i=24.2%, w_f=20.0%					
	1.49	2.7	4.54	4.85	10.1	8.58	5.02	13.13	32.51	24.45	49.87	52.41
	S1W1R2, w_i=25.1%, w_f=21.8%						S2W1R2, w_i=25.8%, w_f=20.3%					
	1.39	2.93	8.42	6.53	14.62	13.64	5.25	12.92	31.69	16.52	36	61.38
	S1W2R1, w_i=28.5%, w_f=23.7%						S2W2R1, w_i=28.4%, w_f=21.7%					
	1.39	1.39	1.39	1.39	1.39	1.39	3.04	6.35	17.14	14.82	33.69	37.22
	S1W2R2, w_i=28.2%, w_f=23.7%						S2W2R2, w_i=27.8%, w_f=21.8%					
	1.39	1.54	3.53	3.38	4.68	5.87	3.16	6.03	6.24	9.63	12.18	13.39

Table 3.4 Mass of $CaCO_3$ (wt.%) results for baseline untreated and MICP treated samples.

	Slime 1	Slime 2
Baseline	0.12	0.93
W1R1	1.25	5.76
W1R2	1.09	6.02
W2R1	0.64	5.60
W2R2	1.27	6.40

Table 3.5 Remaining CaCO3 Mass % at varying pH solutions for Slime 1.

pH	S1W1R1	S1W1R2	S1W2R2	S1W2R1
3.01	0.28	0.26	0.33	0.03
3.58	0.50	0.42	0.48	0.07
4.04	0.65	0.56	0.66	0.12
4.53	0.80	0.67	0.81	0.18
4.97	0.91	0.75	0.89	0.34
5.51	1.03	0.94	1.01	0.49
7	1.25	1.09	1.27	0.64

Table 3.6 Remaining CaCO3 Mass % at varying pH solutions for Slime 2.

pH	S1W1R1	S1W1R2	S1W2R2	S1W2R1
3.01	5.30	5.42	5.15	5.38
3.58	5.47	5.66	5.77	5.63
4.04	5.53	5.78	5.88	5.95
4.53	5.59	5.90	6.05	6.14
4.97	5.64	5.84	6.33	6.21
5.51	5.70	5.90	5.88	6.34
7	5.76	6.02	5.60	6.40

Table 3.7 Remaining % of initial $CaCO_3$ Mass at varying pH solutions for Slime 1.

pH	S1W1R1	S1W1R2	S1W2R2	S1W2R1
3.01	22%	24%	5%	26%
3.58	40%	39%	11%	38%
4.04	52%	51%	19%	52%
4.53	64%	61%	28%	64%
4.97	73%	69%	53%	70%
5.51	82%	86%	77%	80%
7	100%	100%	100%	100%

Table 3.8 Remaining % of initial $CaCO_3$ Mass at varying pH solutions for Slime 2.

pH	S2W1R1	S2W1R2	S2W2R1	S2W2R2
3.01	92%	90%	92%	84%
3.58	95%	94%	103%	88%
4.04	96%	96%	105%	93%
4.53	97%	98%	108%	96%
4.97	98%	97%	113%	97%
5.51	99%	98%	105%	99%
7	100%	100%	100%	100%

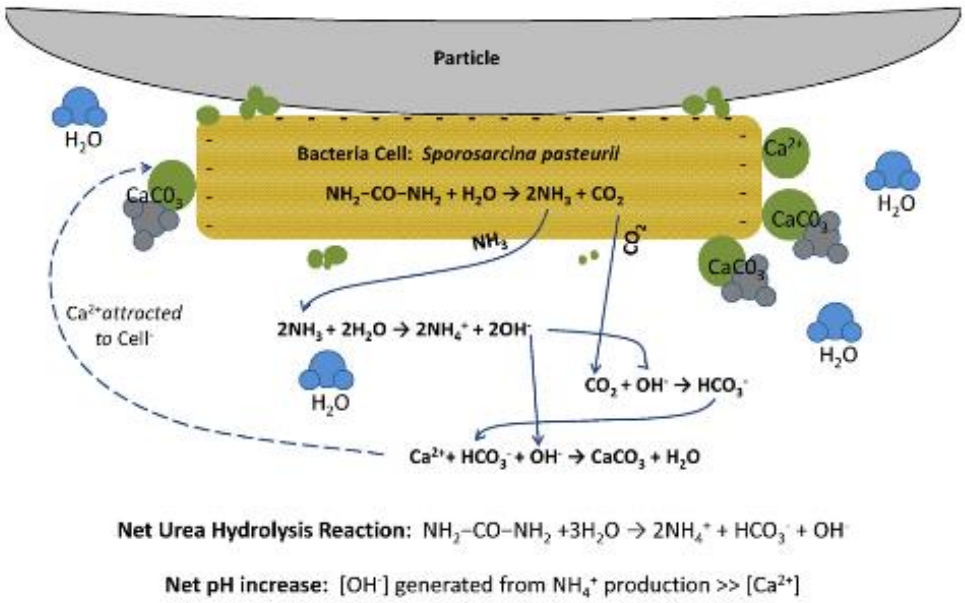

Figure 3.1 from DeJong et al, 2010- An overview of bio-mediated calcium carbonate precipitation and the relevant chemical reactions.

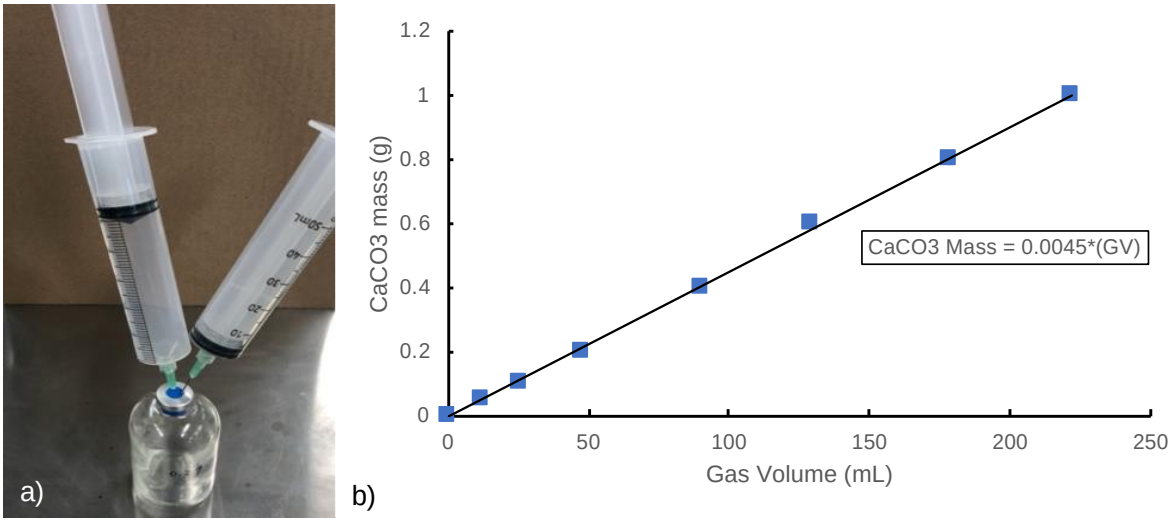

Figure 3.2 a) Gasometric testing apparatus and b) gas volume to $CaCO_3$ mass calibration.

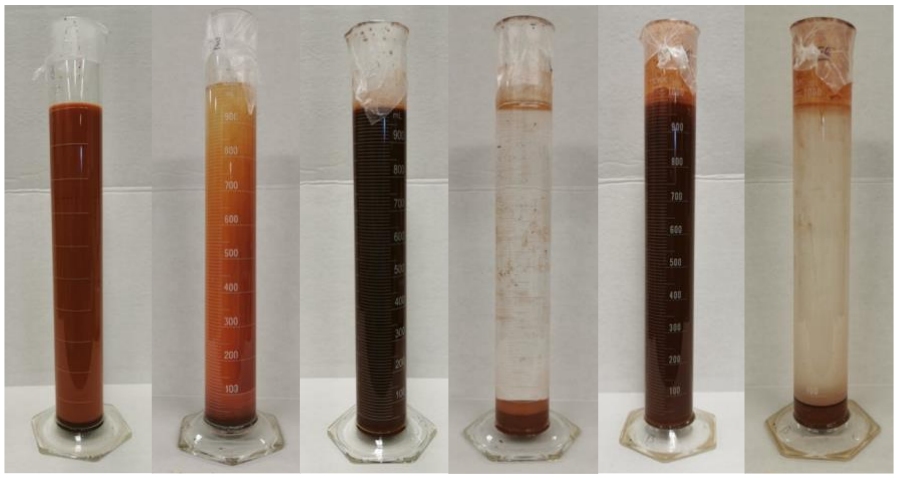

Figure 3.3 Pictures of self-consolidation column tests from beginning of trial (day 0) to end of trial (day 7). *S.p*. in the figure refers to *S. pasteurii*.

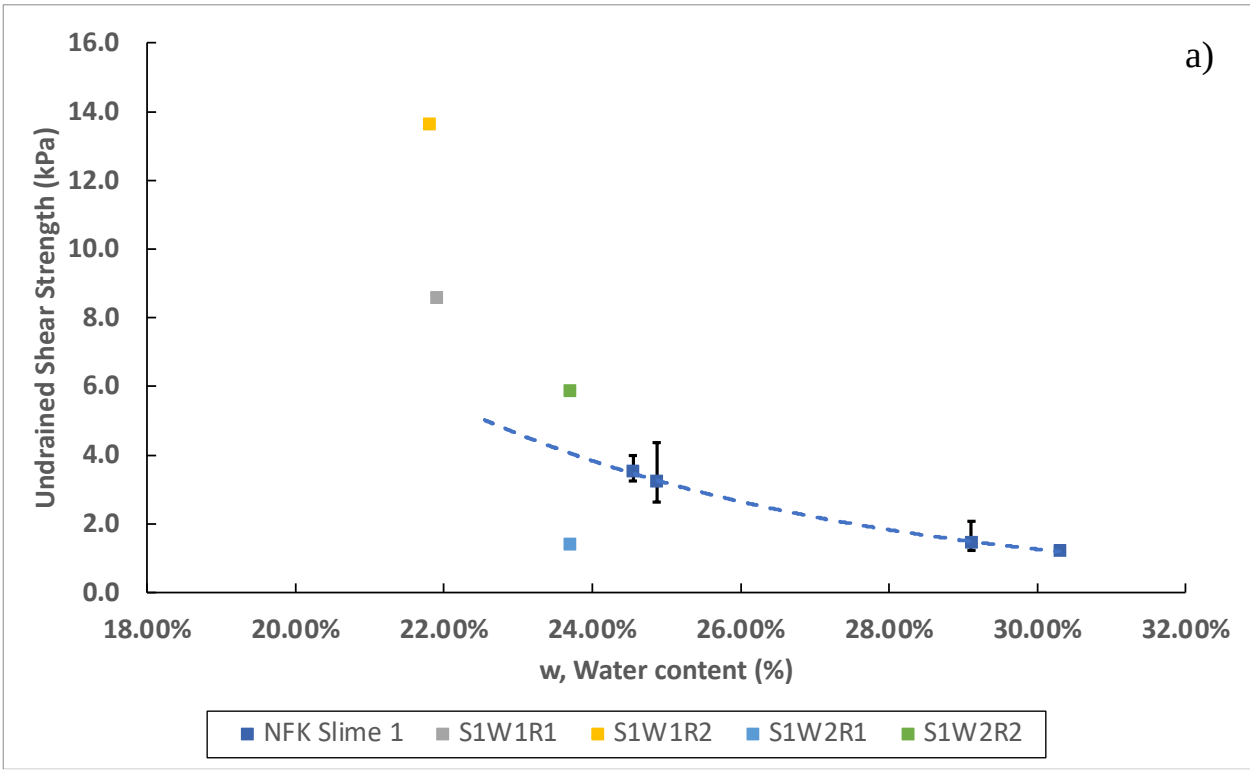

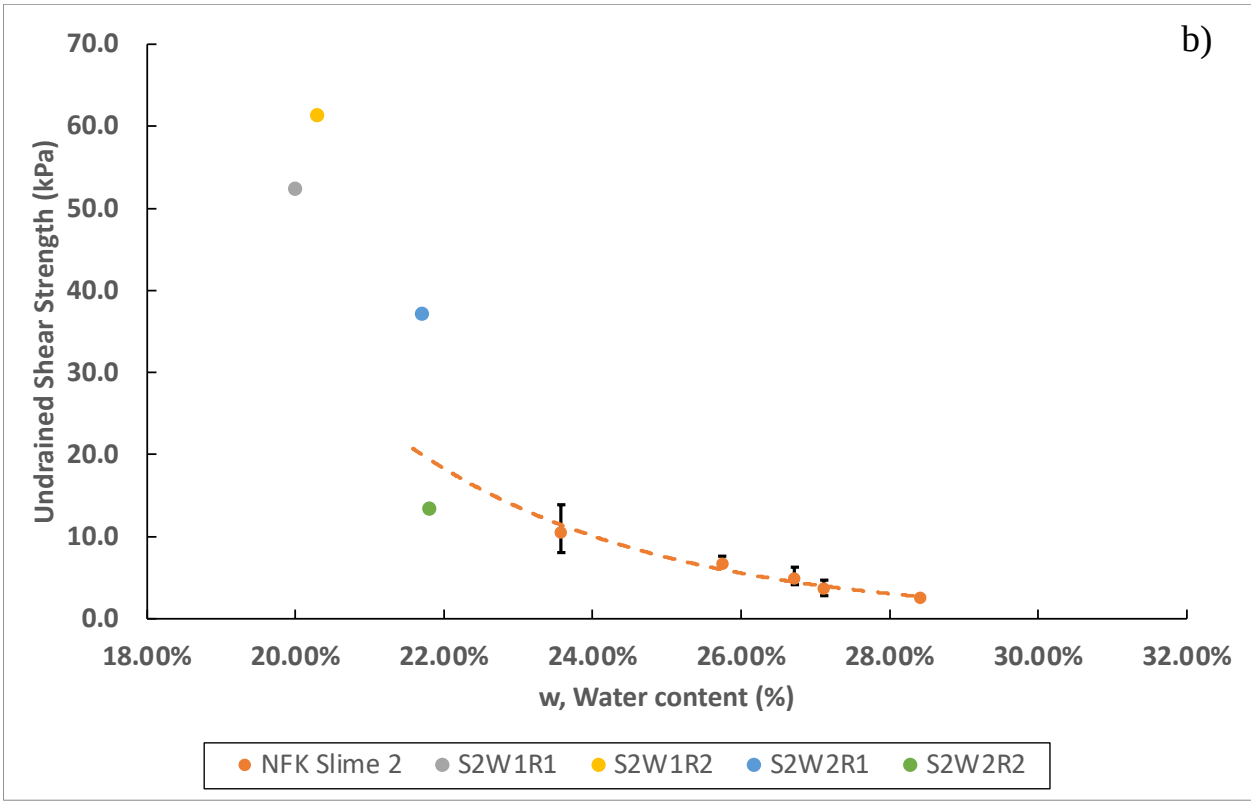

Figure 3.4 FCT S_{ur} results normalized for water content of Slimes 1 (a) and 2 (b) with error bars.

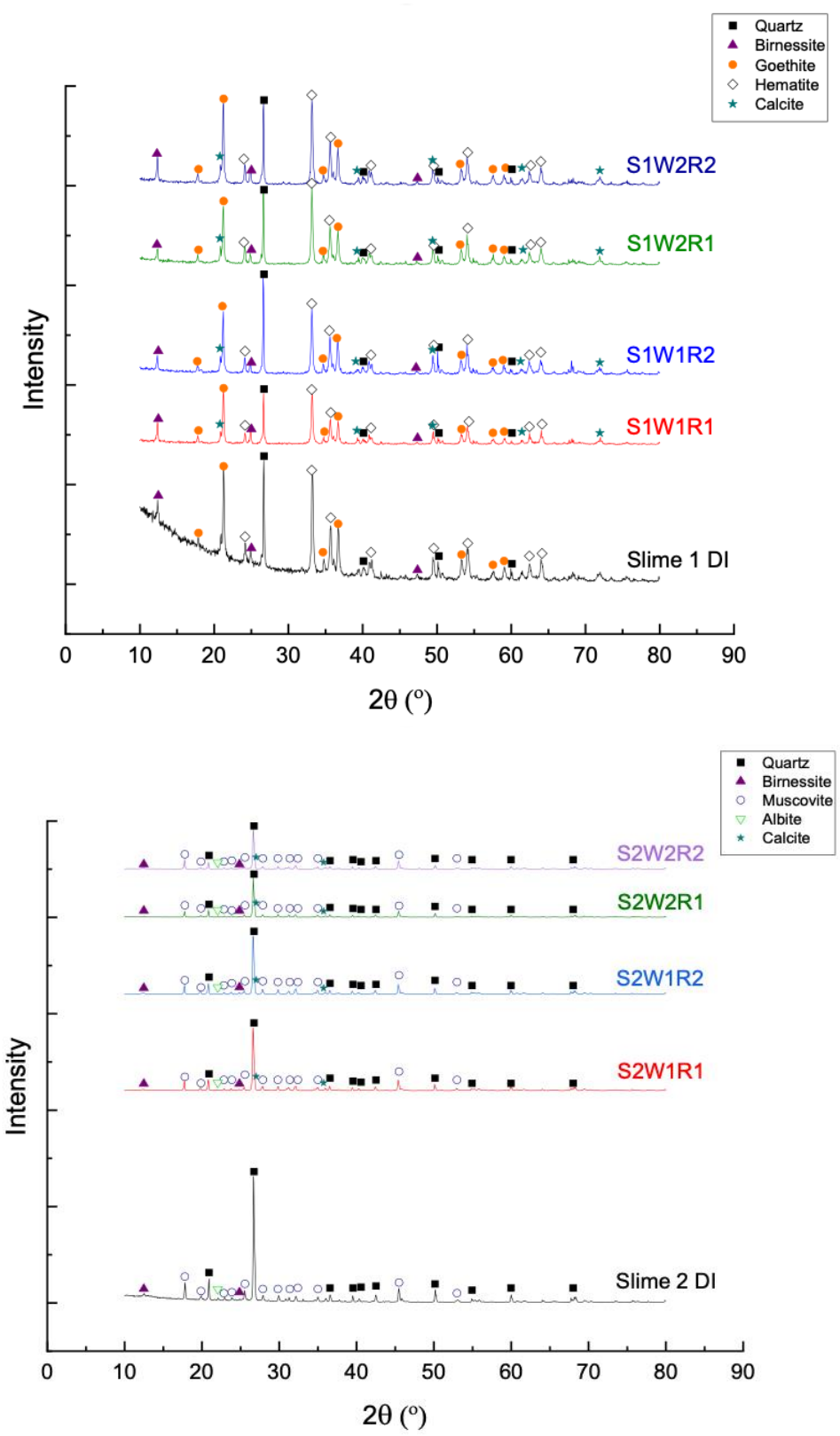

Figure 3.5 XRD results of treated slime samples indicating calcite for both Slime 1 and 2.

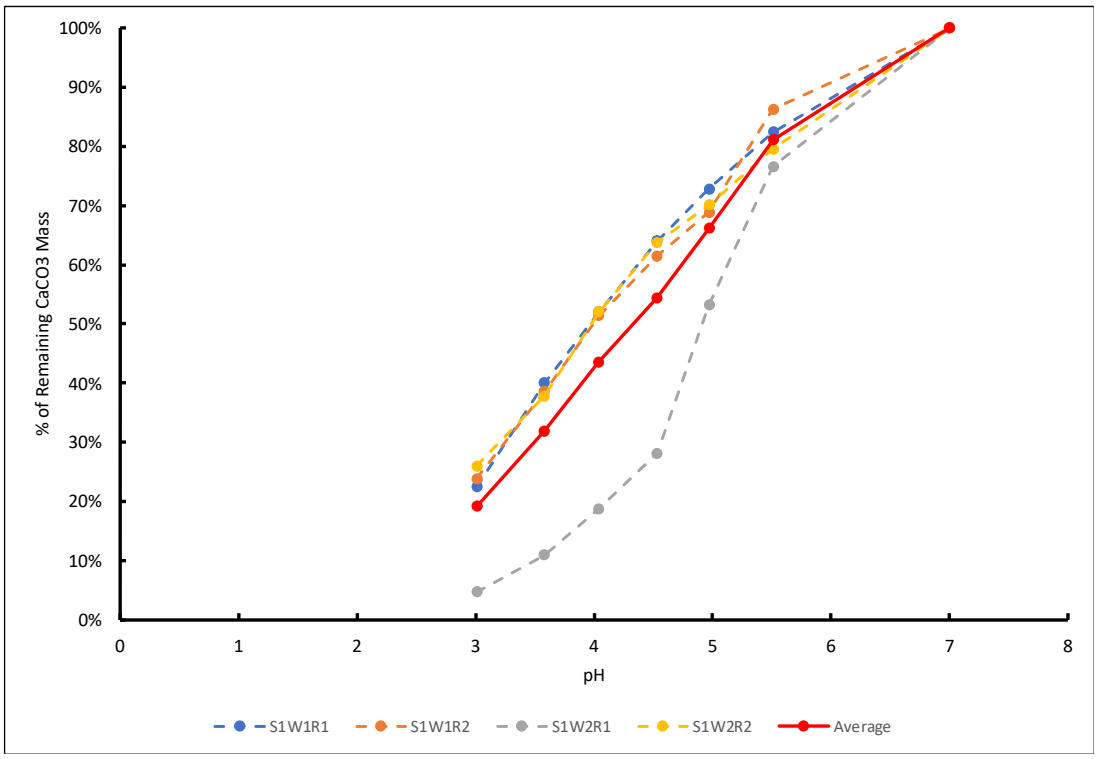

Figure 3.6 Remaining % of original $CaCO_3$ Mass for Slime 1 samples, including average.

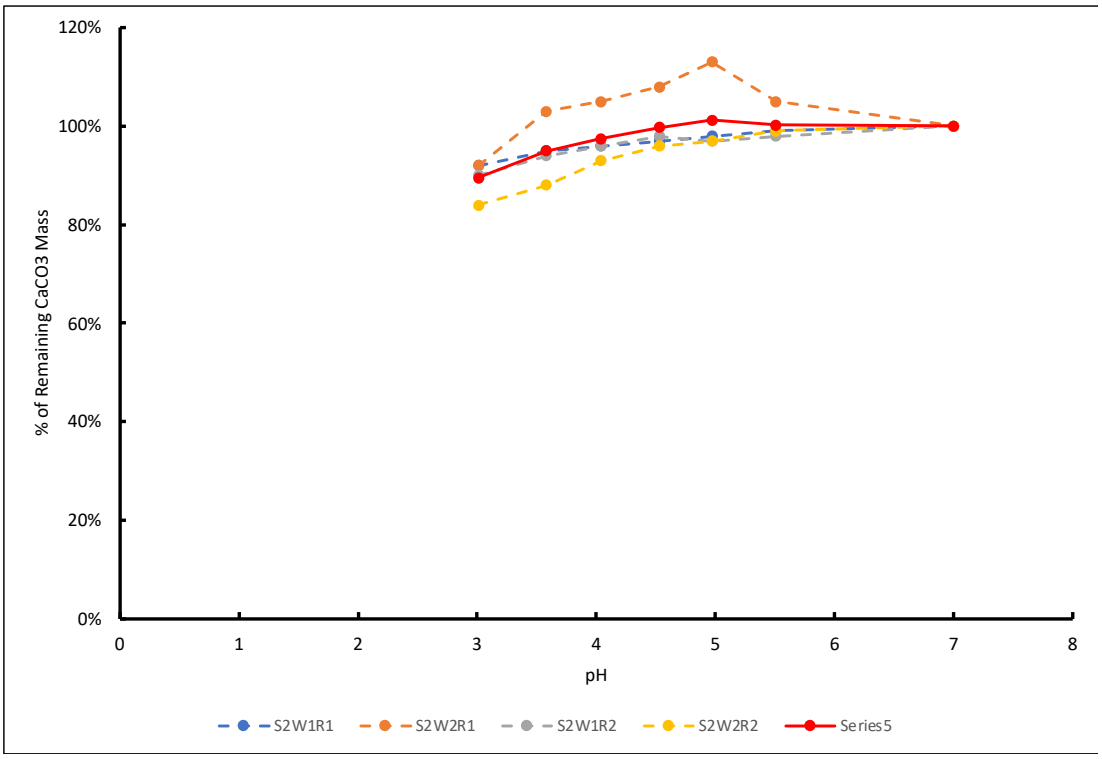

Figure 3.7 Remaining % of original CaCO3 Mass for Slime 2 samples, including average.

Chapter 4 The Ability of Microbial Induced Carbonate Precipitation to Stabilize High Water-Content Tailings

4.1 Objectives

Following the results from Chapter 3, applicability of MICP with the mine tailings at water contents consistent with field conditions was examined. The goal of this testing procedure was to treat samples at water contents that were more representative of field conditions during mining ore processing. Following guidance from NewFields (the sponsors), 150% and 80% water contents for the Slimes and Sands, respectively, were chosen as water contents at which the tests would be performed.

4.2 Materials and Methods

4.2.1 Coarse Grained Materials

The materials used in this testing originated from the same mining complex as Slime 1 and 2. However, a second set of samples taken from the sandy fraction during the mining processing (see Chapter 2) were compared to the materials taken from the fine fraction during processing, Slime 1 and 2. Although these sandy materials were labeled as “Sand 1” and “Dry 2”, for consistency throughout this thesis, they will be referred to as “Silt 1” and “Silt 2”, respectively. Their geochemical and mineralogical make up are identical in that both are predominantly quartz. The iron mine tailings (Slime 1 and Silt 1) contain hematite, and goethite and birnessite, while the gold mine tailings (Slime 2 and Silt 2) contain muscovite, birnessite and albite (see Chapter 2 for XRD analysis).

Similar to Slimes 1 and 2, water contents, using ASTM D2216, of the natural sand tailing samples were tested upon arrival. Both sandy tailings particle size distribution and specific gravity were measured and examined using the appropriate ASTM standard- ASTM D6913,

ASTM D7928 and ASTM D8543. A summary of those test results can be found in Table ***4.1*** and Figure **4.1**, and is compared to results from their fine grained counterparts, Slimes 1 and 2. Silt 1 and 2 both have similar sand (>.075mm), silt (.002-.075mm), and clay (<.002mm) fractions. Though their grain size distributions are similar, Silt 1 has a coefficient of curvature (C_c) and uniformity coefficient (C_u) of 1.1 and 7.4, whereas Silt 2 has values of 1.6 and 14.4, respectively. Slime 2 and Silt 2 have similar specific gravities of 2.85 and 2.69 respectively, whereas Slime 1 and Silt 1 have significantly different specific gravities of 3.46 compared to 2.61. The iron mine tailings specific gravities are consistent with those of metal tailings but much higher than those of natural soils, whereas the gold tailings values are smaller than those of the iron tailings but slightly larger than those of natural soils (Hu et al, 2017).

One note the author would like to make regarding the separation of these two materials; when comparing their grain size distribution, it can be noted that the differences between the two sets of materials is not as significant as expected. Slime 1 is in fact coarser than the Silt 1 from the same mine ore, whereas Slime 2 is finer than Silt 2. Contrary to these results though, the materials were tested and considered as presented by the mines as slimes and coarse grained materials, as they were collected at different times in the mining process, even though their physical characteristics would suggest otherwise.

4.2.2 Methods of High Water Content Testing

To more similarly simulate field conditions, a testing method utilizing both the self-weight consolidation column tests and Fall Cone Test (FCT) were combined into 1 continuous test. Glass cylinders, as shown in Figure **4.2**, were filled with the slurried materials at high water contents, and after 7 days of observation, the effluent water was removed to allow for FCT to proceed. The glass cylinders were compliant with ISO 17892-6:2017, which stipulates that the

testing apparatus must consist of a cup "with a diameter greater than 55 mm and depth of at least 30 mm" (ISO 17892). Similar to testing outlined in Chapter 3, the same 3 testing groups were utilized for this testing procedure- Set 1- Control; Set 2- Chemical additives/ingredients ($CaCl_2$, Urea); Set 3- MICP treated, with 2 duplicates for each group and material combination. Concentrations of $CaCl_2$ and Urea solutions were 100 mM and 333 mM respectively, and *S. pasteurii* (ATCC 11859) was cultivated and centrifuged via the same method as mentioned in Chapter 3 (Liu and Montoya, 2020). Mixing of the samples was done via a blender while adding the corresponding solutions, and then the slurry was poured into the glass cylinders to allow for self-weight consolidation for 7 days. Periodic pictures were taken to see the rate of consolidation over the course of 7 day period, and in between photos, samples were stored in incubator to promote bacteria activity for the MICP treated samples. Lastly, the glass cylinders were capped throughout the self-weight consolidation process and were replaced once transferring of supernatant or periodic FCT was complete. The mass of the system was monitored throughout to account for any changes in evaporation that could affect the shear strength measurements. Additionally, after the tests were completed, mass of calcium carbonate was determined in the same modified gasometric method as described in 3.2.4.

4.3 Results

4.3.1 Sedimentation and Precipitation Results

As can be seen in the photos taken at the beginning and at the end of the test in Figure ***4.3***, the results of this set of experiments differ from the findings in 3.3.1. The sedimentation column heights are summarized in Table **4.2** for the average of the samples from each group. From the table and visually from the photos, we can see that the Set 3 samples, across all 4 materials, have the highest sedimentation column height of the three groups. This seemingly contradicts the

results from Chapter 3, as we would expect Set 3 columns with MICP ingredients + *S. pasteurii* to show increasing levels of flocculation and evidence of calcium carbonate precipitation as compared to Sets 1 and 2. However, during the 7 day period of consolidation, an abnormal behavior was noticed in all of the Set 3 samples. A stiff upper layer, as shown in Figure ***4.4***, developed early in the testing period. By day 2, this stiff upper layer was visibly noticeable and created a significant layer of extruded water that was trapped between the top of the consolidated soil column and the precipitated crust. Through these pictures, it is inferred that the stiff crust prevented further consolidated and extrusion of pore water for the Set 3-MICP samples, which would explain the overall lack of decreased sedimentation height. This stiff crust is theorized to have formed due to the small specimen size and boundary conditions from the glass container. As seen in Table ***4.3***, results from acid washing of Set 3 samples indicated increased levels of $CaCO_3$ content (%) for all samples. Specimens were sampled in the top half and bottom half for characterization of $CaCO_3$ with specimen depth, and the top half of all samples were consistently higher than the bottom half, varying from 2.1 to 6.4 times. Additionally, samples of the stiff crust were acid washed and indicated that the upper layer, that prevented expected dewatering and consolidation to occur, contained 53.5-54.9% calcium carbonate precipitate.

Despite the results regarding the Set 3 samples, results from Sets 1 and 2 aligned with expectations and results from Chapter 3 for the same sets. As previously mentioned, from our understanding and assumptions that the Guoy-Chapman theory for the diffuse double layer (DDL), we anticipate that the Set 1 sedimentation height would be highest, as particles suspended in the DI water have the highest DDL thickness of the samples and the least attraction in particle-particle interactions (Mitchell and Soga, 2005). Set 2 which consisted of the slurries suspended with MICP ingredients (namely $CaCl_2$), introduced an electrolyte with valence 2,

which according to the theory, should show decreased soil thickness (i.e., more consolidated) as compared with Set 1.

For Slimes 1, Silt 2, and Slime 2 this holds true, as results summarized in Table **4.2** indicate that Set 2 sedimentation column height decreased as compared to Set 1. However this was not evident in Silt 1, which could be attributed to low quantity of clay minerals (Figure **4.1**) and therefore less reactive to the pore fluid. Finally, as expected, acid wash of samples from Sets 1 and 2 showed no indications of calcium carbonate due to lack of ureolytic activity to drive the MICP process.

4.3.2 Fall Cone Testing

Following ISO-17892, baseline measurements at varying water contents were conducted for both Silt 1 and Silt 2 and compared to their slime counterparts, which can be found in Figure ***4.5***. Once the consolidation period had concluded, the supernatant water was siphoned off in order to allow for fall cone testing (FCT) to be performed. Though initially prepared at higher water contents- 80% for the Silts and 150% for the Slimes- based on previous results presented in Chapter 3, water contents for these samples would need to decrease below 30% in order to get viable measurements using this method. The mass of each system and specimen had been carefully monitored throughout, and all removed water was weighed and the mass subtracted from the overall system. Using this method and avoiding the destructive method of ASTM D2216, a reasonable water content value could be obtained.

However, as mentioned in the previous section, the Set 3 MICP samples presented some limitations on the viability of the testing procedure. Since the stiff upper layer had formed and prevented more significant consolidation than expected, there was supernatant water that could not be removed from the system without breaking the upper crust. An initial fall cone test

measurement was attempted on all MICP samples of Slimes 1 and 2 and Silts 1 and 2 to test the strength of the stiff crust. However, each measurement broke through the crust and encountered the liquefied unconsolidated bottom portion of the soil column, which resulted in errored values for all samples. A birds-eye view down into the soil column after the initial, unsuccessful FCT measurement can be viewed in the photo in Figure **4.6**, where it can be noted the difference between the stiff upper layer and water layer below.

In order to continue testing the viability of the samples, the stiff upper layer was removed and set aside for acid wash testing. Then, samples were allowed to further consolidate for an additional time period of 2-3 days, and any supernatant water was siphoned off to allow for continued FCT. Results of FCT after removal of the stiff upper layer can be found in Figure **4.7**. The results indicate that Silt 1 showed significant increase in undrained shear strength, S_{ur}, from 4.86 to 5.46 times the estimated value from the baseline curve. Silt 2 did not show any improvement, as values were similar to their estimated shear strength of untreated samples; additionally water contents for silt 2 could not be reduced to fit within the previously tested range of 13 to 32%, despite the removal of the stiff upper layer and additional water. Results using the modified apparatus did not match previously identified trends for Slimes 1 and 2 as seen in Figure **4.7**. Similar to Silt 2, water contents could not be reduced to within the previously tested range of 20-30%. Samples of Slimes 1 and 2 in the modified apparatus were well above the materials respective liquid limits, as seen in Table **4.2**, and therefore showed little to no shear strength.

4.3.3 Mass of Calcium Carbonate

As previously mentioned, mass of calcium carbonate was determined using a modified gasometric method based on ASTM 4373. Samples from each of the groups was tested in the top

and bottom half to get a representative calcium carbonate content estimate. In addition, the stiff upper layer that developed for each of the MICP treated samples was tested to determine calcium carbonate content. The results are also summarized in Table ***4.3***.

4.4 Conclusions and Limitations

For 1 group of samples using the modified testing apparatus, shear strength increases of up to 540% were demonstrated on MICP treated samples of materials from the same iron and gold mines as Slimes 1 and 2. For the Silt 1 samples, fall cone testing indicated that MICP provided significant strength increase from apparent $CaCO_3$ precipitation as evidenced by acid washing. However, samples of Slimes 1 and 2 and Silt 2 showed a lack of increase in shear strength or fabric change expected with levels of cementation confirmed with acid washing results. Limitations of boundary conditions of the glass cylinder seemingly inhibited homogenous calcium carbonate precipitation within the particle-particle contacts, and instead precipitated calcium carbonate at the water-soil interface. This preferential precipitation formed a stiff upper crust which hindered consolidation and caused high water contents and low to non-value measurements of shear strength. While acid washing indicated that precipitation was present in portions of the soil column, the lack of change in fabric associated with MICP treated samples, in addition to the consolidation and sedimentation behavior, suggests that this method of MICP treatment of the mine tailings did not have the intended effect of demonstrating the viability at field scale. Future work with finer grained materials such as these, with low permeability, may look to incorporate testing at a larger scale to reduce any potential boundary effects on the location of precipitation.

References

ASTM. (2010). “D2216 Standard Test Methods for Laboratory Determination of Water (Moisture) Content of Soil and Rock by Mass”. ASTM International, West Conshohocken, PA.

ASTM. (2014). “D854 Standard Test Methods for Specific Gravity of Soil Solids by Water Pycnometer”. ASTM International, West Conshohocken, PA.

ASTM (2014). “D4373 Standard Test Method for Rapid Determination of Carbonate Content of Soils”. ASTM International, West Conshohocken, PA

ASTM (2017b.) “D6913 Standard Test Methods for Particle-Size Distribution (Gradation) of Soils Using Sieve Analysis”. ASTM International, West Conshohocken, PA.

ASTM (2017c). “D7928 Standard Test Method for Particle-Size Distribution (Gradation) of Fine-Grained Soils Using the Sedimentation (Hydrometer) Analysis”. ASTM International, West Conshohocken, PA

ISO. (2017). “ISO 17892-6:2017- Geotechnical investigation and testing - Laboratory testing of soil - Part 6: Fall cone test”. Geneva, Switzerland.

Hu, L., Wu, H., Zhang, L., Zhang, P., and Wen, Q. 2017. Geotechnical proper- ties of mine tailings. Journal of Materials in Civil Engineering, 29(2): 04016220. doi:10.1061/(ASCE)MT.1943-5533.0001736.

Mitchell, J. K., and Soga, K. (2005). *Fundamentals of soil behavior, 3rd ed*. Wiley, Hoboken, NJ.

Table 4.1 Physical Properties of Slime and Silt Samples.

Property	Test Results			
	Slime 1	Slime 2	Silt 1	Silt 2
Water Content (%)	26.24	26.23	8.7	14.3
Liquid Limit (%)	26.8	27.8	25.5	40
Specific Gravity	3.46	2.61	2.85	2.69
Sand Content (%)	42.5	20.6	36.7	36.6
Silt Content (%)	52.7	77.3	62.2	62.2
Clay Content (%)	4.8	2.1	1.1	1.2
D50 (mm)	0.07	0.04	0.05	0.05
C_c	1.08	4.62	1.10	1.60
C_u	26.33	10	7.4	14.4

Table 4.2 Soil column height for modified high water content FCT-sedimentation tests.

Material	Group No.	Height (in.)
Slime 1	Group 1	1.45
	Group 2	1.43
	Group 3	1.78
Silt 1	Group 1	1.23
	Group 2	1.19
	Group 3	1.35
Slime 2	Group 1	1.55
	Group 2	1.44
	Group 3	1.65
Silt 2	Group 1	1.48
	Group 2	1.61
	Group 3	2.00

Table 4.3 Calcium Carbonate content for high water content tests, including control values.

Material	Location	CaCO3 Content (%)
Slime 1	Top	1.44
	Bottom	0.68
Slime 2	Top	0.85
	Bottom	0.35
Silt 2	Top	0.80
	Bottom	0.34
Silt 1	Top	1.57
	Bottom	0.25
Slime 1-1 MICP Stiff Upper Layer		54.85
Silt 1-1 MICP Stiff Upper Layer		53.49
Control		
Material		CaCO3 Content (%)
Silt 1		0.04%
Silt 2		0.09%

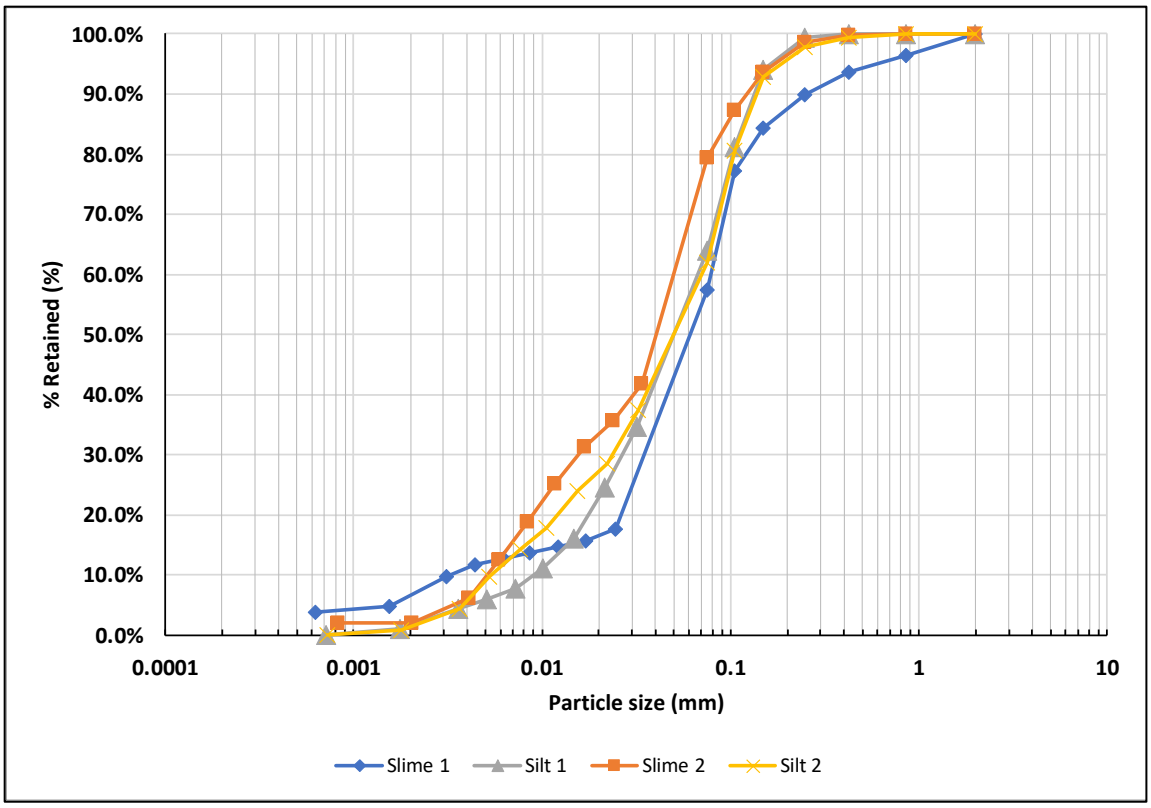

Figure 4.1 Grain size distribution for all 4 materials- Slimes 1 and 2 & Silts 1 and 2.

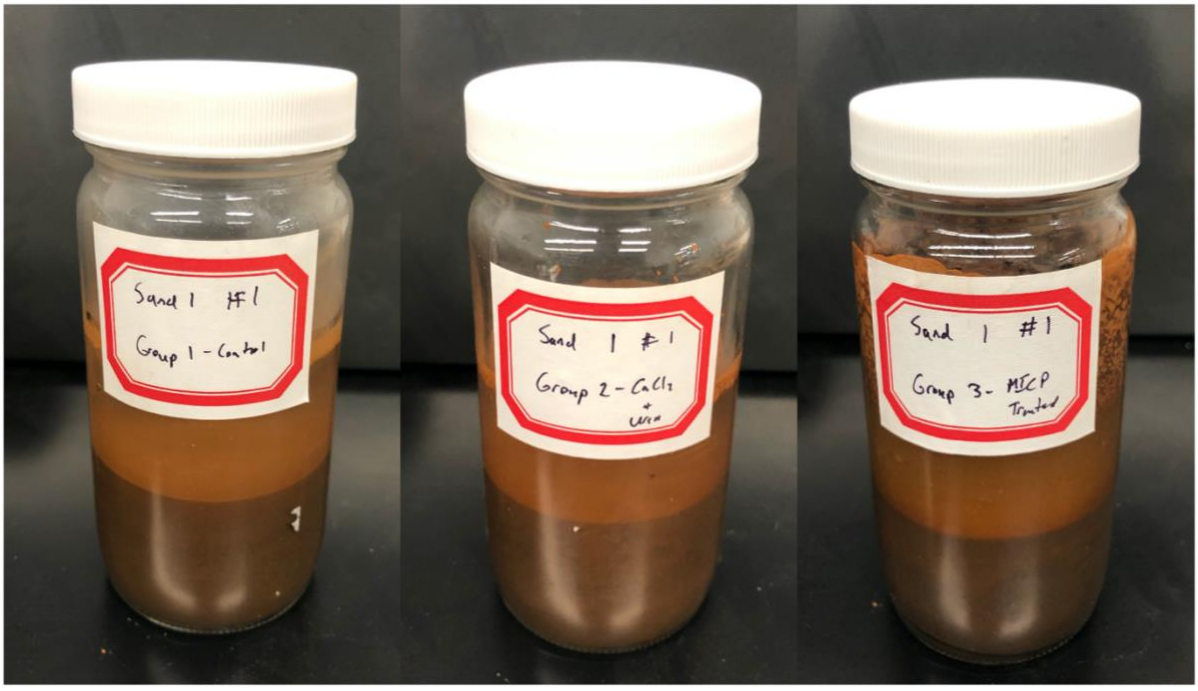

Figure 4.2 Modified high water content testing container to allow visualization of sedimentation behavior and periodic fall cone testing measurements once consolidation is complete.

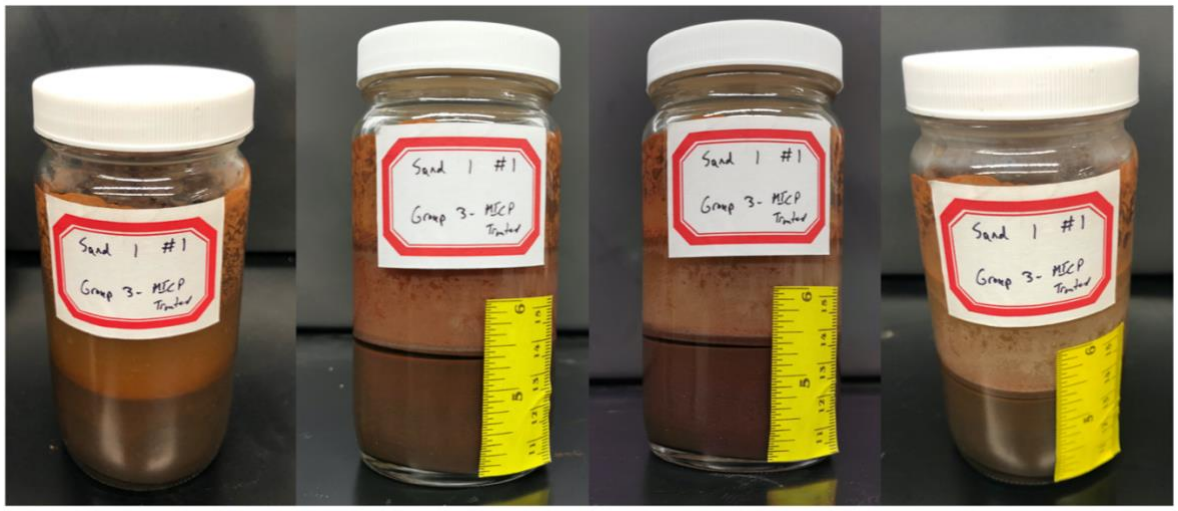

Figure 4.3 Pictures of modified self-consolidation-fall cone column tests from beginning of trial (day 0, left) to end of trial (day 7, right). Photos were also taken on days 2 and 5.

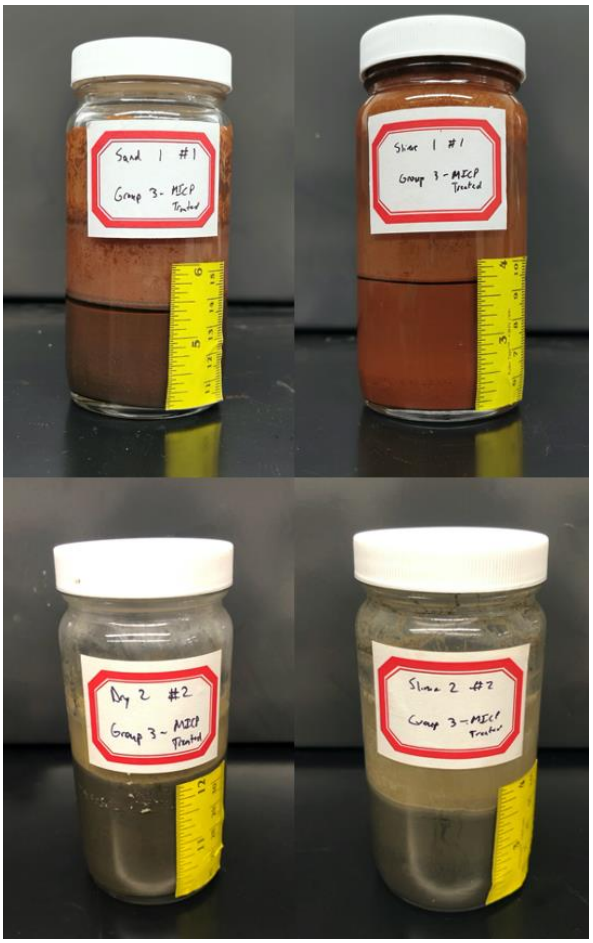

Figure 4.4 MICP treated samples in modified column-FCT tests that developed stiff upper layer that inhibited consolidation and dewatering.

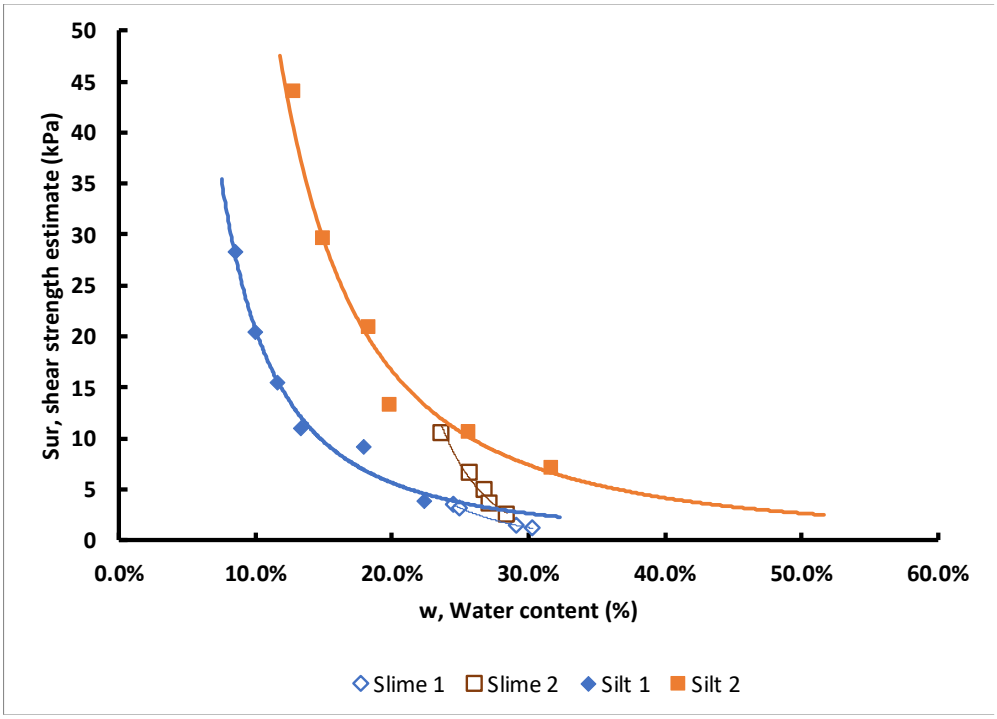

Figure 4.5 Untreated undrained shear strength estimates from Fall Cone Tests for both Slimes and both Silts at varying water contents.

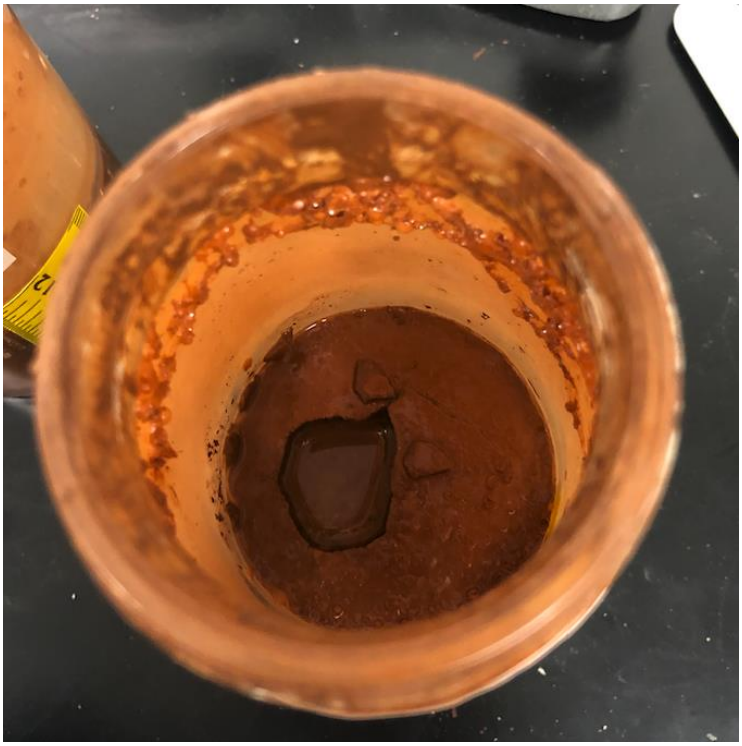

Figure 4.6 Top down view of FCT measurement of modified column test with stiff upper layer present, showing impact crater where cone broke through precipitate into soft soil.

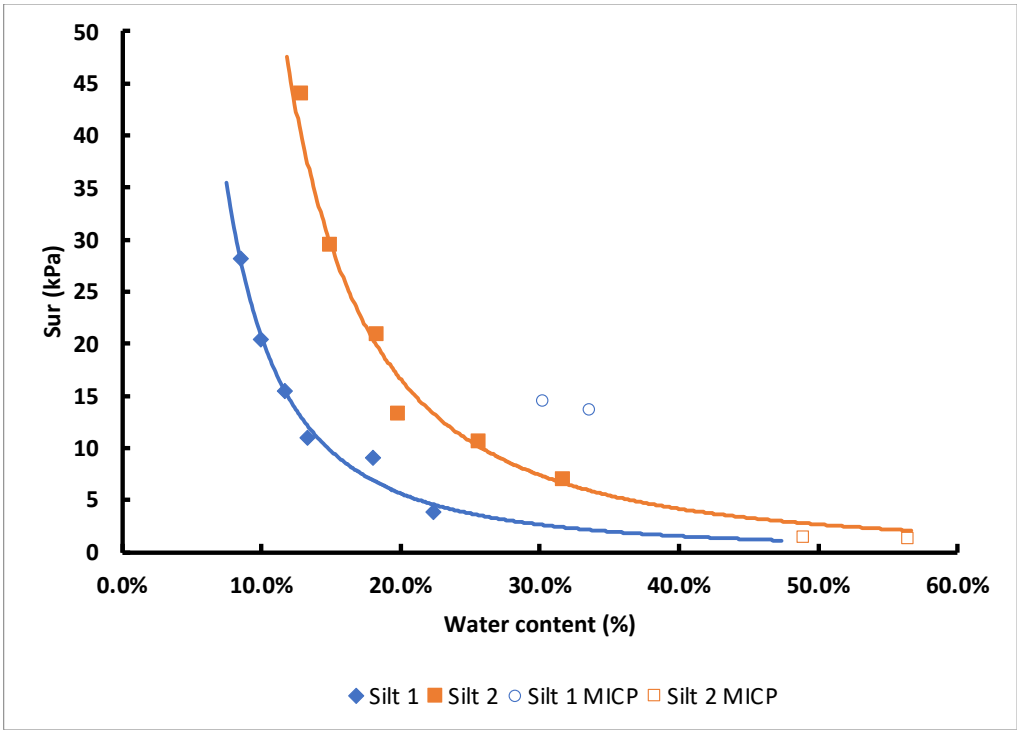

Figure 4.7 Undrained shear strength behavior from FCT for MICP treated Silts via modified column testing.

Chapter 5 The Effect of Microbial Induced Carbonate Precipitation on the Undrained Shear Strength of Silty Mine Tailings

5.1 Introduction

Due to the nature of their processing and deposition, as described in Chapter 2, these mine tailings are often susceptible to static liquefaction triggering. These fine-grained mine tailing soils, the silts and slimes examined in this thesis, negatively affect the overall performance of tailings impoundments and dams, and have previously contributed to catastrophic failures of these structures. These failures have had damaging economic and environmental effects to the surrounding communities and ecosystems impacted by the vast quantity of stored mine waste released during a failure. Such failures are often caused by changes in effective stress, lateral deformation, and liquefaction of the loose silt and slime tailings (Fotovvat and Sadrekarimi 2022). The loose state of mine tailings material results in their higher susceptibility to liquefaction, and static liquefaction of mine tailings material is one of the major causes of failure, in which the material behaves like a liquid under applied stresses (Xu and Wang, 2015, Davies, 2002, Fourie et al., 2001).

One note about the materials, ASTM (2016a) D4253 and ASTM (2016b) D4254 standard procedures for measuring the maximum and the minimum index densities of granular soils were not applicable for these tailings because of its high fines content (>15%). Additionally, ASTM D4254 and ASTM (2012) D1557, which are used to measure the maximum void ratios (e_{max}) and minimum void ratios (e_{min}), respectively, could not be performed due to the limited quantity of material provided for testing. As such, commonly used parameters to describe pre-shearing configurations like relative density (D_r) are unable to be utilized in this study.

5.2 Methods

5.2.1 Direct Simple Shear

The monotonic shearing behavior of the sandy tailings samples was investigated in this study using a direct simple shear (DSS) apparatus manufactured by Trautwein GeoTAC. Vertical and horizontal stress and displacement readings are collected throughout both consolidation and shearing stages. During an undrained DSS test, the specimen height is kept constant (i.e., maintaining a constant volume) and changes in pore water pressure are measured indirectly through the change in normal stress. The constant height and undrained test are comparable as previous studies show that the results are consistent (Dyvik et al. 1987).

The specimens were consolidated under 100 kPa of vertical stress and then sheared with a rate of 10% strain per hour recommended by Dahl (2010). The tests were stopped after the specimen had reached a minimum shear strain of 15%. In the DSS testing setup, the shear strain is the ratio of horizontal displacement at top of the specimen to its pre-shear height.

5.2.2 Sample Apparatus and Preparation Method

As shown in Figure **5.1**, a stack of thin Teflon-coated steel rings provides a rigid radial boundary for the specimen while allowing unrestricted movement during the shearing stage. When assembled, the lower acrylic end cap, the stacked rings, and the vacuum mold serve as the specimen preparation mold. The internal circumference of the specimen is lined with a latex membrane, which is secured to the top and the bottom end caps by O-rings.

5.2.3 Sample Preparation Method

With fine grained materials such as these mine tailings, there are two preparation methods that can be used- slurry deposition and moist tamping. Specimens prepared by slurry deposition indicate tendencies of grain size segregation for well graded silty sands and often allow limited

control over the final consolidation density (Riveros and Sadrekarimi, 2020). Therefore, these DSS tests were conducted on specimens prepared by moist tamping method first outlined in Ladd 1978, in order to enhance specimen homogeneity and promote strain-softening and liquefaction behavior. Because of its ease of use and better control over the specimen's void ratio, moist-tamping has been used extensively for reconstituting tailings specimens for laboratory testing (Al-Tarhouni et al. 2011; Chen and van Zyl 1988; Fourie and Tshabalala 2005; Hu et al. 2017; Reid et al. 2018; Schnaid et al. 2013). The DSS specimens have a diameter of 66.8±0.2 mm and a height between 18-20 mm. The specimens are prepared to have a target pre-shear void ratio of 1.15±0.05 for Silt 1 and 1.2±0.05 for Silt 2. These ranges were determined based on previous test results of monotonic DSS testing of mine tailings with similar characteristics, notably grain size distribution (Riveros and Sadrekarimi, 2020). Differences in particle size and shape could explain the variations in void ratios between the Silt specimens, however these void ratios produced repeatable results. Thus the provided ranges of target void ratio were specified to obtain a loose configuration to facilitate strain softening behavior.

5.2.4 MICP Treatment Method

Sporosarcina pasteurii (American Type Culture Collection (ATCC 11859), Manassa, Virginia), a common alkalophilic soil bacterium with high urease activity, was used in this study to catalyze the biochemical reaction for calcium carbonate precipitation. The method of cultivation of *S. pasteurii* (ATCC 11859) suspension and incubation of the growth media followed previous studies (Zamani, 2017, Liu and Montoya, 2020). The ingredients were autoclaved individually and mixed after sterilization. The growth medium was inoculated with the *S. pasteurii* stock culture and incubated aerobically at 30°C in an incubator at a speed of 200 rpm for 40 hrs to reach an optical density (OD_{600}) of 0.8 to 1.2. Cultures were centrifuged at 4000g for 20 min in

15 ml volumes and replaced with fresh growth media. Harvested bacteria were stored in centrifuge vials at 4°C for a maximum of 14 days. Further details for preparing bacteria used in MICP treatments can be found in Mortensen et al. (2011).

A two-phase injection was implemented for the treatment of the Silt specimens, as presented in Table ***5.1***. A falling head injection procedure was used to treat the soil, where both the biological and cementation treatment solutions permeated through the soil from the bottom to the top of the specimen as shown in Figure **5.2**.

Through the first phase, in excess of two pore volumes (approximately 100 mL) of the inoculation treatment solution (Table ***5.1***) were injected into the specimen to inoculate the soil with bacteria. The inoculation treatment and bacteria were left for 6 hours to allow the bacteria to attach to soil particles. As presented in Table ***5.1***, the biological treatment media did not contain calcium chloride to ensure that cementation would not occur during this first injection.

The second phase consisted of a series of cementation media injections (Table ***5.1***). 100 mL of cementation treatment (>2 pore volumes) were injected in 6-6-12 h intervals. Shear wave velocity measurements were recorded for samples throughout the injection cycle. The number of injections varied depending upon the target level of cementation and soil type. Two cementation levels of Low and Moderate were chosen for the Silt materials, as previous studies have shown that increased resilience against liquefaction can occur at light to moderate levels of cementation corresponding to ~1-3% mass of carbonate (Darby, 2019). Previous studies have shown that light and moderate levels of cementation are attainable at 7 to 10 and 13 to 15 injections, respectively (Nafisi, 2019). The variation of these number was dependent on the soil type and confining pressure utilized during treatment. Therefore, for these silt materials, 9 and 18 injections were chosen for the light and moderate levels of cementation, respectively. All specimens were treated

in the same temperature (about 22°C) to prevent any possible temperature effects on the precipitation process and bacteria activity (Sun et al. 2019).

During injection, the pH of the effluent was measured in each cementation treatment to directly monitor the bacterial activity during treatment. Based on the recipe used in the current study (Table ***5.1***) a pH value of 9 or higher would indicate that the pore fluid is alkaline and that bacteria are hydrolyzing the urea. Bio-dosing, or the process by which a small amount of bacteria suspension (~3.75ml per 100 mL of treatment media) is injected into the specimen along with the cementation treatments, promotes additional bacterial activity (Martinez 2012). Bio dosing intervals of once every fourth injection were determined based on previous guidance and results from other studies (Nafisi et al. 2020). Once the target number of injections was reached, ten pore volumes of water were flushed through the specimen to stop the cementation process and remove excess salts and other reagents.

The treatment of 8 samples was performed while the specimens were under ~10 kPa of vertical stress. Names for samples from each of the Silt 1 and 2, both untreated and treated at each cementation level, can be found in Table **5.2**. Duplicates of each combination, for repeatability, were prepared in accordance with the previously mentioned sample preparation.

5.2.5 Shear Wave Velocity Measurements

Shear wave velocity (Vs) measurements were performed to track the cementation progress while treating the samples. Bender elements had been previously assembled in the acrylic end caps as shown in Figure 5.3. These were assembled to perform the V_s measurements through the treatment process, and were measured on specimens that had working bender elements. Shear wave velocity (Vs) measurements were calculated using the known distance between bender elements embedded in top and bottom acrylic caps. The bender elements are typically prepared

to operate in the highly conductive environment during MICP treatment (Montoya et al. 2012). A 5-V, 100 Hz sine waves were generated by a function generator model Agilent 33522A, through the sending bender element, through the soil and receiving bender element, and were received by a digital oscilloscope model Agilent MSO6014A. The oscilloscope and wave generator are able to determine the travel time of the shear wave, and from the known distance we are able to calculate the V_s value. Bender elements are most efficient when the benders transmit the shear wave at its resonant frequency, which is dependent on the bender properties, the anchorage of the bender elements, and the shear wave velocity of the soil (Montoya et al, 2012). The travel time was determined by using the first crossover of the received signal, recommended by Lee and Santamarina (2005).

5.2.6 Mass of Calcium Carbonate Acid Washing

The same modified method previously mentioned and outlined in Chapter 3 was used to determine mass of calcium carbonate in these MICP treated sample. With the previously established relationship, samples of the silts can be tested to determine their $CaCO_3$ mass, for both untreated samples as a control group and for treated samples to determine the increase due to MICP. Treated specimens were sampled in multiple places to obtain a representative value for each.

5.3 Results and Discussion

5.3.1 General Instability

Instability refers to a general behavior in which large plastic strains are accumulated due to the inability of a soil element to sustain a given load or stress (Chu et al. 2003, Riveros and Sadrekarimi, 2020). Static liquefaction is considered as a special form of instability that occurs in a loose soil as a result of excess pore pressure generation induced by an undrained shear loading

prior to the stress state reaching failure (Chu et al. 2003). A loss of shear strength could follow the development of pore-water pressure or the reduction of effective stress (Terzaghi et al. 1996).

Results from previous studies on specimens tested in DSS devices suggest that failure in a DSS test occurs on a horizontal plane containing the maximum shear stress (Cole 1967; Roscoe 1970; Muir Wood et al. 1979), which is observed during shearing for these silt specimens as shown in Figure **5.4**. For the purposes of our discussion, this measured peak shear stress measured by the DSS device during testing will be interpreted as the undrained shear strength.

5.3.2 Undrained Shear Response of Untreated Silts

The undrained shear behavior of the untreated silts was assessed observing changes in shear strength (τ) and excess pore water pressure (Δu) with respect to shear strain (γ), as well as change in normalized shear stress (τ/σ'_{vc}) with normalized vertical stress (σ/σ'_{vc}). The untreated silt materials' stress strain and stress path behaviors of constant volume DSS tests can be seen in Figure **5.5**. For DSS testing a minimum shear strain of 15% was targeted as allowed to ensure specimens to fully develop their stress strain behavior (similar to Zamani and Montoya, 2018).

Strain-softening is evident in all untreated silt specimens, indicating the specimens are likely loose of critical. The strain-softening behavior observed in all the samples is followed by a weak strain-hardening behavior at large strains (γ > 10%–14%), which is typical of these liquefiable materials (Riveros and Sadrekarimi, 2020). The minimum undrained strength mobilized after yielding at large strains is referred to as the undrained post-liquefaction strength (S_u(residual)) (Stark et al, 1999). Baseline untreated specimens of Silt 1, prepared with moist tamping at e_0 =1.174 to 1.182 exhibited significant strain-softening behavior, with a S_u(yield) between 14.4 and 14.61 kPa occurring between 1-2.4% strain, and a S_u(residual) of 5.49 to 5.65 kPa. Meanwhile Silt 2, which was also prepared using the moist tamping method, but with

e_0=1.211 to 1.257, showed weak strain-softening behavior. Yield strength values for Silt 2 were 16.41 to 17.12 kPa between 2.5 and 3.9% strain, with residual strength of 13.56 to 14.25 kPa.

Both sets of undrained DSS tests can be seen in Figure **5.5**. Overall, Silt 2 had higher yield and residual strength as compared to Silt 1, which is consistent with the results from Chapter 3 and 4 with regards to the FCT tests conducted on untreated specimens of Slimes 1 and 2. Future SEM analyses may elucidate fabric differences between Silt 1 and Silt 2 and their slime counterparts that may provide insight into their untreated undrained shear behavior.

5.3.3 Undrained Shear Behavior of MICP Treated Silts

Shear wave velocity was measured throughout treatment to monitor the cementation process in real time. Figure **5.6** shows the trend of increasing shear wave velocity for all samples measured. Due to time constraints, the treatment and testing plan was started with working benders on 6 of the 8 specimens, at least 1 on each group (S1-Low, S2-Mod, etc.). However, 2 stopped working once specimens were prepared, and 1 stopped receiving and/or transmitting a signal after the 2nd injection.

Additionally, during the treatment schedule, minor revisions to the injection volume for Injection #'s 8 and 9 were required for 2 samples. With changes to the void ratio through cementation and effects to the permeability of samples, 2 of the Silt 2 Moderate specimens only allowed 80 mL of cementation solution into the sample over the course of 3+ hours, and for the sake of consistent treatment durations, the volumes were shortened. A summary of the planned volumes can be found in Table ***5.3***, while the actual injection volumes for all samples can be found in Table ***5.4***.

Differences in properties of MICP treated Silt specimens were examined using shear wave velocity measurements, mass of calcium carbonate via acid washing, and undrained shear

strength, both yield and residual. Before treatment and shearing, the untreated void ratio of each specimen was calculated accounting for the mass of water added due to moist tamping.

The undrained shear strength and normal stress at yield, yield friction angle (ϕ'_{yield}), and maximum (yield) normalized shear stress $(\tau/\sigma'_{vc})_{max}$ for both MICP treated and untreated silt specimens at different cementation levels is presented in Table **5.5**, and can be viewed in the shear response curves in Figure **5.7** and Figure **5.8**. Additionally, the differences in maximum normalized shear strength at yield between treated and untreated specimens can be seen in Table ***5.6***. These results show improvement in the shear response for all specimens, and the extent of improvement is higher for both Silts at the moderate level of cementation compared to the low level of cementation.

All treated Silt 1 specimens display progressive initial mobilization of undrained strength S_u, up to S_u(yield), after which instability and strength loss occur until S_u(liq) is reached as shown in Figure **5.9**. The MICP-treated samples exhibit both steeper mobilizations of shear strength (i.e., a stiffer response) up to S_u(yield) and higher S_u(yield) values as compared to the original material. Additionally, as evident in Figure **5.7**, the significant strain softening behavior exhibited in the untreated Silt 1 samples, while still present in the treated samples, is significantly reduced, as shown by higher S_u(liq) values at high strain levels (>12-14%).

Silt 1-2M exhibited some odd behavior shortly after the peak or yield stress was reached. In Figure **5.7** (a) and (c), Silt 1-2M indicates higher dilatancy with increasing shear stress with decreasing vertical stress. This is often behavior seen with heterogeneous distribution of calcium carbonate occurring during shearing. However this is not quite what we see in Figure **5.7** (b), as as the pore pressures generated do not dissipate with increasing shear strain.

While treated Silt 2 did not exhibit the same behavior seen in Silt 1 in regards to stiffer initial shear response as compared to the untreated samples, the yield and residual shear stresses increased with increasing cementation level as shown in Figure **5.8**. Additionally, low levels of cementation increased the shear strain needed to reach residual shear stress after yielding, while providing a minor increase in yield shear stress. These increases in yield and residual shear strength can be attributed to calcium carbonate cementation and particle bonding in the treated samples.

The extent of improvement in shear strength as a result of MICP treatment is a function of the number of particle contacts, their contact area, change in relative density and the fabric governing the material's behavior (Zamani, 2017). The number of particle contacts highly influences the effectiveness of MICP since there is a general preference for precipitation at contact points. The number of contact points increases with decrease in void ratio (e) and increase in silt content. This behavior held true for Slime 1 as compared to Slime 2, as Slime 2 was finer and had higher untreated and treated undrained shear strength estimates (Figure **3.4**).

According to Table ***4.1***, Silt 1 and 2 have similar silt and clay fractions, however Silt 2 is slightly finer between particle sizes of .03 to .003 mm, as evidenced by their grain size distributions in Figure **4.1**. Though Silt 2 showed higher untreated and low cementation level shear strength as compared to Silt 1, the higher fine fraction between .03 and .003 did not lead to higher shear strength values for Silt 2 over Silt 1 for moderate levels of cementation. Further investigation via analytical method (i.e.- SEM imaging) are needed to confirm calcium carbonate precipitation location (e.g.- bonds between particle-particle contacts) and to understand the behavior that the fine fraction has on these treated silt materials. Additionally, XRD analysis of both the untreated and treated silt materials should be completed in order to: 1) ensure that the

components present in the Slimes and Silts are the same, and 2) confirm precipitation structure is metastable calcite or another polymorph of calcium carbonate.

The calcium carbonate content was measured using the gasometric acid washing technique previously described for all the treated specimens and can be seen in Table **5.5**. Calcium carbonate content was averaged between top and bottom of the sample, with 2 duplicates for each portion of the sample, to obtain a representative value for each specimen. The treated Silt 1 specimens reached low and moderate values of calcium carbonate content as theorized by the number of injections chosen in the treatment schedule. Silt 1 specimens treated at low levels of cementation with 9 injections showed calcium carbonate content of 1.34-1.56%. The moderate samples are a little less consistent, both within samples and within groups. Silt 1-1M was in the range as expected, close to 3%, but Silt 1-2M had a large discrepancy between the top half and bottom half of the sample, from 1.34% to 6.7%, respectively. This partially explains the behavior seen in the stress strain and stress path curve for this sample (Figure **5.7** (a) and (c)), as we saw increased dilatancy and behavior consistent with heterogeneous distribution of calcium carbonate.

Silt 2 samples treated at low cementation showed consistency of 1.34%-1.45% calcium carbonate content, however, the moderate levels of cementation were not as consistent, with 2-1M and Silt 2-2M showed 4.86% and 2.64%, respectively. Silt 2-2M had a greater discrepancy between the top and bottom halves, with carbonate contents of 2.9% and 2.38%, respectively.

Further work needs to examine the differences between the amount of calcium carbonate that precipitates on each of the tailings materials. Some possible reasons are that iron oxides present in the Slime 1 and Silt 1 could inhibit increased calcium carbonate precipitation, but the shape and size of the particles could allow for bonding between particles, leading to lower

calcium carbonate content but higher strength. On the other hand, the plate-like material of Silt 2, seen in SEM images, could cause difficulties with nucleation of calcium carbonate precipitation. Work completed by Lee and Burns, 2020, was unable to conclude whether the presence of iron oxides affected calcium carbonate precipitation, but were able to show that the cementation solutions injected were dissolving iron oxides into ferrous iron. Future and ongoing work will hopefully provide indications as to whether iron oxides affect MICP.

5.4 Conclusions

Silts typically show more unstable and liquefiable behavior compared to sands due to their differences in fabric and structure. In this study, MICP treatment is applied to silt materials to observe its effect on the monotonic shear response of the silt specimens. The improved strength and stiffness of the MICP-treated silt samples resulted from not only the effect of calcite cementation, but also from the reduced void ratio and densification of the sand fabric by the precipitated calcite grains. While cementation certainly affected the initial stiffness (V_S and G_{max}) of the specimens at small strains, the strong effect of densification was apparent from the consistent trends of $S_u(liq)/\sigma'_{vc}$ and yield the treated silts.

The results of this study indicate that applying MICP improved the liquefiable resistance of these silt mine tailings materials. According to the results, the MICP method is a viable method in improving the shear strength of the silt materials, indicating yield stress increase in low and moderate level cementations of 9.3% and 210% for Silt 1 and 2.3% and 19.4% for Silt 2, respectively. In addition, the post-liquefaction or residual shear strength response was improved for all samples- Silt 1 showed higher residual strength over the untreated samples, while Silt 2 reached residual strength at higher levels of strain over untreated samples.

References

Al-Tarhouni, M., Simms, P., and Sivathayalan, S. 2011. Cyclic behaviour of reconstituted and desiccated-rewet thickened gold tailings in simple shear. Canadian Geotechnical Journal, 48(7): 1044–1060. doi:10.1139/t11-022.

ASTM. 2007b. Standard D6528: Standard test method for consolidated undrained direct simple shear testing of cohesive soils. In Annual Book of ASTM Stand- ards. ASTM International, West Conshohocken, Pa.

Chen, H.W., and van Zyl, D.J.A. 1988. Shear strength and volume-change behavior of copper tailings under saturated conditions. In Hydraulic fill structures. Edited by D.J.A. Van Zyl and S.G. Vick. American Society of Civil Engineers (ASCE), New York, NY, pp. 430–451.

Chu, J., Wanatowski, D., Leong, W.K., Loke, W.L., and He, J. 2015. Instability of dilative sand. Geotechnical Research, 2(1): 35–48. doi:10.1680/gr.14.00015.

Darby, K. M., G. L. Hernandez, M. G. Gomez, J. T. DeJong, D. W. Wilson, and R. W. Boulanger, 2019. Centrifuge Model Testing of Liquefaction Mitigation via Microbially Induced Calcite Precipitation. Journal of Geotechnical and Geoenvironmental Engineering, 145(10): 2136– 2144

Dyvik, R., Berre, T., Lacasse, S. & Raddim, B., (1987), “Comparison of Truly Undrained and Constant Volume Direct Simple Shear Test”. Geotechnique 37, No. 1, 3-10.

Fourie, A.B., and Tshabalala, L. 2005. Initiation of static liquefaction and the role of K0 consolidation. Canadian Geotechnical Journal, 42(3): 892–906. doi:10.1139/t05-026.

Fotovvat, A.R., Sadrekarimi, A., 2022. Instability of a Gold Mine Tailings Subjected to Different Stress Paths. Journal of Geotechnical and Geoenvironmental Engineering, 148(5)

Hu, L., Wu, H., Zhang, L., Zhang, P., and Wen, Q. 2017. Geotechnical proper- ties of mine tailings. Journal of Materials in Civil Engineering, 29(2): 04016220. doi:10.1061/(ASCE)MT.1943-5533.0001736.

Idriss, I.M., and Boulanger, R.W. 2008. Soil liquefaction during earthquakes. Engineering Monographs on Miscellaneous Earthquake Engineering Topics. No. MNO-12. Earthquake Engineering Research Institute, San Francisco.

Ladd, R. S., "Preparing Test Specimens Using Undercompaction," Geotechnical Testing Journal, GTJODJ,Vol. 1, No. 1, March 1978, p. 16-23.

Lade, P.V. 1992. Static instability and liquefaction of loose fine sandy slopes. Journal of Geotechnical Engineering, 118(1): 51–71. doi:10.1061/(ASCE)0733- 9410(1992)118:1(51).

Lee, J. S., & Santamarina, J. C. (2005). Bender elements: performance and signal interpretation. Journal of geotechnical and geoenvironmental engineering, 131(9), 1063-1070

Lee, J., Burns, S., Coldwell, F., Ntarlagiannis, D., Ohan, J., and Saneiyan, S. Dissolution and Recrystallization of Iron Oxide during MICP. Geo-Congress 2020: Biogeotechnics

Martinez, B. C. (2012). "Experimental and numerical upscaling of MICP for soil improvement." Uni. of California, Davis, CA.

Mortensen, B. M., Haber, M. J., DeJong, J. T., Caslake, L. F., & Nelson, D. C. (2011). Effects of environmental factors on microbial induced calcium carbonate precipitation. *Journal of applied microbiology*, *111*(2), 338-349.

Montoya, B. M., Gerhard, R., DeJong, J. T., Wilson, D. W., Weil, M. H., Martinez, B. C., and Pederson, L. (2012). "Fabrication,Operation, and Health Monitoring of Bender Elements for Aggressive Environments." Geotechnical Testing Journal, 35(5), 1-15

Nafisi, A. 2019. Elucidating the failure behavior and bond mechanics of biocemented sands. Ph.D. thesis, North Carolina State University, Raleigh, N.C

Reid, D., Fanni, R., Koh, K., and Orea, I. 2018. Characterisation of a suba- queously deposited silt iron ore tailings. Géotechnique Letters, 8: 278– 283. doi:10.1680/jgele.18.00105.

Riveros, G.A, Sadrekarimi, A. Static liquefaction behaviour of gold mine tailings. Canadian Geotechnical Journal. 58(6): 889-901. https://doi.org/10.1139/cgj-2020-0209

Schnaid, F., Bedin, J., Viana da Fonseca, A.J.P., and de Moura Costa Filho, L. 2013. Stiffness and strength governing the static liquefaction of tailings. Journal of Geotechnical and Geoenvironmental Engineering, 139(12): 2136– 2144. doi:10.1061/(ASCE)GT.1943-5606.0000924.

Sladen, J.A., D'Hollander, R.D., and Krahn, J. 1985. The liquefaction of sands, a collapse surface approach. Canadian Geotechnical Journal, 22(4): 564– 578. doi:10.1139/t85-076.

Sun, X., Linchang Miao, Tong, T., and Wang, C. (2019). "Study of the effect of temperature on microbially induced carbonate precipitation." *Acta Geotechnica*, 14, 627–638.

Stark, T., Olson, S.M., Kramer, S.L., and Youd, T.L. 1997. Shear strength of liquefled soils. In Proceedings of the Workshop on Post-Liquefaction Shear Strength of Granular Soils, University of Illinois at Urbana-Champaign, Urbana, Illinois, 17–18 April 1997. National Science Foundation, p. 288.

Zamani, A., Montoya, B.M. (2018). "Undrained Monotonic Stress-Strain Behavior of Silty Sand Improved with Microbial Induced Cementation." *ASCE Journal of Geotechnical and Geoenvironmental Engineering*, 144(6).

Table 5.1 Chemical Recipe for MICP treatment of Silts 1 and 2.

Recipe component	Phase 1	Phase 2
	Inoculation Treatment Concentration	Cementation Treatment Concentration
Urea (mM)	333	333
$CaCl_2$ (mM)	-	100
S. Pasteurii	~10^7 cells/mL	-

Table 5.2 Naming convention for samples of Silt 1 and 2 and their cementation levels.

Cementation Level	Silt 1	Silt 2
Untreated	Silt 1-3u	Silt 2-2u
	Silt 1-4u	Silt 2-3u
Low	S1-1L	S2-1L
	S1-2L	S2-2L
Medium	S1-1M	S2-1M
	S1-2M	S2-2M

Table 5.3 Planned injection volumes for treatment of Low and Moderate cementation.

Cementation Level		Injection #	Injection Type	Volume (mL)
Low Cementation	**Moderate Cementation**	0	A	115
		1	B	100
		2	B	100
		3	B	100
		4	B*	103.75
		5	B	100
		6	B	100
		7	B	100
		8	B*	103.75
		9	B	100
		10	B	100
		11	B	100
		12	B*	103.75
		13	B	100
		14	B	100
		15	B	100
		16	B*	103.75
		17	B	100
		18	B	100
		19	WF	500

Table 5.4 Actual injection volumes for treatment of Low and Moderate cementation.

Low Cementation (All Samples)		
Injection #	Injection Type	Volume (mL)
0	A	115
1	B	100
2	B	100
3	B	100
4	B*	103.75
5	B	100
6	B	100
7	B	100
8	B*	103.75
9	B	100
10	WF	500

Moderate Cementation			
		S1-1M, S1-2M	S2-1M, S2-2M
Injection #	Injection Type	Volume (mL)	Volume (mL)
0	A	115	115
1	B	100	100
2	B	100	100
3	B	100	100
4	B*	103.75	103.75
5	B	100	100
6	B	100	100
7	B	100	100
8	B*	103.75	80^
9	B	100	80^
10	B	100	100
11	B	100	100
12	B*	103.75	103.75
13	B	100	100
14	B	100	100
15	B	100	100
16	B*	103.75	103.75
17	B	100	100
18	B	100	100
19	WF	500	500

A= Inoculation Solution (100 mL 333mM Urea+ 15 mL *S. Pasteurii*)
B= Cementation Solution (100 mL of 333mM Urea+ 100 mM $CaCl_2$
B*= Cementation Solution + Bio-dose (100 mL of 333mM Urea+ 100 mM $CaCl_2$+ 3.75 mL of *S. Pasteurii*)
WF= Water Flush and saturation at end of treatment and for DSS testing
^= S2-1 and S2-2M only allowed 80 mL of the proposed 100 mL of cementation solution

Table 5.5 Effect of MICP on shear strength behavior of Silts.

	Yield (Peak)				Liq (Residual)		e_0 (initial void ratio)	$CaCO_3$ Content (%)
Sample	S_u (kPa)	σ'_{vc} (kPa)	ϕ' (°)	S_u/σ'_{vc}	S_u (kPa)	S_u/σ'_{vc}		
Silt 1-3u	14.6	62.6	13.14	0.146	5.7	0.057	1.174	.04%
Silt 1-4u	14.4	60.9	13.30	0.144	5.5	0.055	1.182	.04%
Silt 1-1L	16.4	50.5	18.00	0.164	11.5	0.115	1.165	1.56%
Silt 1-2L	15.3	51.7	16.51	0.153	9.4	0.094	1.145	1.34%
Silt 1-1M	42.8	56.5	37.16	0.428	26.7	0.267	1.189	2.61%
Silt 1-2M	47.2	53.2	41.58	0.472	44.6	0.446	1.161	4.04%
Silt 2-2u	17.1	60.1	15.91	0.171	14.2	0.142	1.211	.09%
Silt 2-3u	16.4	62.9	14.63	0.164	13.5	0.135	1.257	.09%
Silt 2-1L	17.1	53.8	17.65	0.171	13.9	0.139	1.248	1.34%
Silt 2-2L	17.2	54.2	17.57	0.172	13.7	0.137	1.213	1.45%
Silt 2-1M	20.7	47.8	23.42	0.207	18.6	0.186	1.240	4.86%
Silt 2-2M	19.3	56.2	18.99	0.193	17.0	0.170	1.277	2.64%

Table 5.6 Effect of MICP on the maximum normalized shear strength at yield and residual of Silts.

	Yield			Residual (Liq)		
Sample Name	Untreated S_u/σ'_{vc}	Treated S_u/σ'_{vc}	Δ S_u/σ'_{vc}	Untreated S_u/σ'_{vc}	Treated S_u/σ'_{vc}	Δ S_u/σ'_{vc}
Silt 1-3u	0.146	-	-	0.057	-	-
Silt 1-4u	0.144	-	-	0.055	-	-
Silt 1-1L	-	0.164	0.019	-	0.115	0.059
Silt 1-2L	-	0.153	0.008	-	0.094	0.038
Silt 1-1M	-	0.428	0.283	-	0.267	0.211
Silt 1-2M	-	0.472	0.327	-	0.446	0.390
Silt 2-2u	0.171	-	-	0.142	-	-
Silt 2-3u	0.164	-	-	0.135	-	-
Silt 2-1L	-	0.171	0.003	-	0.139	0.000
Silt 2-2L	-	0.172	0.004	-	0.137	0.000
Silt 2-1M	-	0.207	0.039	-	0.186	0.048
Silt 2-2M	-	0.193	0.026	-	0.170	0.032

Figure 5.1 Sample preparation tools used in assembly of DSS specimens.

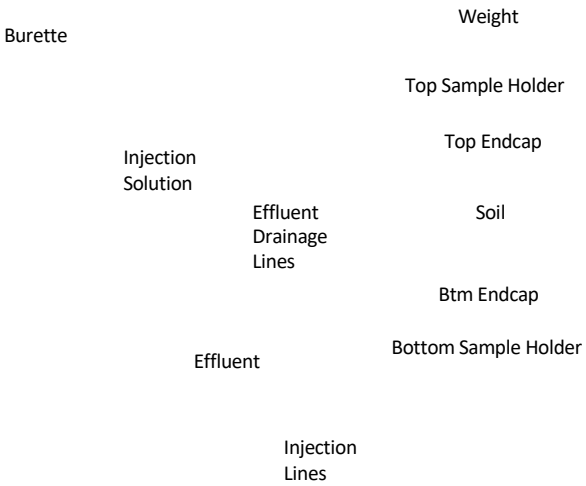

Figure 5.2 Photo and illustration of bottom-up injection setup for gravity drainage MICP treatment undergoing MICP treatment at 10 kPa confining pressure.

Figure 5.3 DSS end cap with bender element for shear wave velocity measurements.

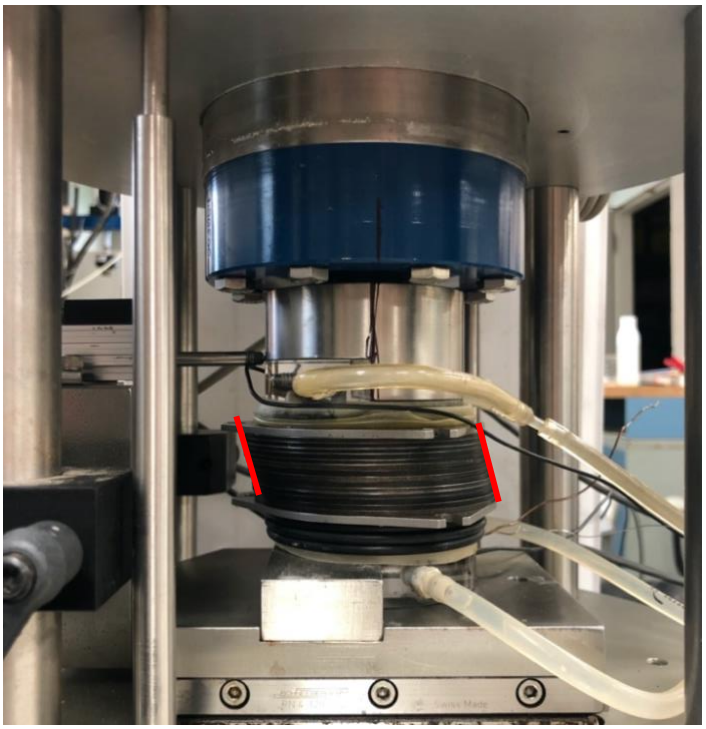

Figure 5.4 Example of specimen in DSS device during shearing with distinct failure plane developed along weakest plane of sample.

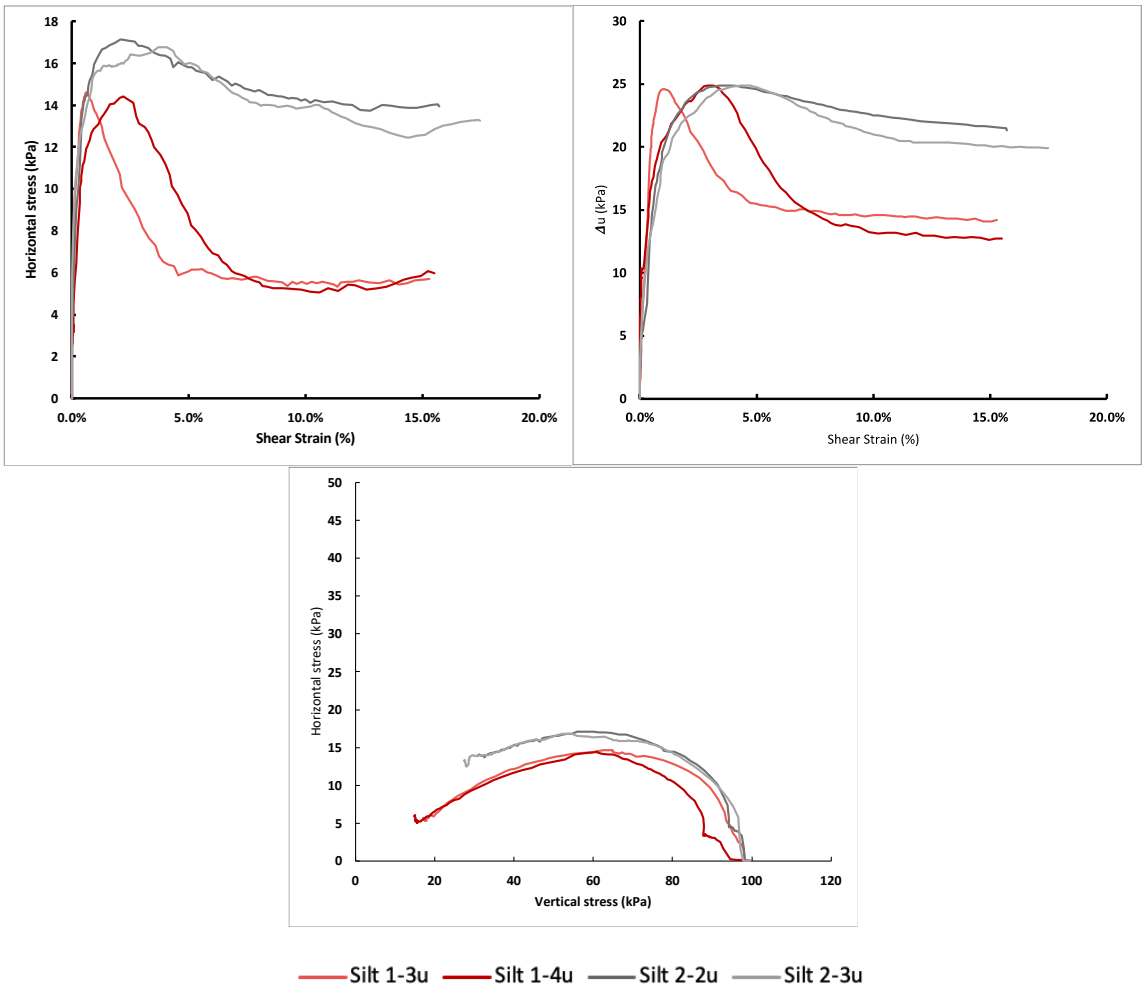

Figure 5.5 a) Stress–strain plots, b) change in pore water pressure, c) and stress paths of constant-volume DSS tests on moist-tamped, untreated Silt 1 and 2 specimens.

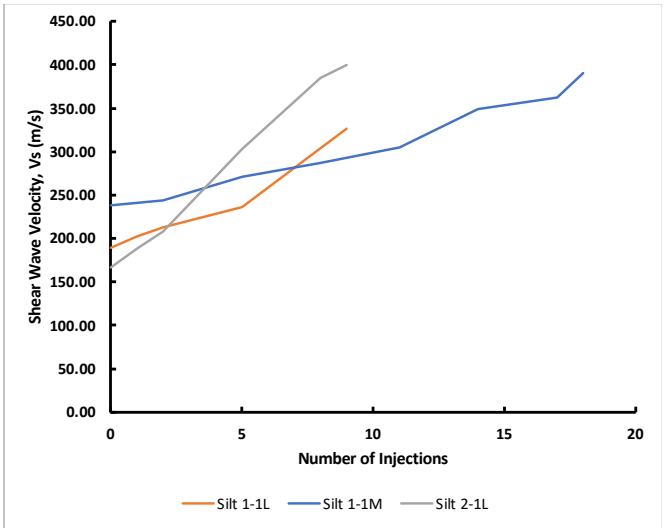

Figure 5.6 Increases of V_S after application of Low and Moderate levels of MICP treatment over the course 9 and 18 injections, respectively, for Silt 1 and 2 as measured by bender elements.

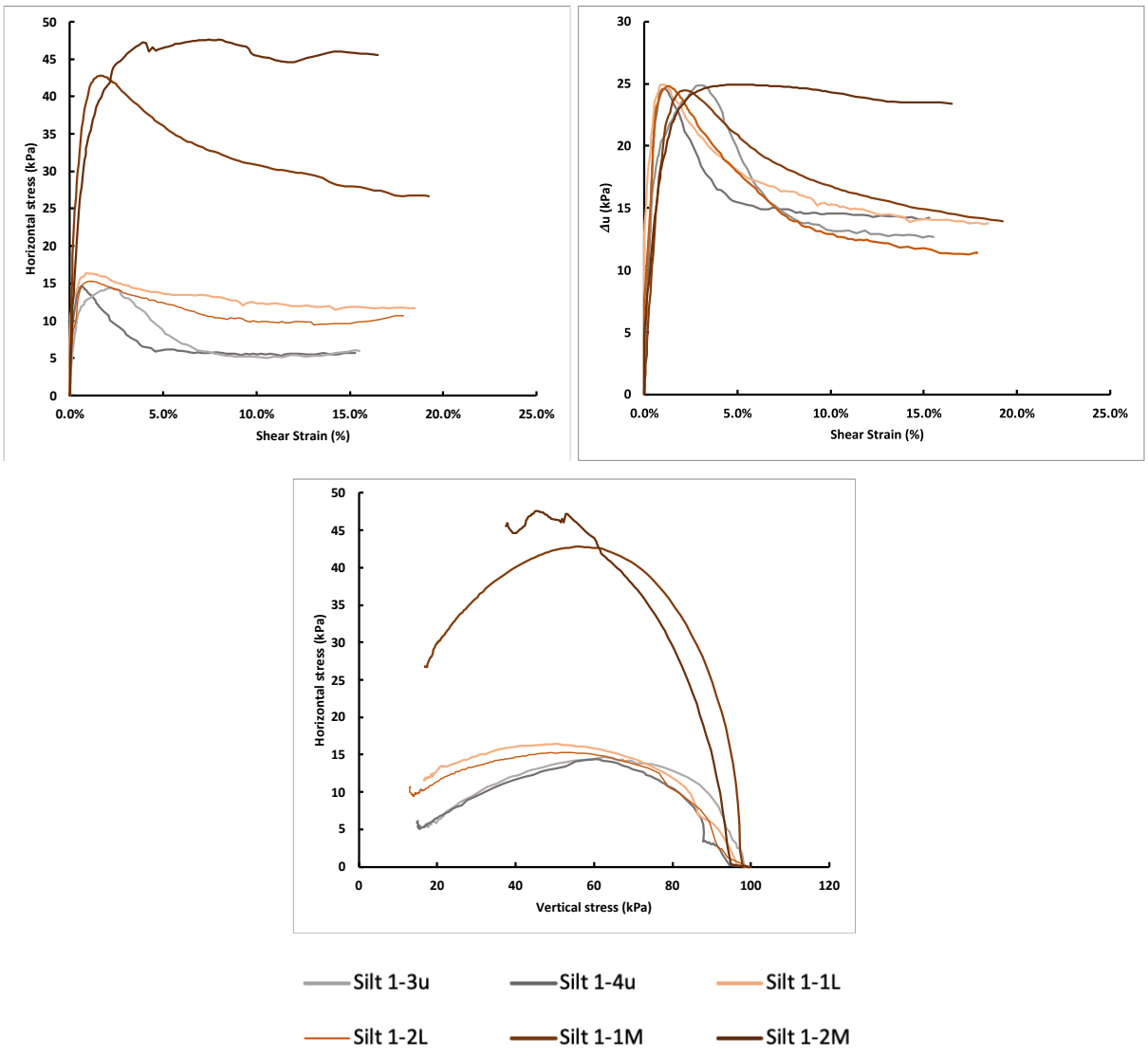

Figure 5.7 a) Stress–strain plots, b) change in pore water pressure, c) and stress paths of constant-volume DSS tests on moist-tamped, MICP-treated Silt 1.

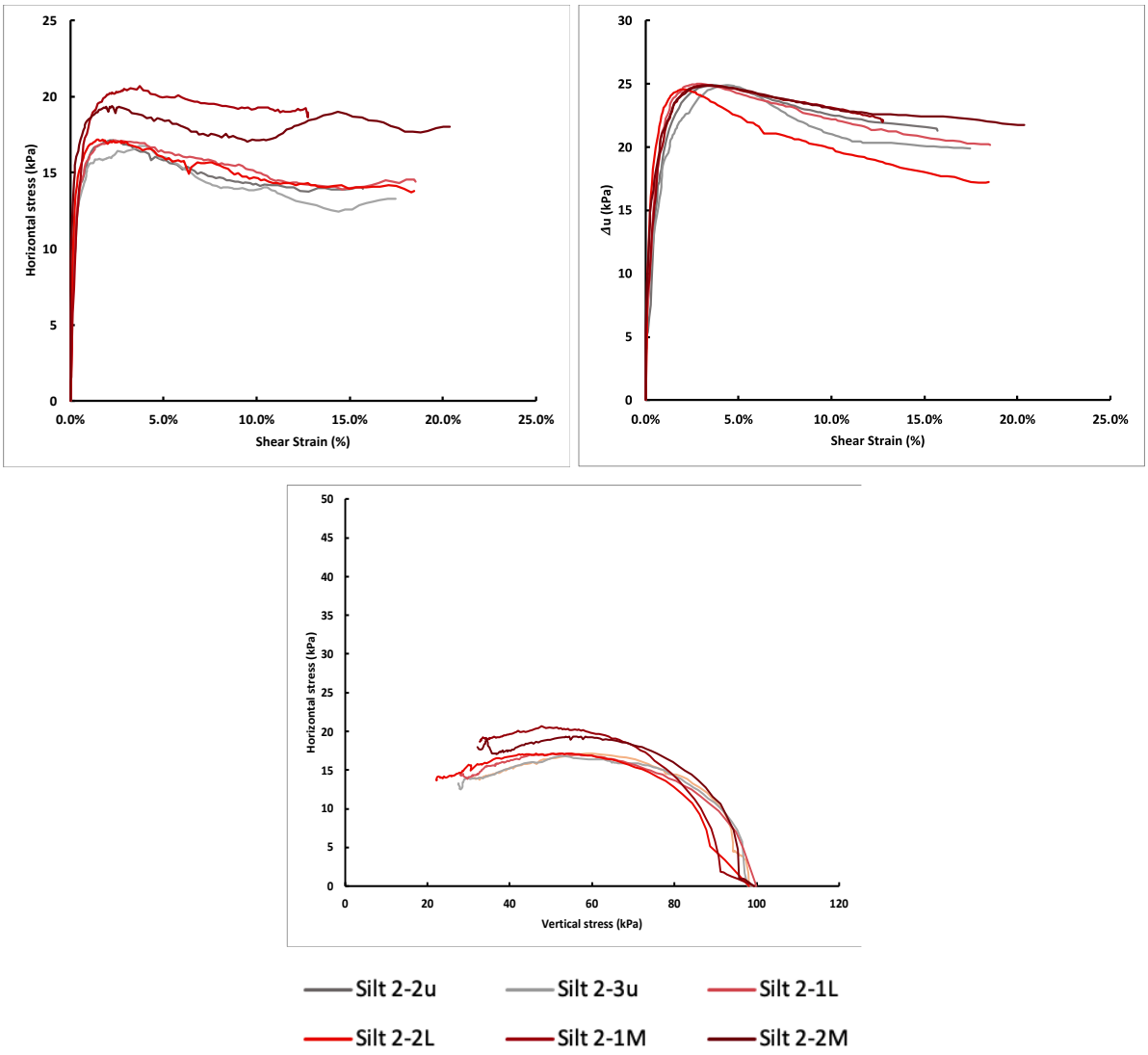

Figure 5.8 a) Stress–strain plots, b) change in pore water pressure, c) and stress paths of constant-volume DSS tests on moist-tamped, MICP-treated Silt 2.

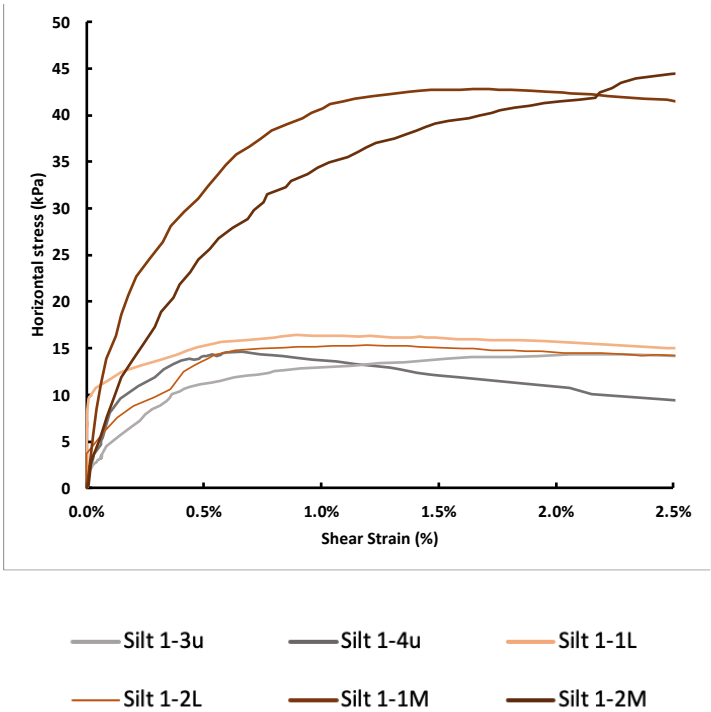

Figure 5.9 Early shear-strain behavior indicating higher mobilization of shear strength up to peak stress in MICP treated samples over untreated samples of Silt 1.

Chapter 6 The Impact of Hydraulic Design Practices on Resiliency of Infrastructure

Portions of this chapter are published in a literature review for NCDOT, "Improving Resilience of Transportation Infrastructure to Hurricane Damage," where the author was a significant contributor to the literature review report.

6.1 Introduction

Infrastructure resilience has become an important topic for North Carolina. Recent hurricanes and other extreme events have caused more than $450 million in damage to the States' transportation infrastructure. In addition to the cost of the infrastructure, the North Carolina Department of Transportation (NCDOT) spent considerable resources to redesign and repair many elements after each event. In particular, Hurricane Matthew in October of 2016 and Hurricane Florence in September of 2018 are of great focus for the NCDOT. Hurricane Matthew caused considerable damage to the State's transportation infrastructure. Though indications were that Hurricane Florence was less damaging to roadway infrastructure as compared to Hurricane Matthew, a review of the NCDOT records following Hurricane Florence suggest that more than 3,000 disruptions to roadways occurred. Further review of NCDOT records indicated that some of the locations identified in Florence were identical to those damaged during Hurricane Matthew.

However, since the amount and degree of damage, at least anecdotally, was different between the two events, this suggested that DOT design strategies between the two hurricane events were effective. The potential reasons for this are included, but not limited to:

1. when the infrastructure was initially designed and constructed (pre-Matthew) the design codes and standards were not the same as those used post-Matthew (i.e. installation of headwalls)

2. the infrastructure pre-Matthew was older and perhaps had accumulated damage that had weakened the infrastructure and a replacement or repair caused the structure to be resilient,
3. flooding intensities, though similar and well above normal expectations, may have differed, and
4. debris flow/actual capacity due to deferred maintenance may have also differed in the two events.

This study will look to identify and evaluate the specific elements, design features, or repair options used in the new infrastructure that positively contributed to the improved performance during Hurricane Florence and those that did not positively contribute. The NCDOT tasked us with this project with this simple overarching goal in mind- "Quantitatively prove what we already qualitatively know- that sites re-designed following Matthew were successfully resilient when Florence occurred." Though guidance on improved and/or resilient design exists from the FHWA, AASHTO, NCHRP, and others, these issues are highly context sensitive with many contributing factors including age of structure, maintenance levels, region, rainfall intensity, etc. which has necessitated a North Carolina specific investigation. The goal of this research will be to a) evaluate the design process for roadway infrastructure that was repaired following Hurricanes Matthew and Florence, b) identify the specific elements of the new infrastructure that positively contributed to improved performance during Hurricane Florence, and c) develop recommendations on design elements that improve the resilience of NCDOT roadways.

In order to carry out this investigation, a review of some important topics is required. This chapter is divided into five primary sections. Section 1 (this section) provides an introduction and overview of the research conducted. Section 2 describes the relevant studies and

general practice of NCDOT hydraulic design procedures, including appropriate hydrologic methods in estimating peak discharge for a given site. In addition, section 2 will review guidelines for hydraulic design on regional and state level. Section 3 will look to provide insight and analysis into the decision making from the different hydrologic methods and how they inform the hydraulic design. Section 4 will outline multiple case studies to demonstrate the effectiveness of NCDOT practices between Hurricanes Matthew and Florence. Finally, Section 5 and 6 provides an overview and conclusion of lessons learned throughout the project, and future work that is ongoing.

6.2 Overview of Hydraulic Design Practice

In the following sections, the basic process of hydraulic design will be outlined at a national level. According to Federal Highway Administration (FHWA) design philosophy, the primary purpose of highway drainage facilities is to prevent surface runoff from reaching the roadway and to remove rainfall or surface water efficiently from the roadway. Two disciplines utilized in highway drainage design that this research project will focus on are hydrology and hydraulics. The determination of the quantity and frequency of runoff is the hydrologic portion of the design process. The hydraulic design of a drainage structure is determining the appropriate capacity to divert water from the roadway, remove water from the roadway, and pass collected water under the roadway.

For a given structure that services a specific drainage area, an estimate of the amount of runoff that will occur for a storm is considered to be a major component of the hydraulic design process (Kilgore et al, 2016). A number of hydrologic methods are available in order to analyze and determine peak runoff for a given storm. From these runoff estimates, design engineers utilize the runoff in conjunction with frequency analyses to characterize the risk for a given

drainage area and structure. During design, terms of annual exceedance or recurrence intervals are used to describe the probability of occurrence of a given precipitation event. Based on the probability of occurrence of an event and the peak runoff that will occur for that event, a hydraulic engineer can design the drainage structure to be able to withstand that precipitation event.

When designing for drainage facilities, a range of discharges with a range of flood frequencies are used, typically termed the "base flood" and "super flood". A base flood is defined as the flood or storm having a 1 percent chance of being equaled or exceeded in any given year, or 1% annual exceedance probability (AEP). Owing to the fact that the inverse of the AEP is a whole number indicative of occurrence in a given year (i.e., a 1% AEP is equivalent to a 1 in 100 probability), this event is often referred to as simply the 100-year flood. This terminology may give the impression that there is certainty that this event will only occur once every 100 years. However, in reality it is simply a probabilistic assessment of its likelihood. Thus, a 1% AEP event has a 39.5% probability of occurrence at least once during a given 50-year time frame, a 8.9% chance of happening at least twice over the same 50 year time frame, and a 1.4% chance of happening three times over the same time period.

In the following sections, this literature review will examine the design process utilized by national and state agencies, outline hydrologic methods utilized to inform those design decisions, and design practices of NCDOT and how the design process and best practices can differ from other state agencies in the region.

6.2.1 Resources for Estimating Probability of Annual Exceedance

There are many methods in use to estimate rainfall intensity. Peak discharge estimates from these methods are dependent on precipitation data recorded from national agencies, specifically the

National Weather Service (NWS) and National Oceanic and Atmospheric Administration (NOAA). The most recent widespread analysis of precipitation data for North Carolina is presented in NOAA Atlas 14, Vol 2. This volume was released in 2006 and the last data for the estimates presented therein was gathered in 2004. Mention of an updated contract with NOAA indicated that the Southeastern US dataset will be updated again in 2023, published as Vol 13.

Rainfall intensity is the rate at which precipitation occurs. Intensity is usually stated irrespective of the duration of the rainfall, although it can be stated as total rainfall in a particular time period or duration. Frequency is expressed as the probability of a given rainfall intensity being equaled or exceeded (Kilgore et al, 2016). Rainfall data are used to derive intensity-duration-frequency curves necessary in hydrologic analysis, as mentioned in the Rational Method (see 6.3.1.1.2). Two methods for selecting rainfall data used in such frequency analyses are: (1) annual-series and (2) partial-duration series. Annual-series analysis considers only the maximum rainfall for a given year and ignores the remaining rainfalls, even though these lesser rainfalls could exceed the maximum of other years. The partial-duration series analysis considers all of the high rainfalls, regardless of the number occurring within a given year. The FHWA guidelines recommend when designing highway drainage facilities for return periods greater than 10 years, the difference between the two series is unimportant and can be ignored. However, when the return period or design frequency is less than 10 years, the partial-duration series is believed to be more appropriate.

6.2.2 Uncertainty and Extreme Events Consideration in Current Guidelines

Design events carry statistical uncertainty from the estimation process due to the sample size and statistical techniques adopted. The uncertainty can be translated into confidence intervals using the mean intensity or the mean return period. For example, the largest value of a record of 50

samples may be assumed as the expected value of the 50-year event. The exceedance probability of this event is often estimated through the Weibull plotting position as (1 – 50/51) = 0.0196, whose 95% confidence interval has been demonstrated to be included between 0.0005 to 0.071 (Serinaldi et al 2015). These values, in turn, correspond to return periods of 2000 and 14 years, respectively. Similar considerations can be drawn when the sample is analyzed statistically by fitting a probability distribution function. To account for this type of uncertainty, NOAA Atlas 14 provides the expected value for the precipitation intensity associated with a given return period and duration and the 90% confidence intervals, a feature that was not provided in previous governmental releases of this precipitation information. Despite this, design is almost always based on mean estimates. For example, precipitation data was pulled from one NOAA station located at North Carolina State University to illustrate the available data. For a 24-hour storm duration, the mean 1% AEP is 7.57 in. with a 90% upper limit estimate of 8.18 in. and a 90% confidence lower limit estimate of 6.97 in. This mean precipitation frequency estimate and its associated limits place the band of uncertainty of the 1% AEP equivalent to a 1.7% AEP and a 0.6% AEP. These differences translate into a range of probabilities that a 24-hour storm that produces 7.57 in. of precipitation will occur at least once in a 30-year period somewhere between 39.6% and 16.4%. Although the probabilities of these events occurring would classify them as rare events, the high impact of these rare events have been given special values in many newly rising fields such as smart city and autonomous driving (She et al, 2019).

6.2.3 Effects of Non-Stationarity and Climate Change in Hydraulic Design

Hydraulic designers are well aware of the fact that the built environment is non-stationary and that historical precedence is not always a great predictor of future conditions. This effect is evident in cases where new developments or other socio-economic/demographic changes change

run-off levels and affect existing hydraulic structures. It has also become increasingly evident that climatological factors represent another type of non-stationarity that may need to be considered when defining design storm events (Serinaldi et al, 2015; Cheng et al, 2014; Salas et al, 2014; CHy, 2012; Milly et al., 2008; Jain et al., 2001).

This effect has been examined within the NOAA Atlas 14, Vol. 2 release. Here, extreme event precipitation and its change over time was evaluated by performing a linear trend test on the 1-day maximum precipitation levels and its variance. Linear models were fitted to the time-series data for stations with a minimum of 50 years-worth of precipitation data. The results of this analysis are shown in Figure 6.1 (trend of means) and Figure 6.2 (trend of variances). Stations where the mean or variance increased are denoted with a '+' symbol in green and those where the trends decreased are denoted with a red '-' symbol. From these figures, a number of stations in Eastern NC show a positive linear trend with respect to the magnitude and variance, suggesting that it is very important (more so than many other locations in North Carolina and around the region) to consider the most up-to-date precipitation data in order to properly identify the design intensity levels.

FHWA has released a manual (Kilgore et al, 2016) to provide technical guidance grounded in the best available and actionable engineering and scientific data and approaches with a framework that is adaptable to future design situations. The manual provides specific information on risk and vulnerability assessments, planning activities, and design. The FHWA further believes that incorporating the potential effects of extreme events and climate change on flooding and then designing transportation system for more resilience when exposed to extreme flood events will enhance the lifecycle benefits.

The North Carolina DOT mentions that the Hydraulics unit has made a commitment to follow FHWA policy in regard to climate change and its impact on infrastructure design (Chang, 2016). Specifically, NCDOT highlights that "infrastructure is designed to handle impacts of a changing climate, such as sea level rise, increased frequency and magnitude of heavy precipitation and tropical storms, etc. Preparing for extreme weather events is critical to protecting the integrity of transportation and ecological (floodplain and wetland) systems and prudent investment of taxpayer dollars. The NCDOT staff will seek to follow FHWA's policy and guidance to develop cost-effective strategies to minimize climate and extreme weather risks and protect transportation infrastructure. For example, the design engineer will follow the FHWA publication, "Highways in the River Environment – Floodplains, Extreme Events, Risk, and Resilience, HEC-17 (FHWA-HIF-16-018), June 2016 (26)."

In addition, the National Cooperative Highway Research Program (NCHRP) produced a guide to provides a comprehensive framework for considering and incorporating climate change into the design processes for inland and coastal applications. Climate science and modeling is a dynamic field that is constantly changing and advancing and this guide is based on the current state of knowledge and understanding of possible future conditions developed by the climate community. The models from the Coupled Model Intercomparison Project (CMIP), are utilized to project a wide range of possible changes in future climate conditions. The main objective of these projections is to provide the data for engineers to better understand past, present and future climate changes arising from natural, unforced variability or in response to changes in radiative forcing in a multi-model context. The objective of the NCHRP guide is not to replace existing state DOT or other guidance, however it does provide additional tools, notably the CMIP5

climate processing tool, for evaluating the potential effects of climate change on transportation infrastructure (Kilgore et al., 2019).

6.3 National, State, and Regional Hydraulic Design Practices

As mentioned previously, national guidelines outlined by FHWA for hydraulic design are utilized in order to prevent surface runoff from reaching the roadway and to remove rainfall or surface water efficiently from the roadway. National guidelines produced from FHWA do not differ greatly when looking at state guidelines, as the state guidelines reference often the FHWA reports. In particular, North Carolina's hydraulic design guidelines recommend engineers referencing the NCDOT's guidelines to also be up to date on FHWA guidelines (Chang, 2016).

NCDOT's hydraulic design guidelines, titled *Guidelines for Drainage Studies and Hydraulic Design,* was published in November, 2016 and is the result of consolidation and revised guidance from previous Guidelines, most notably the 1999 Guidelines, with the emergence of new environmental, regulatory, and design challenges (Chang, 2016). These Guidelines are for use in design, analysis, and maintenance of drainage structures and systems designed and constructed by or in association with NCDOT-funded projects. The guidelines outline recommendations for design of drainage systems, and highlights the methods and procedures for calculations of runoff and storm discharges for a designed structure. The literature review that focused on the state of hydraulic design guidelines can be described in 2 parts: 1) the current state of design guidelines for extreme storm events and 2) best practices during the design process. In particular decisions made between the current state of design guidelines and how they may deviate from the guidelines when put into practice will be applied to the major storm events, Hurricane Matthew and Hurricanes Florence, which occurred in 2016 and 2018, respectively.

6.3.1 Current State of Practice in North Carolina

Current hydraulic guidelines utilized by the NCDOT rely on hydrologic methods that estimate peak storm discharge rates. Quantitative knowledge of these storm rates from watersheds is relevant to understanding and controlling a number of environmental processes, including erosion and sediment transport, pollutant loadings and travel times, and most notably for the purposes of this project, flooding and drainage (Genereux, 2011). Accurate estimation of peak storm discharge rates from watersheds is important to the design of drainage works along roadways and related infrastructure. The NCDOT guidelines state that the design engineer should select from a number of peak discharge methods, depending on the site's watershed characteristics. The methods utilized by the NCDOT for calculating peak storm discharges are based on the type of structure being designed, as shown in Table ***6.1***. Once a hydrologic method has been selected and implemented, the results from that hydrological method calculations should be calibrated and compared with historical site information. In addition, the design engineer should consider potential future land use changes within a watershed over the life of a roadway structure and include this effect when estimating design discharges.

6.3.1.1 Hydrologic Methods Used by the North Carolina DOT

6.3.1.1.1 Flood Insurance Study (FIS) Method

If a project study site is on a FEMA-regulated stream that is included in a published effective FEMA Flood Insurance Study (FIS), in conjunction with the National Flood Insurance Program (NFIP), then the discharges specified in the FIS should be used in the hydraulic model to demonstrate FEMA regulatory compliance. Streams studied by limited detailed methods will list the 100-year discharge and this information can be used directly by the designer. This method is utilized when structures or roadways have been designated to be within the NFIP and are

required for FEMA compliance. The method is used in conjunction with a Floodway Map to determine whether or not a site is located in a Special Flood Hazard Area (SFHA), V Zone (front row beachfront properties), or a floodway.

6.3.1.1.2 Rational Method

The Rational Method is a simplified approach of calculating peak runoff based on rainfall intensity, drainage area, and land use coefficient, as seen in Equation LIST OF TABLES below.

$$Q = CIA \tag{1}$$

where;

Q = peak discharge (ft^3/s)

C = runoff coefficient (units are consistent with other terms),

I = rainfall intensity (in./hr), and

A = drainage area (acres).

The Rational Method is utilized for corresponding structures as outlined in Table ***6.1*** and is employed when structures are being designed with drainage areas up to 64 acres. Typical runoff coefficients can be found in Table 6.2 (Genereux, 2011). The rainfall intensity (I) can be obtained from NOAA Atlas 14, where they have already been calculated for a range of durations and storm event frequencies at specific locations.

6.3.1.1.3 NCDOT Highway Hydrologic Charts (1973) Method

The NCDOT method uses a series of design charts known as the 'Highway Hydrologic Charts'. This method is only suggested for use in sizing small pipes (Chang, 2016). The method utilizes a hydrologic contour map of North Carolina Figure ***6.3*** and the corresponding contour is used in conjunction with the runoff charts Figure 6.4 to estimate peak runoff at a 50-year design frequency (Q50) (Chang, 2016). There are correction factors that can be used to obtain peak

runoff at other design frequencies, as well as correction factors for drainage area cover and shape, all of which can be seen in Figure 6.4. If the drainage area is larger than 20 acres, NCDOT recommends that the design engineer should consider if the Rational Method would provide a more appropriate estimate for peak discharge.

6.3.1.1.4 USGS Methods

The United States Geologic Survey (USGS) has a number of reports that describe the estimation of peak discharge based on regional statistical regression analysis of watershed area and other characteristics such as land use. These reports outlines methods and procedures for utilizing stream gage data to calculate peak discharge for a specific location. The NCDOT recommends that precedence should be given to this analysis when a USGS stream gage is available at or near the study site. NCDOT also outlines peak discharge estimation procedure for sites where gages are available and unavailable, as presented in USGS report SIR 2009-5158 (Feaster et al, 2009) and USGS report SIR 2014-5030 (Feaster et al., 2014). For sites with gaged data available, there are three types of estimates for peak discharges that USGS provides:

- the recorded annual regulated peak flows are fitted to the log-Pearson Type III distribution,
- the appropriate regionalized regression equation developed for the hydrologic area of the gage location is used, and
- the first two types are used to make the estimate and are then combined using a weighted estimate method.

Additionally, if the site is not located at a reference stream gauge station, and the drainage area is within 50% of the drainage area of the reference gauge station, then the peak discharge estimate from the reference station can be adjusted (or transposed) for the study location (Chang, 2016). If the ungauged site is located between two gaged stations on the same

stream, NCDOT guidelines recommend that two peak discharge estimates can be made using the above procedure and engineering judgment applied to determine which is the more appropriate of the two estimates.

Lastly, two reports have been produced by USGS outlining how the above procedures and methods can be used to calculate and estimate magnitude and frequency of floods varying from land use type and drainage area. The USGS method (2014) is utilized for any drainage area under land use designated as urban, and any rural drainage area that is from 64 acres up to 1 square mile (640 acres). The USGS, 2009 is utilized for any rural drainage area from 1 square mile up to 400+ square miles. These reports utilized multi-variate regression analysis and determined equations that require inputs of site characteristics to obtain peak discharge flows for a given site. As shown in Figure **6.5**, these equations rely on 4 types of data inputs- 1) Drainage area, 2) Percent Impervious Area, 3) Percent Developed Land, and 4) 24-hr 50 year max precipitation from NOAA Atlas 14 Vol 2. Additionally, the design engineer will need to decide at which frequency, or Annual exceedance probability (AEP), to design the structure for, as shown in the equations. Each AEP provides a different set of coefficients to use in the regression analysis.

6.3.1.1.5 Natural Resources Conservation Service (NRCS) Method

The Natural Resource Conservation Service produced a method that estimates discharge primarily based on land use and soil mapping as input parameters. Soil conditions such as hydrologic cover, soil type, and runoff conditions that are incorporated into the estimation method as Curve Numbers (*CN*). These *CN* values and rainfall estimates (*P*) can be utilized in conjunction with Figure 6.6 to determine a runoff estimate for a given site's soil conditions.

6.3.1.2 Design Frequency

Once the appropriate method has been selected based on the land use and drainage area size from guidance in the NCDOT guidelines, the design frequency for that roadway or structure must be determined as well. The design storm frequency for NCDOT drainage structures is determined based on variables such as the roadway classification, traffic volume, level of service, flooding potential to properties, and maintenance costs, among others (Chang, 2016). A summary of these frequencies as they relate to the peak discharge calculations mentioned previous shown in Table ***6.3***. These return period based (frequencies) flood events that have been established by NCDOT as acceptable level of return period flood events for roadway overtopping, or when roadway overtopping is not involved, it will be the level of flood used for establishment of freeboard and/or backwater limitations.

6.3.2 State of Practice from Nearby State Highway Agencies

For comparison, hydraulic guidelines for the states surrounding North Carolina were examined, and a brief summary of highlights is presented. The surrounding states mentioned below were considered for regional comparison to North Carolina. As mentioned previously, state agencies guidelines did not differ greatly from national guidelines outlined by FHWA. However minor variations on terms and definitions can have an impact on how the design process can be done.

6.3.2.1 Virginia (2002, revised 2021)

Virginia DOT utilizes hydrologic methods including the Rational Method, USGS Method (Rural and Urban), the NRCS method and a Modified Rational Method, and the Anderson Method. The Andersen Method was developed by USGS to evaluate the effects of urban development on floods in Northern Virginia, and is therefore not recommended for use outside of this region (VDOT, 2002, r. 2021). The max drainage area recommended for the application of the

Anderson method is 570 sq. miles. Similar to the NCDOT guidance on the Rational Method, the Rational Method and the Modified Rational Method in Virginia are recommended for sites up to 200 acres.

6.3.2.2 Tennessee (2012)

Tennessee's hydraulic design guidance has indicated that there are preferred methods for hydrologic design calculations. The Rational and USGS Methods are preferred when the drainage area is less than 100 acres or greater than 100 acres, respectively. As mentioned previously, this drainage area criterion differs from NCDOT guidance (200 acres for Rational Method). However, there are certain situations where additional methods are required and utilized. Depending on the extent of man-made structures and the size of the drainage area, hydrograph methods such as the NRCS method and similar to the NCDOT Highway Hydrologic Charts may be utilized (TDOT, 2012). Additionally, the TDOT has determined that based on the design location, there are differing drainage area limits that affect the applicability of the USGS methods.

6.3.2.3 South Carolina (2009)

South Carolina has minor variations to the overall design process for hydraulic structures. For definitions, the agency refers to all drainage structures that are greater than 20 feet in length as bridges. All others (i.e. less than 20 feet in length) are labeled as culverts.

SCDOT uses different design frequencies for hydrologic estimates based on roadway classification (i.e. major primary routes, secondary routes, etc). For secondary roads, 25-year peak discharge is used, as these are frequently smaller drainage areas and service less utilized roadways. Overdesigning for these secondary routes would present South Carolina with increased costs (SCDOT, 2000). Primary and interstate routes utilize 50-year discharge, and all

stream crossings are analyzed for 100-year events, similar to current practices employed by NCDOT.

Typical hydrologic methods utilized include the Rational Method, USGS Method (Rural and Urban), and NRCS method. Differing from NCDOT, the Rational Method in South Carolina is recommended to be used for sites up to 100 acres. The NRCS method is recommended to be utilized for locations from 100 acres to 640 acres. For locations with greater than 640 acres (1 square mile), the two USGS methods are employed depending on land usage (urban or rural).

6.3.2.4 Georgia (2020)

The Georgia DOT hydraulic guidelines are similar to those of the SC DOT guidelines, but differ on the drainage area limitations for recommending which hydrologic method to be used in a hydrologic analysis (GDOT, 2020). The 3 methods recommended and their drainage area limitations were:

- Rational method – up to 200 acres, with a recommendation of utilizing for drainage areas less than 64 acres (similar to NCDOT),
- NRCS Method – up to 2000 acres and hydrologically homogenous, and
- USGS Methods – following referenced methodologies' recommendations (mentioned in Section 6.3.1.1.4)

6.3.2.5 Florida (2012)

Although a comparative study undertaken by Genereux, 2011 suggests that Florida uses USGS for some hydraulic design calculations, Florida's guidance from 2012 makes no mention of either USGS method (FDOT, 2012). It does suggest that the Rational Method is utilized along with FHWA HEC-12, which appears to be a precursor to the NCDOT Highway and Hydrologic

Charts. Design frequencies for drainage systems range from 3-year to 50-year discharges, with the most common being 3-year design frequency.

6.3.3 Hydraulic Design Procedures

6.3.3.1 HDS-5

Hydraulic Design Series-5, or HDS-5 as the report will be referred to in this thesis, was released by FHWA as a publication to provide information for the planning and hydraulic design of culverts. The common practice for designing using HDS-5 relies on established nomographs to obtain a ratio of HW/D (head water to depth inside pipe). These nomographs are established based on flow theory and vary by pipe type, inlet arrangement, slope, diameter, etc. For design, HDS-5 nomographs are provided for different material types (i.e.- concrete, metal, etc.) and the design engineer will choose the appropriate chart for the pipe being designed for. Figure **6.7** shows an example of a nomograph provided in HDS-5 for concrete pipe culverts. For example, using this nomograph and after determining the appropriate peak discharge Q_{25} value, the engineer would start at the left with the diameter of the pipe in inches (ex: 42 in.) and cross a straight line with the discharge in ft^3/s (ex: 120 cfs) and take the value provided from that straight line to the HW/D values given- 2.5 in the example. Depending on the type of culvert being designed for, the engineer can choose different Entrance Types- square edge with headwall, groove end with headwall, or groove end projecting- which control the entrance loss coefficient (K_e), and affect the outcome of the nomograph. For the same scenario listed in Figure **6.7**, the value of 2.5 obtained for Entrance Type 1 would be 2.1 and 2.2 for Entrance Types 2 and 3, respectively.

NCDOT utilizes a computerized implementation of the HDS-5 report and nomographs, and is shown in Figure **6.8**. This computer program version of these nomographs is similar to the

physical nomographs and require inputs of peak discharge and culvert diameter in inches. One slight variation as compared to the physical nomographs is that the computer version requires an input of culvert barrel slope, but NCDOT Hydraulics unit guidance is to assume this value is to be 0.0 ft/ft for practical design purposes. Headwater value is the output, and based on the inputs provided, critical depth and critical velocity are calculated as well. The NCDOT Hydraulics unit notes that it most commonly uses this software during the design process to determine HW/D ratios.

One additional guidance gleaned from NCDOT during the design using HDS-5 that is not explicitly written out in the Hydraulic guidelines has to do with buried depth. In the hydraulic recommendation report, there is consideration to use a buried depth of 1 ft for a given pipe size and design- "at jurisdictional crossings proposed culvert(s) analyzed buried 20% of diameter up to 1' for aquatic fish passage." This consideration is important for the hydraulic design process for HDS-5, as the software does not have the ability to differentiate between buried or fully open pipe diameter. To get around this, the Hydraulics unit "down-sizes" the pipe size, where the cross-sectional area of that open pipe area would be determined, and the nearest cross sectional area of a non-buried pipe would be used in its place. For example, a 60'' diameter pipe would normally have an area of 19.64 ft^2, but buried 1 ft has an area of 16.84 ft^2. The nearest non-buried area is 15.90 ft^2 for a 54'' diameter pipe, and so a D of 54'' would be used in HDS-5.

6.3.3.2 HY-8

HY-8 is a computerized implementation of the same FHWA culvert hydraulic analysis approach outlined in HDS-5. However, HY-8 utilizes the head loss equations and Manning's flow equations directly to estimate the flow through pipes and on the outlet side instead of the categorical nomographs in HDS-5. Additionally, HY-8 allows the user to more accurately

portray the structure and site characteristics that HDS-5 does not take into account, most notably buried vs non-buried pipe diameter. In HY-8, there are five main input windows as illustrated in Figure **6.9**; 1) Discharge Data; 2) Tailwater Data; 3) Roadway Data; 4) Culvert Data; and 5) Site Data. The types of inputs and how they were utilized is detailed in the following sections.

6.3.3.2.1 Discharge Data

Users in HY-8 can choose from among three different discharge methods for inputting data for a site: Min/Design/Design, User Defined, and Recurrence Interval as shown in Figure **6.10**. The "User-Defined" option provides a convenient avenue for an analysis that the research team had been pursuing with adjusted precipitation values, as it allows the user to create a list of sample discharges to analyze the structure with. One minor limitation is that the values must be listed in increasing value. The 'Min/Max/Design' option allows the user to set a minimum and maximum discharge values between which HY-8 populates discharge intervals will interpolate and use for analysis along with the design discharge. Finally, the 'Recurrence' option allows the user to set the annual exceedance probability (AEP) design discharges for 1 through 500 year intervals. Each of these design discharge values can be estimated using the appropriate hydrologic method (i.e. using equations from USGS Rural 2009, USGS Urban and Small Rural 2014, or the Rational Method).

6.3.3.2.2 Tailwater Data

In the Tailwater data section input window, the user must first choose from either a list of different channel shapes- Rectangular, Triangular, Trapezoidal, and Irregular or enter either the channel rating curve or a constant tailwater elevation. As can be seen in Figure **6.11**, when selecting from the channel shapes, the user enters the appropriate geometric descriptors for that channel and the invert elevation. For the regular geometries, these descriptors include width

(rectangular and trapezoidal) and side slope (triangular and trapezoidal). For an irregular geometry, the user defines the shape through a station-elevation table. In both regular and irregular channels the Manning's n value and the channel slope should also be input. If a user elects to input a channel rating curve they must enter the relationship between flow, elevation, and velocity for that channel as well as the invert elevation. For the case of a constant tailwater elevation the user enters the tailwater and invert elevations. A more detailed view of the inputs window for this section can be seen in Figure **6.11**.

Channel slope has to be greater than zero for the model to run. Since this value is not typically available or reported in the North Carolina DOT design it was set through trial and error to 0.01 ft/ft because HY-8 results obtained using this value were close to HDS-5 results, which the research team had wanted to replicate. Manning's n value can be found from various resources, but is typically assumed to be 0.04 for all channels as is typical for natural channels (Manning's Roughness Coefficients, n.d.) Finally, Channel Invert Elevation is typically designated to be 0 ft barring otherwise provided data. The flexibility to consider different channel types allows HY-8 analysis to consider site specific data that cannot be considered in HDS-5.

6.3.3.2.3 Roadway Data

The third input window that HY-8 is used to construct a site is the Roadway Data window, which allows one to define the roadway characteristics with values for Crest Length, Crest Elevation, and Top Width. Crest Length is the length of the roadway perpendicular to flow that the pipe is placed, including the headwall. Additionally, the user can define an Irregular roadway profile shape. While this value does not have an effect on the flow characteristics while completing the analysis, it is necessary to use a value that allows for the pipe cross section to fit between the top

of roadway and bottom of channel. Similarly, Crest Elevation defines the value from the bottom channel depth to the top of the roadway. The NCDOT utilizes this value in their hydraulic calculations to define the HW/D ratio, but refers to it as Bed to Crown (BTC). While also not inherently effecting the hydraulic capabilities of the site, it is equally important to build the cross section as close to site conditions as possible in order to estimate the possibility that a site will overtop for a given flow. Additionally, considerations can be made as to whether the road is paved or unpaved. The research team has not specifically explored the effects of this choice because all sites analyzed so far are paved with asphalt concrete. Lastly, the Top Width is defined as the width of the roadway along the pipe/flow direction. This parameter, along with the other parameters in the Roadway Data window can be visualized in Figure **6.12**.

6.3.3.2.4 Culvert Data

One important area where HY-8 has a distinct advantage over HDS-5 is the ability to determine the exact cross sectional area of a pipe based on the type of culvert, dimensions, material, and number of barrels. Users are able to define the shape of the culvert, which can be found in greater detail in Table **6.4**, as well as choose from a list of standard pipe sizes for each of those shapes. Manning's number values are automatically filled in based on the material type chosen; however, the user can define that number to their judgement. Additionally, HY-8 allows the user to define an embedment depth. Figure **6.13** depicts a 66″ x 51″ CAAPA (Corrugated Aluminum Alloy Pipe Arch) with 1 ft embedment depth. In HDS-5 nomographs, a simple approximation is made for embedded pipes wherein a pipes buried cross sectional area is compared to the closest unburied cross section and this unburied pipe is used in place of the buried pipe. Finally, similar to HDS-5 coefficients for entrance loss (K_e) need to be defined. Specific options exist along with

their default values: thin edge (0.09), mitered (0.7), square edge (0.5), headwall (0.5), beveled edge (0.2), and others.

6.3.3.2.5 Site Data

Lastly in the inputs window, Site Data defines how the culvert is placed within the previously defined site conditions in Roadway Data. Inlet and outlet elevation values can be defined; however, it is standard practice in to set culvert slope as 0. The Outlet station value should match the length of the pipe that is put in place. Finally, the number of barrels can be defined, as compared to HDS-5 nomographs in which the design discharge flow would be divided by the number of barrels to get the equivalent HW values.

6.3.3.2.6 Output- Analyze Crossing

Once these values have been defined and the input window is complete, HY-8 allows the user to analyze the design by pressing the "Analyze Crossing" button in the bottom right section of the main screen. If the input window is error free, the software will provide a variety of calculated values as shown in Figure **6.14**. These outputs include the Crossing Summary Table, Culvert Summary Table, Water Surface Profile, Tapered Inlet Table, and Customized Table. The Culvert Summary table provides values of design discharges previously defined in Discharge Data, Headwater Elevation, Inlet Control Depth, Outlet Control Depth, USGS Flow Type, Critical depth, Outlet Depth, Tailwater Depth, and Outlet and Tailwater Velocities. HDS-5 nomographs only provide values of HW, Critical depth and velocity. Additionally, the Water Surface profile allows the user to visualize the modeled water level through the pipe, which can be viewed in Figure **6.14**.

6.4 Case Studies and Variances of Q_{25} vs Florence and Matthew Flow Conditions

To compare performances of infrastructures during two events and patterns associated with them, four categories were considered to develop case studies. These identification criterion are as follows: 1) Damaged in both events, 2) Not damaged in Matthew, damaged in Florence, 3) Not damaged in Florence, damaged in Matthew, 4) Not damaged in either events. This matrix can be found in Figure **6.15**, and was the basis for determining case studies for further analysis.

Next, in order to identify potential areas to focus on for an extended and deeper analysis, the objective of characterizing and understanding the impact the storms had on the infrastructure. In order to do that, precipitation estimates were required for the whole of North Carolina. National Oceanographic and Atmospheric Administration, or NOAA, provides datasets that have rainfall estimates for the country, and so ArcGIS was used to overlay a map of North Carolina with the precipitation. These maps can be seen in Figure **6.16** and were created for both Matthew and Florence. Areas with high levels of cumulative precipitation are highlighted in red and yellow, and we can see that the highest levels seen in Matthew and Florence are in the Southeast in Divisions 2, 3, 4, 5, 6, and 8. These Divisions were the ones considered for our case study analysis, and specifically narrowed in on Division 6 and Robeson county. Robeson county had the highest number of Scenario 1- damaged in both- sites that overlapped in the NCDOT provided databases. From the NCDOT datasets provided for Matthew and Florence, a map of the identified sites within Robeson county was created as seen in Figure **6.17**. Robeson county outlined below contained 78 Matthew (M) only damaged sites, 57 Florence (F) only damaged sites, and 7 Matthew and Florence (MF) overlapped sites. Of these, all 7 MF sites, 16 M sites, and 9 F sites were selected to continue with the analysis.

For a more in-depth analysis and to demonstrate the NCDOT design process, 2 cases from each of the 3 available Scenarios were chosen: Case 5-MF Kitchen St Road, Case 7-MF Fairley Road, Case 6-M Vester Road, Case 8-M McCrimmon Road, Case 1-F Evon Road and Case 2-F Pearsall Road. Sites that fit into Scenario 4- Not damaged in either, are still being investigated on how best to approach and obtain data from NCDOT, as the dataset for this Scenario is not explicitly available.

6.4.1 Precipitation Intensity Analysis

The hourly rainfall data was obtained from the NCDOT project RP2021-03. The daily maximum 24-hour rainfall data along with corresponding AEP% from NOAA are summarized in Table ***6.5***. The AEP% values were calculated by interpolating the existing NOAA precipitation levels and their AEP values. In Table ***6.5***, the Maximum 24-hr rainfall values are estimated by using the conventional NOAA definition of a 24-hr event (starting at 12:00 AM GMT or 7:00 AM ET and going until 6:59 AM ET the following calendar day). The absolute (overall) maximum 24-hour rainfall, regardless of start time, was also calculated for each event and each location and the results are also summarized in Table 6.

The table shows that the majority of sites had AEP values for the 24-hr duration events, defined according to the NOAA definition of a 24-hr period, below 4%, or corresponding to a 25-year return interval. When using the overall maximum 24-hr period, all sites have AEP's below 4% and many are at the 0.2% or 0.1% (500 year and 1000 year return interval), which would suggest that the flow levels at these sites greatly exceeded their design during the events, which would have been for a 4%, 25 year return period storm. In order to characterize the precipitation into a metric that could be used in analysis, a ratio of the observed 24-hr

precipitation, $P_{\text{observed,24-hr}}$, to the 24-hr 4% AEP, $P_{\text{4\% AEP}}$, to estimate the likely flow rates during the events.

$$Ratio = \frac{P_{\text{observed,24-hr}}}{P_{\text{4\% AEP}}} \quad (2)$$

Table 6 also shows these ratios calculated using their respective definitions of the 24-hr precipitation levels. Ratio 1 is determined using the NOAA definition of 24-hr event and Ratio 2 is calculated from the heaviest 24-hr period. Examining the overall maximum 24-hr precipitation ratio, it can be observed (as expected) that both Florence and Matthew events have ratios greater than one and in most cases the ratio for Matthew was higher than for Florence.

6.4.1.1 Adjusted Peak Discharge

Using the ratios described above, in order to examine the potential flow scenarios during both Hurricane Matthew and Hurricane Florence, the values shown in Table ***6.6*** were calculated using the appropriate 4% AEP, or Q_{25} peak discharge for the sites listed. These original Q_{25} values were then multiplied by the ratios to calculate the adjusted peak discharge rates, shown in Table 7. The discharge levels shown as Ratio 1 are the ones calculated using the NOAA definition of 24-hr event and the levels shown as Ratio 2 are the ones calculated using the ratio from the heaviest 24-hr period.

6.4.2 Comparing HDS-5 and HY-8

In order to demonstrate the design process for the shortened case study list, an example procedure is outlined below for Case 8-M. This site was evaluated in detail using both HDS-5 and HY-8 in order to illustrate the design process and analysis outcomes from each software. This site was damaged in only Matthew, and the hydraulic design used for the analysis consisted of 2-60'' diameter Corrugated Metal Pipes (CMP) with a headwall (2@60''CMP w/ HW).

NCDOT hydraulic guidelines dictated that this site, with a drainage area of 3.52 sq. miles, would be designed hydrologically using USGS Rural 2009 equations, which yielded a design discharge Q_{25} of 525.3 cfs.

6.4.3 HDS-5 Analysis

The first step for the HDS-5 analysis was to choose the applicable nomograph for the pipe. Since this is a CMP pipe, Chart 2 was chosen and the 'Headwall' option was selected. In order to allow HDS-5 to correctly calculate the headwater depth, Q_{25} was divided by two yielding a per barrel discharge of 175.1 cfs, which is what was input into HDS-5 in discharge. As mentioned before, based on input from the North Carolina DOT, the culvert slope was set to 0 ft/ft. Lastly, the diameter of the pipe being analyzed, and 5 ft was input. No guidance in the hydraulic report or other documents mentioned a buried depth, so it was assumed fully open. If buried, the process described in the HDS-5 section would be followed. Using this process and the input screens found in the appropriate windows, a value of headwater value of 10.22 ft is calculated, which yielded a HW/D value of 2.04 (10.22 ft/5 ft).

6.4.4 HY-8 Analysis

HY-8 involves many more inputs and some additional assumptions as compared to HDS-5. First the discharge data was defined the same way it was input into HDS-5 except that the input discharge was the total Q_{25} (525 cfs) instead of 1/2 of the total Q_{25}. Since the number of barrels is defined later under the Site Data section, it is not necessary to divide the Q_{25}. For this example, Min/Design/Max will be used as we are analyzing for a single design discharge, 525 cfs.

Next, the tailwater data was defined. Since the channel geometry was not provided in the existing design documents and the research team has not visited the site yet, it was assumed to model the channel as a trapezoid and use a bottom width of 25 ft. Varying the value chosen here

does not affect the HW calculation, but does affect the calculations for tailwater velocity. The trapezoidal channel was also assumed to have a 2:1 H:V side slope, a channel slope of 0.01 ft/ft, and a Manning's n of 0.04 were chosen. No channel invert elevation or rating curve were defined.

The roadway data, including the crest length, crest elevation (BTC), and top width were defined. Similar to channel bottom width mentioned above, crest length, crest elevation, and top width do not specifically have an effect on the outcome of the analysis of the site, but is best for complete accuracy when building the cross sections. BTC values can be obtained from hydro reports when they are initiated and other relevant site data can be obtained from site visits. The culvert data input reflected what was available in the design documents, 60'' diameter Circular shaped metal pipe; corrugated aluminum pipes was chosen despite not being specifically defined in the design documents. Corrugated steel will provide a slightly higher headwater depth because the Manning's number that is auto-populated is 0.024 for Steel as compared to 0.031 for Aluminum. The pipe was assumed to be resting on the channel bottom given that the design in this case pre-dates Hurricane Matthew. The inlet configuration was assumed as Straight and Square Edge w/ Headwall (with K_e value of 0.5) and assumed to have no inlet depression.

The final input step for HY-8 was the site data. The difference between the inlet station and outlet station values should be the length of the pipe. For this site, the length of the pipe is 60 ft, so the inlet station value is 0 and the outlet station value is 60. Additionally, the culvert barrel slope can be defined using the inlet and outlet elevations. HY-8 manually calculates the computed culvert slope off those values, and for this example it is calculated to be zero. Finally, the number of barrels is defined, and for this example there are two barrels.

Finally, this procedure was repeated for the 5 other sites from each Scenario, and the results of this analysis can be found in Table **6.7**. The above process as described for Case 8M was also completed using the adjusted peak discharge values and the results can be found in Table **6.8**.

6.4.5 Comparison of Base Discharge Results

A direct comparison with the outputs from HDS-5 and HY-8 was completed to evaluate the similarities and differences in analysis outcomes for all of the chosen case study sites. As expected, a majority of the sites damaged in either storm were under-designed according to the standard of HW/D < 1.25. Only 1 site had adequate-designed pipes pre-Matthew according to HDS-5 and HY-8. This site, Case 6M, from discussions with Division 6 personnel, is an unpaved road, and the damage was almost entirely to the embankment and roadway, and not to the pipes itself. This site can be considered an outlier for this reason.

There are some minor differences when comparing the base discharges results from the two software programs, with all 6 sites arriving at the same conclusion based on the NCDOT design criterion of HW/D<1.25 for Matthew and Florence. Only 1 site, Case 2-F has disagreeing values for HDS-5 and HY-8 for the current in place structure. This site has HW/D values above 1.25 for HDS-5, but has HW/D values less than 1.25 in HY-8. While there is variation to the exact value that each analysis provides for a given site, this site offers an interesting look into the potential benefits of using HY-8 over HDS-5. This site, if analyzed in its current structure, would be determined “under-designed” and would be more likely to overtop according to HDS-5. However, HY-8 indicates that this site is properly designed with a HW/D value of 1.11.

6.4.6 Comparison of Adjusted Discharge Results

As mentioned previously, the procedure as described for Case 8M was also completed using the adjusted peak discharge values. The results show that for HY-8, almost all sites had HW/D values > 1.25 for adjusted peak discharge values, except Case 7MF and Florence Ratio 1 (R1). Whereas for HDS-5, there were only 5 combinations of adjusted peak discharge values that provided HW/D values < 1.25. Comparing the values from Table **6.7** and Table **6.8**, we see that for Case 7MF, the structure was repaired after Matthew, and the new structure, according to HY-8 and HDS-5, was adequately designed for the base peak discharge. However, using the method to estimate the potential flow these structures experienced during the storms, we see that for Florence, this site was prone to overtopping with a HW/D value of 1.39 for Ratio 2.

In addition, Cases 6M and 8M provide interesting sites to consider. 6M was adequately designed according to both hydraulic analyses, 8M was not. Both were damaged in Matthew, and both upgraded following that damage, but neither was re-damaged in Florence. Hydraulic analysis of HY-8 and HDS-5 indicated both were adequately designed in their post-Matthew/pre-Florence structure using the base peak discharge values. And although for Case 6M in HDS-5, the HW/D values for the adjusted Florence discharges are shown in red, their values of 1.29 and 1.26 are very close to the overtopping criterion of 1.25, and thus could be considered adequately designed if provided a buffer. If so, then we can consider that the re-designing of these two sites following Matthew was sufficient in providing additional resilience when Florence occurred. These two sites demonstrate what the NCDOT was hoping to determine, that some of the design practices put in place for Matthew aided in the state's infrastructure resilience for following storm events.

Though the HY-8 values for Case 6M and 8M are above the criteria for adequate design, as shown previously, the number of inputs for HY-8 greatly outnumbers the inputs for HDS-5, and any one of those inputs could account for this minor difference between the two analyses. One input that could cause the HY-8 value to be slightly higher than the HDS-5 value is that the HY-8 model incorporates the length of the pipe into the analysis, whereas HDS-5 does not. However, this is just speculation and a comparative analysis should be completed on a larger sample size and more counties and Divisions to definitively determine this. Ongoing work on this project is looking to address this observation and other discrepancies determined through this analysis.

6.5 Analysis of Decision Making from Different Hydrologic Methods

6.5.1 Key Updates to Hydraulic Design Guidelines

Upon further examination of the design process for sites through the case study analysis, the previous versions of the NCDOT Hydraulic Design Guidelines, in particular the 1999 version, were investigated. Comparison was made between the current iteration of the guidelines and the previous version, with a focus on the hydrologic method determination criteria.

As summarized in Table **6.9**, The 1999 guidelines' criteria states that for a given site, the designation of Rural or Urban should be made, and once determined, the size of the drainage area will establish which hydrologic method to utilize. For rural sites with greater than 640 acres (1 sq. mile), the use of USGS Rural Regression Equations (1999) is recommended, while drainage areas less than 1 sq. mile should use the Highway Hydrologic Charts 1973. For urban sites, Highway hydrologic charts 1973 are used for drainage areas less than 10 acres if mainly residential (otherwise use the Rational Method) and for drainage areas between 10 and 100 acres.

For drainage areas greater than 100 acres, the USGS Rural Regression Equations are recommended to be used.

As compared to the 1999 guidelines, the current hydrologic method determination criteria are somewhat simpler in deciding which to use, and are summarized in Table **6.10**. For drainage areas of 0 to 64 acres, the Rational Method is used. For drainage areas between 64 acres and 640 acres (1 sq. mile), USGS Urban and Small Rural (2014) should be used, while all other drainage areas (>640 acres) should use USGS Rural (2009). The hydraulics unit started moving away from the Highway Hydrological Charts method to estimate peak discharge sometime in 2009, as design engineers were finding the estimates to be under-valued compared to USGS equations. As seen in Table ***6.11***, for the 6 sites examined in this brief case study, the 2 sites, Case 5-MF and Case 1-F would have used the NCDOT Highway Hydrologic Charts (1973) under the 1999 guidelines. Using a correction factor of 1.5 (see 6.5.3.2), as there is not information provided from NCDOT as to what correction factors were actually used, the Q_{23} was estimated for each site using the NCOT 1973 method. Compared to the 2016 guidelines, which would have dictated the design engineer use USGS 2014 regression equations, the NCDOT 1973 method underestimates the Q_{25} by 15 and 7.4 cfs respectively. However, the method is still used throughout the state in some situations as determined by the design or division engineer. Inquiries into the specific situations referenced here did not provide useful insight into when this method would be used.

6.5.2 Timing of Matthew and Florence Storms

As shown previously Hurricane Matthew occurred on October 8th through 9th of 2016. In late November of 2016, the updated 2016 Hydraulic guidelines were released. A timeline of relevant events, as well as some of the larger storms experienced by North Carolina, are shown in Figure

6.18. Whether put into use immediately or subject to a brief grace period of adopting the guidelines, there is a significant amount of time between the end of Matthew and the guidelines being released. NCDOT typically desires to re-open damaged roadways as soon as safely and feasibly possible given the extent of damage. For example, Case 5MF was damaged during Matthew, and by October 19th, Hydraulics had already determined that the structure was under-designed and recommended a replacement pipe of 1@54'' CMP to address the HW/D value> 1.25 and bring it down to .9. However, in that recommendation, the Hydraulics engineer was following the 1999 guidelines for hydrologic method determination. Under those guidelines, with this site being rural and having a DA of .4 sq miles, below the 1 sq. mile threshold, the design engineer used the Highway Hydrological Charts 1973 to determine a peak discharge of 90 cfs. Using this value, the HW/D value was determined to be .9. However, if the 2016 guidelines had been followed, the USGS Rural and Small Rural Regression Equations (2014) would have been used, and a peak discharge of 150 cfs would have been determined. Putting this value into HDS-5, this 54'' CMP that was recommended would have a HW/D value of 1.45, which would be above the criterion for sufficient size pipe. Although ultimately this pipe was not put in place and only a minor repair was conducted at this site, this example illustrates the timing of events and shows the impact that these updated guidelines could have had on the re-design of structures post-Matthew.

6.5.3 Practice vs Guidelines

Unless otherwise noted, the design practices below from NCDOT personnel are guidelines, not policies. As such, the hydraulic design that is put into practice can vary slightly from the policy as set in the Hydraulic Guidelines, as each project can have unique circumstances that might require the design engineer to deviate from the guidelines. Discussions with NCDOT hydraulics

engineers on design practices and how they might differ from the guidelines provided the following:

6.5.3.1 USGS Methods

The NCDOT has noted that USGS estimates for Region 3 (Sand Hills Region) are greatly underestimated according to design engineers experience. The Hydraulics Unit has adopted a composite calculation when designing structures within the Sand Hills area, utilizing a percentage of the estimates the USGS method(s) provides for Region 3 and from either Region 1 or Region 4.

6.5.3.2 NCDOT Highway Hydrologic Charts

Both Western and Eastern NC divisions have indicated that this method is somewhat outdated and underestimates discharge values for design calculations. Discussions with the Eastern Hydraulics Unit indicated that their unit's design procedure started moving away from this method around 2009. However, this method is still used on occasion according to brief interactions with the Western Hydraulics Unit.

However, when the Highway Hydrologic Charts are necessary and utilized by NCDOT personnel in design practice, below are some guidelines on how to effectively use the method:

- When determining the drainage area cover factor as seen in Figure 6.4-c, labeled Appendix C Chart C200.5, the percent forested area is estimated from Google Earth, Google Maps, or other detailed satellite imagery.
- Once a drainage area correction (cover) factor and shape factor are determined, their product will not be greater than 1.5. In other words, if the shape factor is 1.5 and the cover

factor is 1.5, then the total correction factor applied to the Q_{25} determined by the method is 1.5.

- Lastly, according to Hydraulics Unit personnel, when determining the Hydrologic contour, as shown in Figure ***6.3***, a minimum value of 5 is used.

6.5.3.3 NRCS Method

Although rarely utilized currently, there is increasing interest to put into practice this method. However, from discussions with Hydraulics Unit members, the Rational Method is likely a faster method to develop an adequate discharge estimate, and allows the design engineer to make more general assumptions on variables and inputs to the design procedure.

6.5.3.4 Hydraulic Reports

Hydraulic reports are produced from NCDOT when an existing structure suffers failure or damage from an extreme storm event. These reports consist of the Hydraulics Unit recommendation for upgrading the structure based on one of the previously mentioned hydrologic methods (USGS, Rational, etc.) and hydraulic analysis. According to NCDOT and comparing sets of reports from both storms, these reports became more detailed and structured after Hurricane Matthew in 2016.

6.6 Summary and Conclusions

In this study, the design processes of NCDOT in regards to highway infrastructure, with particular interest in how those structures reacted to Hurricanes Matthew and Florence, were examined and investigated. The NCDOT Hydraulic Guidelines provide the most thorough instruction on how to appropriately design highway infrastructure to be more resilient to extreme weather events. However, there is deviation from the guidelines as outlined previously, highlighted here but not inclusive:

- USGS equations have historically offered higher estimates of peak discharge as compared to the NCDOT Highway Hydrologic charts, which prior to the 2016 updated guidelines, was the recommended method to estimate peak discharge via the 1999 Guidelines. Though indications are that some at NCDOT started moving away from this procedure prior to the guidelines release based on anecdotal evidence, the new guidelines would not have been adopted in time for Matthew, and depending on how quickly the guidelines were put into practice, may not have been in place for structures to be replaced post Matthew, or in time for Florence.
- Updating Hydraulic guidelines and the application of Hydrologic methods to use should have a large impact on resilience of structures. Under the updated guidance, 100% of structures investigated in the case studies that failed in Hurricane Matthew showed susceptibility to overtopping/failure in one or both of the hydraulic analysis, using HY-8 or HDS-5
- Discrepancies between the hydraulic design software programs of HY-8 and HDS-5 needs to be further investigated, but the results of this study show that even though they are inconsistent in their recommendation, they can be used as complementary tools to better inform design decisions when structures are damaged.

Although these conclusions have been reached on research completed thus far, additional analysis is ongoing. More case studies have been identified in another county in Division 6 as well as another county in a different Division, to determine if lessons learned in Robeson county stay true for additional sites. Future work will include analyzing the additional identified case study sites using the appropriate hydrologic methods and in HDS-5 and HY-8, as well as site visits to get first-hand look at the structures to gain any insight that reports may not convey.

References

Chang, D. S. Guidelines for Drainage Studies and Hydraulic Design. North Carolina Department of Transportation, Raleigh, NC, 2016.

Cheng, L., and A. Aghakouchak. Nonstationary Precipitation Intensity-Duration-Frequency Curves for Infrastructure Design in a Changing Climate. Scientific Reports, Vol. 4, 2014, pp. 1–6. https://doi.org/10.1038/srep07093.

Commission for Hydrology (CHy). Fourteenth Session of the Commission for Hydrology. 2012.

Feaster, T. D., A. J. Gotvald, and J. C. Weaver. Magnitude and Frequency of Rural Floods in the Southeastern United States, 2006—Volume 3, South Carolina. U.S. Geological Survey Scientific Investigations Report 2009–5156, 2009.

Feaster, T. D., A. J. Gotvald, and J. C. Weaver. Methods for Estimating the Magnitude and Frequency of Floods for Urban and Small, Rural Streams in Georgia, South Carolina, and North Carolina, 2011. U.S. Geological Survey Scientific Investigations Report 2014–5030, Version 1.1, 2014.

Florida DOT (FDOT). Drainage Manual. Florida DOT, Tallahassee, FL, 2000.

Genereux, D. P. Comparison of Methods for Estimation of 50-Year Peak Discharge from a Small, Rural Watershed in North Carolina. Environmental Geology, Vol. 44, No. 1, 2003, pp. 53–58. https://doi.org/10.1007/s00254-002-0734-5.

Georgia DOT (GDOT). Drainage Design for Highways. Georgia DOT, Atlanta, GA, 2020.

Hulbert, W. H. Requirements for Hydraulic Design Studies. South Carolina Department of Transportation, Columbia, SC, 2000.

Jain, S., and U. Lall. Floods in a Changing Climate: Does the Past Represent the Future? Water Resources Research, Vol. 37, No. 12, 2001, pp. 3193–3205. https://doi.org/10.1029/2001WR000495.

Kilgore, R. T., G. Herrmann, W. O. Thomas, and D. B. Thompson. Highways in the River Environment- Floodplains , Extreme Events, Risk, and Resilience. Report No. FHWA-HIF-16-018, Federal Highway Administration, Washington, D.C., 2016.

Kilgore, R., W. Thomas, S. Douglass, B. Webb, K. Hayhoe, A. Stoner, D. Thompson, G. Herrman, E. Douglas, and C. Anderson. Applying Climate Change Information to Hydrologic and Coastal Design of Transportation Infrastructure. NCHRP Project 15-61, Washington, D.C., 2019.

Milly, P. C. D., J. Betancourt, M. Falkenmark, R. M. Hirsch, Z. W. Kundzewicz, D. P. Lettenmaier, and R. J. Stouffer. Climate Change: Stationarity Is Dead: Whither Water Management? Science, Vol. 319, No. 5863, 2008, pp. 573–574. https://doi.org/10.1126/science.1151915.

Salas, J. D., and J. Obeysekera. Revisiting the Concepts of Return Period and Risk for Nonstationary Hydrologic Extreme Events. Journal of Hydrologic Engineering, Vol. 19, No. 3, 2014, pp. 554–568. https://doi.org/10.1061/(asce)he.1943-5584.0000820.

Serinaldi, F., and C. G. Kilsby. Stationarity Is Undead: Uncertainty Dominates the Distribution of Extremes. Advances in Water Resources, Vol. 77, 2015, pp. 17–36.

She, R., S. Liu, S. Wan, K. Xiong, and P. Fan. Importance of Small Probability Events in Big Data: Information Measures, Applications, and Challenges. IEEE Access, Vol. 7, 2019, pp. 100363–100382. https://doi.org/10.1109/ACCESS.2019.2926518.

Tennessee DOT (TDOT). Design Division Drainage Manual. Tennessee DOT, Nashville, TN, 2012.

Virginia DOT (VDOT). Drainage Manual. Virginia DOT, Richmond, VA, 2002.

Table 6.1 Hydrologic Methods Utilized by NCDOT from NCDOT Guidelines for Drainage Studies and Hydraulic Design, 2016.

Feature \ Hydrologic Method	FIS (for NFIP compliance)	USGS Methods	Rational Method (up to 20 ac)	Highway Hydrologic Charts	NRCS Method (for routing)
Bridges	X	X			X
Culverts	X	X			X
Storm Drain Systems			X	X	X
Cross Pipes (≤ 72 in. dia.)	X	X	X	X	X
Gutter Spread			X		
Ditches and Channels	X	X	X	X	
BMP Devices			X		X
Natural Stream Design	X	X	X		X
Storage Facilities					X
Floodplain Impacts	X	X			X

Table 6.2. Typical Runoff Coefficients to be used in Rational Method Calculations.

Type of Surface	**C**
Pavement	0.7 – 0.9
Gravel surfaces	0.4 – 0.6
Industrial areas	0.5 – 0.9
Residential (single-family)	0.3 – 0.5
Residential (Apartments, etc.)	0.5 – 0.7
Grassed, steep slopes	0.3 – 0.4
Grassed, flat slopes	0.2 – 0.3
Wood/Forest	0.1 – 0.2

Table 6.3 Storm Design Frequency for NCDOT Structures from NCDOT Guidelines for Drainage Studies and Hydraulic Design, 2016.

Roadway Classification	Frequency			
	Bridges, Culverts, and Cross Pipes	Storm Drain System		Ditches
		On Grade	At Sages (without relief)	
Major Arterials (e.g., I, US, NC)	50	10	50	10
Minor Arterials, Collectors, and Local Roads	25	10	25	10
Temporary/ Detours	10	-	-	10

Table 6.4 Culvert Data Shape and Material choices in HY-8 software.

Shape	Material	Shape	Material
Circular	Concrete	User-Defined	Corrugated Metal Riveted or Welded
	Corrugated Steel		Concrete
	PVC	Arch, Open Bottom	Corrugated Steel
	Smooth HDPE		Corrugated Aluminum
	Corrugated PE	Low Profile Arch	Corrugated Steel
Concrete Box	Concrete		Corrugated Aluminum
Elliptical	Steel or Aluminum	High Profile Arch	Corrugated Steel
	Concrete		Corrugated Aluminum
Pipe or Arch	Concrete	Metal Box	Corrugated Steel
	Steel or Aluminum		Corrugated Aluminum
	Aluminum Structural Plate	Concrete Open Arch Bottom	Concrete
	Steel Structural Plate	South Dakota Concrete Box Culvert	Concrete

Table 6.5 Maximum 24 hours rainfall intensity data for selected case studies.

Case ID	Event	Max 24-hr (in.)	24-hr AEP (%)	Ratio 1 (Max 24-hr/4% AEP rainfall)	Overall Max 24-Hr (in.)	Overall Max 24-Hr AEP (%)	Ratio 2 (Overall Max 24-hr/4% AEP rainfall)
Case 5-MF	Matthew	6.8	4	1.0	10.2	0.5	1.5
	Florence	6.7	4	1.0	9.2	1.0	1.4
Case 7-MF	Matthew	6.3	4	0.9	9.5	0.5	1.4
	Florence	6.6	4	1.0	8.9	1.0	1.3
Case 1-F	Matthew	8.1	1	1.2	10.7	0.2	1.6
	Florence	7.7	2	1.2	9.3	0.5	1.4
Case 2-F	Matthew	8.1	1	1.2	10.7	0.2	1.6
	Florence	7.7	2	1.2	9.3	0.5	1.4
Case 6-M	Matthew	10.2	0.5	1.5	12.4	0.2	1.8
	Florence	8.6	1	1.3	11.7	0.2	1.7
Case 8-M	Matthew	6.3	4	.9	9.5	0.5	1.4
	Florence	6.6	4	1	8.9	1	1.3

Table 6.6 Adjusted Peak Discharge Values based on precipitation ratios.

Case ID	Original Q_{25}	Adjusted Peak Design Discharge			
		Matthew (Ratio 1)	Matthew (Ratio 2)	Florence (Ratio 1)	Florence (Ratio 2)
Case 5-MF	143	144	217	143	197
Case 6-MF	255	279	402	269	421
Case 1-F	86	107.1	142.2	102.2	122.7
Case 2-F	251	310.4	412.4	296.2	355.9
Case 6-M	526	785.9	951.6	662.1	897.7
Case 8-M	525	493.9	742.7	513.6	694.3

Table 6.7 Results of analysis completed utilizing HDS-5 and HY-8 for base peak discharge in identified sites in Robeson County (red cells have calculated HW/D > 1.25 and green cells have calculated HW/D ≤ 1.25).

	Base Discharge HDS-5 HW/D			Base Discharge HY-8 HW/D		
Case ID	Base Matthew	Base Florence	Base Current	Base Matthew	Base Florence	Base Current
Case 5-MF	4.05	4.05	1.00	3.33	3.33	1.04
Case 7-MF	2.50	1.00	1.00	2.32	1.17	1.17
Case 6-M	0.95	0.81	0.81	1.23	0.99	0.99
Case 8-M	2.04	0.89	0.89	1.75	1.07	1.07
Case 1-F	4.10	4.10	4.10	4.07	4.07	4.07
Case 2-F	42.28	42.28	1.57	3.86	3.86	1.13

Table 6.8 Results of analysis completed utilizing HDS-5 and HY-8 for peak discharge values adjusted using Ratios 1 and 2.

	Adjusted Discharges HD-S HW/D				Adjusted Discharges HY-8 HW/D			
Case ID	Matthew R1	Matthew R2	Florence R1	Florence R2	Matthew R1	Matthew R2	Florence R1	Florence R2
Case 5-MF	4.10	8.45	4.05	7.08	3.33	3.58	3.33	1.76
Case 7-MF	2.30	4.33	0.99	1.21	2.26	2.69	1.15	1.39
Case 6-M	1.45	1.23	1.29	1.26	1.68	1.36	1.55	1.50
Case 8-M	1.89	1.99	1.18	1.07	1.71	1.74	1.50	1.44
Case 1-F	6.44	5.92	10.84	8.30	4.21	4.18	4.37	4.29
Case 2-F	16.54	15.14	1.61	1.46	3.99	3.94	1.88	1.62

Table 6.9 NCDOT Hydraulic Guidelines 1999 in determining appropriate hydrologic method to use in estimating peak discharge.

1999 Hydraulic Guidelines				
Rural		Urban		
DA>640 acres	DA<640 acres	DA<10 acres	10<DA<100 acres	DA>100 acres
USGS Regression Equations	Highway Hydrological Charts	Highway Hydrological Charts, or Rational	Highway Hydrological Charts	USGS Regression Equations

Table 6.10 NCDOT Hydraulic Guidelines 2016 in determining appropriate hydrologic method to use in estimating peak discharge.

2016 Hydraulic Guidelines		
0<DA<64 acres	64<DA<640 acres	DA> 640 acres
Rational Method	USGS Urban and Small Rural '14	USGS Rural '09

Table 6.11 Comparison of Peak Discharge using 1999 vs 2016 NCDOT Guidelines

Case ID	DA (sq. mi.)	DA (acres)	1999 Method	1999 Q_{25} (cfs)	2016 Method	2016 Q_{25} (cfs)	ΔQ_{25}
Case 5-MF	0.38	243	NCDOT 1973	135	USGS 2014	150	-15.0
Case 7-MF	2.90	1856	USGS 1999	467	USGS 2009	467.1	0.0
Case 6-M	3.53	2259	USGS 1999	526	USGS 2009	526.2	0.0
Case 8-M	3.52	2253	USGS 1999	525	USGS 2009	525.3	0.0
Case 1-F	0.18	115	NCDOT 1973	79	USGS 2014	86.4	-7.4
Case 2-F	1.04	666	USGS 1999	251	USGS 2009	251	0.0

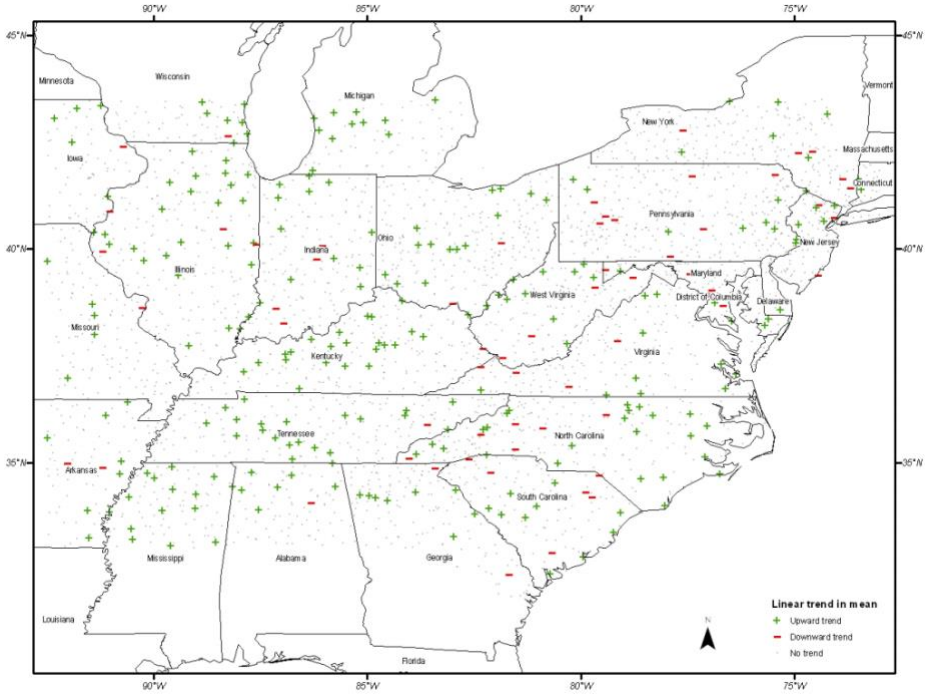

Figure 6.1 Linear trend of 1-day annual maximum from rainfall stations with minimum of 50 years data, NOAA Atlas 14 Vol 2.

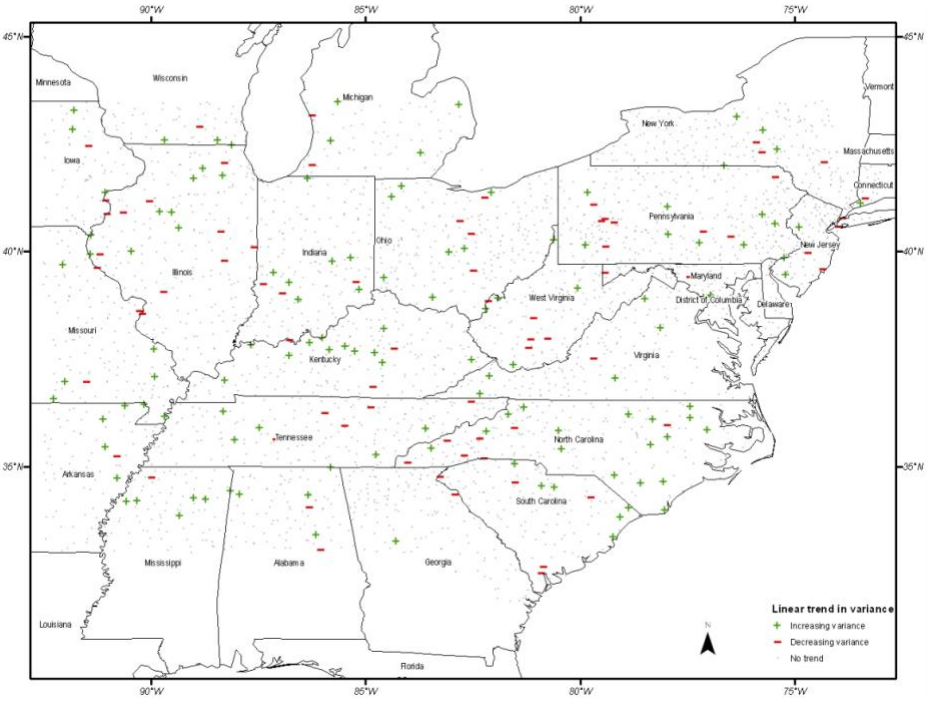

Figure 6.2 Variance of 1-day annual maximum from rainfall stations with minimum of 50 years data, NOAA Atlas 14 Vol 2.

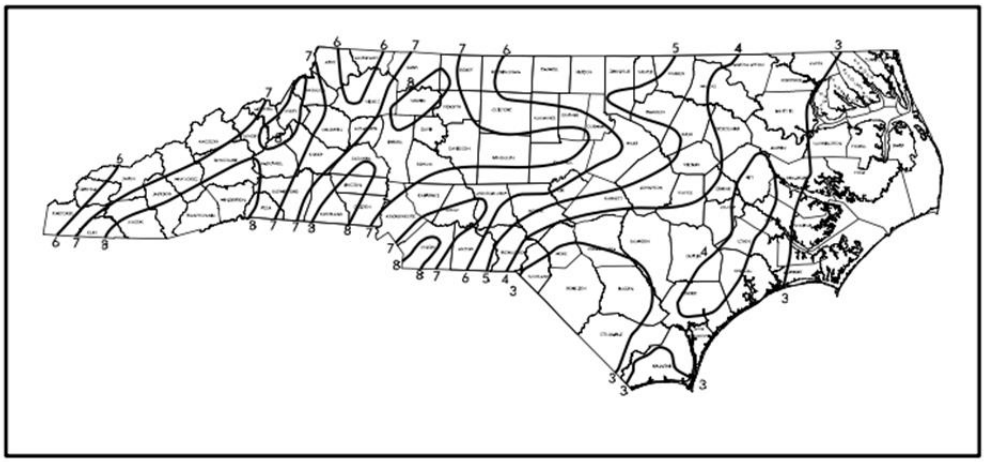

Figure 6.3 Hydrologic contour map for North Carolina utilized in the NCDOT Method.

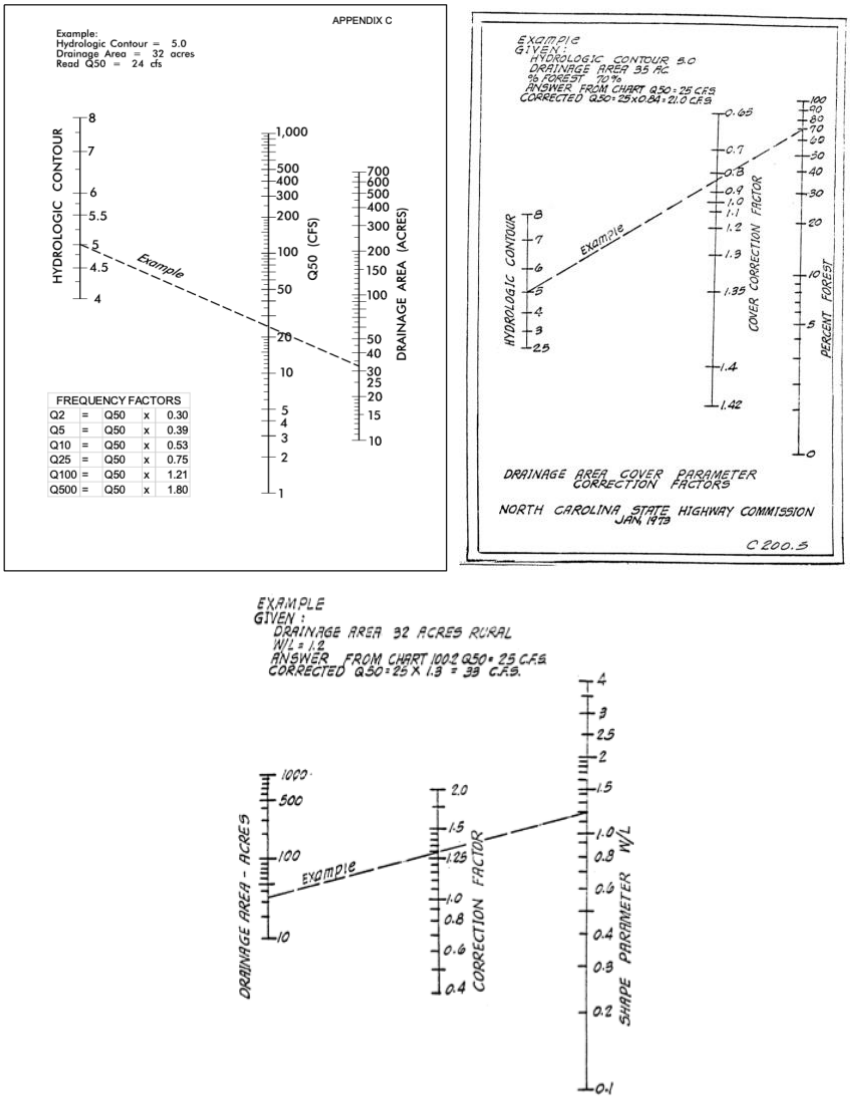

Figure 6.4 a) Runoff Chart with relevant frequency correction factors, b) drainage area cover factor chart, and c) shape correction factor chart used in NCDOT Method (1973) **.**

Percent annual exceedance probability	Hydrologic Region 1		Hydrologic Region 3
	0.10 mi² ≤ DRNAREA ≤ 3 mi²	3 mi² < DRNAREA ≤ 436 mi²	0.22 mi² ≤ DRNAREA ≤ 459 mi²
50	$163(DRNAREA)^{0.7089}10^{(0.0133*IMPNLCD06)}$	$198(DRNAREA)^{0.5735}10^{(0.0101*IMPNLCD06)}$	$30.0(DRNAREA)^{0.6605}10^{(0.0122*DEVNLCD06)}$
20	$284(DRNAREA)^{0.7351}10^{(0.0096*IMPNLCD06)}$	$359(DRNAREA)^{0.5605}10^{(0.0074*IMPNLCD06)}$	$51.4(DRNAREA)^{0.6535}10^{(0.0109*DEVNLCD06)}$
10	$381(DRNAREA)^{0.7536}10^{(0.0076*IMPNLCD06)}$	$484(DRNAREA)^{0.5539}10^{(0.0060*IMPNLCD06)}$	$68.4(DRNAREA)^{0.6507}10^{(0.0102*DEVNLCD06)}$
4	$518(DRNAREA)^{0.7752}10^{(0.0053*IMPNLCD06)}$	$657(DRNAREA)^{0.5470}10^{(0.0046*IMPNLCD06)}$	$93.3(DRNAREA)^{0.6472}10^{(0.0095*DEVNLCD06)}$
2	$632(DRNAREA)^{0.7903}10^{(0.0037*IMPNLCD06)}$	$794(DRNAREA)^{0.5428}10^{(0.0037*IMPNLCD06)}$	$114(DRNAREA)^{0.6451}10^{(0.0090*DEVNLCD06)}$
1	$753(DRNAREA)^{0.8038}10^{(0.0024*IMPNLCD06)}$	$941(DRNAREA)^{0.5386}10^{(0.0028*IMPNLCD06)}$	$138(DRNAREA)^{0.6430}10^{(0.0086*DEVNLCD06)}$
0.5	$884(DRNAREA)^{0.8181}10^{(0.0011*IMPNLCD06)}$	$1096(DRNAREA)^{0.5351}10^{(0.0021*IMPNLCD06)}$	$163(DRNAREA)^{0.6413}10^{(0.0082*DEVNLCD06)}$
0.2	$1045(DRNAREA)^{0.8160}$	$1319(DRNAREA)^{0.5305}10^{(0.0011*IMPNLCD06)}$	$201(DRNAREA)^{0.6386}10^{(0.0077*DEVNLCD06)}$

Percent annual exceedance probability	Hydrologic Region 4	Hydrologic Region †5
	0.10 mi² ≤ DRNAREA ≤ 53.5 mi²	0.20 mi² ≤ DRNAREA ≤ 10 mi²
50	$26.3(DRNAREA)^{0.5908}10^{(0.0173*IMPNLCD06)}10^{(0.0515*I24H50Y)}$	$165(DRNAREA)^{0.537}$
20	$40.6(DRNAREA)^{0.5958}10^{(0.0125*IMPNLCD06)}10^{(0.0623*I24H50Y)}$	$265(DRNAREA)^{0.583}$
10	$51.8(DRNAREA)^{0.6004}10^{(0.0101*IMPNLCD06)}10^{(0.0666*I24H50Y)}$	$349(DRNAREA)^{0.600}$
4	$67.1(DRNAREA)^{0.6067}10^{(0.0075*IMPNLCD06)}10^{(0.0708*I24H50Y)}$	$473(DRNAREA)^{0.615}$
2	$78.4(DRNAREA)^{0.6111}10^{(0.0058*IMPNLCD06)}10^{(0.0738*I24H50Y)}$	$574(DRNAREA)^{0.624}$
1	$90.5(DRNAREA)^{0.6154}10^{(0.0043*IMPNLCD06)}10^{(0.0762*I24H50Y)}$	$684(DRNAREA)^{0.632}$
0.5	$103(DRNAREA)^{0.6201}10^{(0.0029*IMPNLCD06)}10^{(0.0785*I24H50Y)}$	$804(DRNAREA)^{0.639}$
0.2	$119(DRNAREA)^{0.6261}10^{(0.0012*IMPNLCD06)}10^{(0.0813*I24H50Y)}$	$971(DRNAREA)^{0.649}$

DRNAREA= Drainage Area, mi²
IMPNLCD06= percentage of impervious area from the 2006 National Land Cover Dataset, in percent
DEVNLCD06, percentage of developed land from the 2006 National Land Cover Dataset
I24H50Y, 24-hour, 50-year maximum precipitation, in inches from current as of this writing NOAA Atlas 14 Vol 2, or updated version

Figure 6.5 Regional flood-frequency equations for un-gaged urban and small, rural streams in Georgia, South Carolina, and North Carolina, from USGS, 2014.

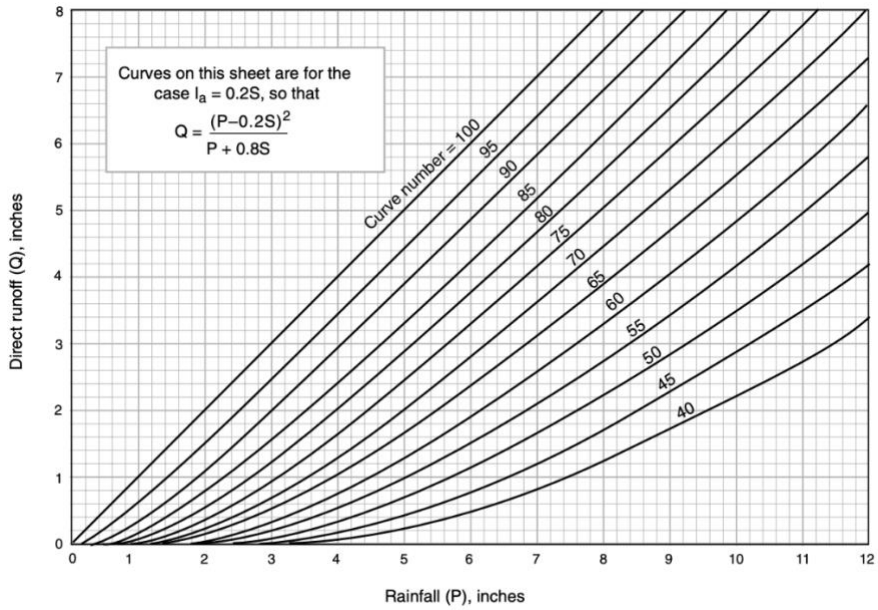

Figure 6.6 Solution for runoff equation to be used in NRCS Method.

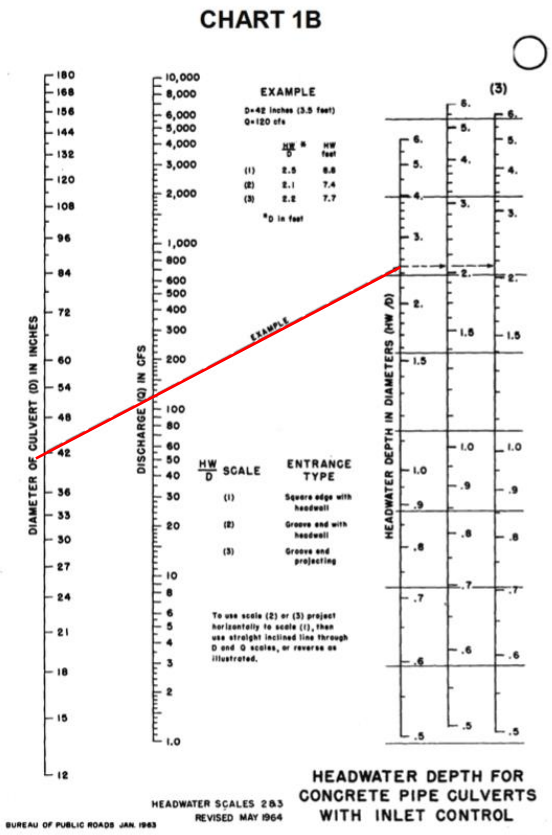

Figure 6.7 Example of digitized HDS-5 nomographs used in hydraulic design of culverts.

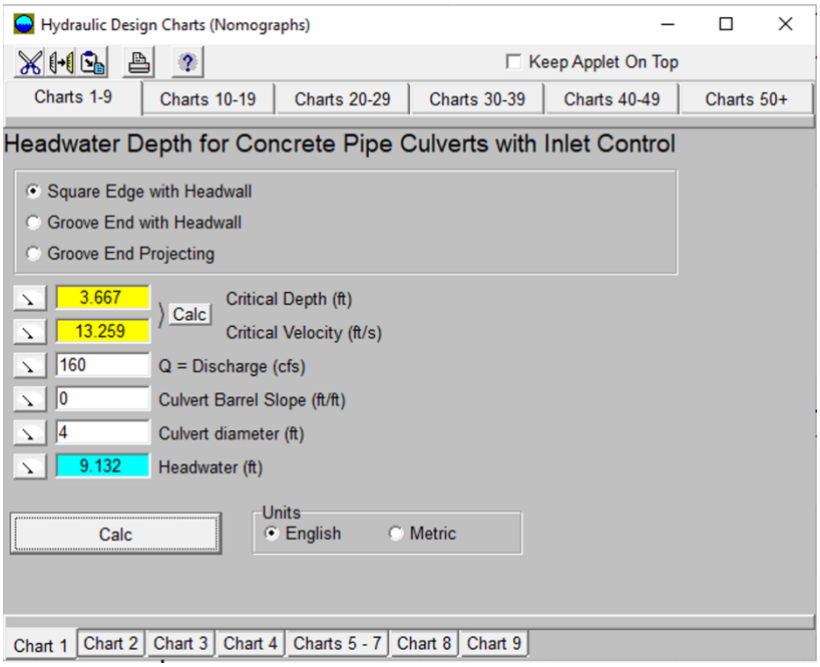

Figure 6.8 Computerized program version of HDS-5 Nomographs.

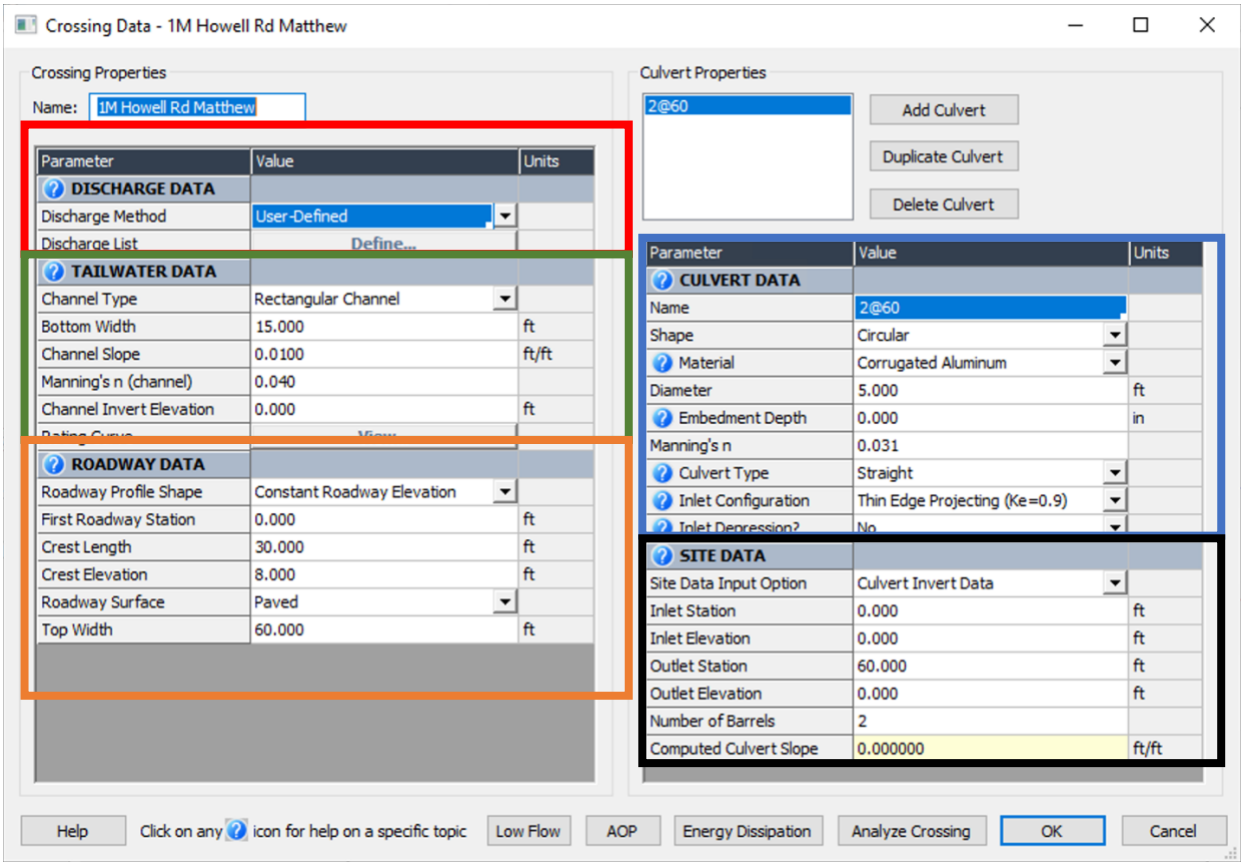

Figure 6.9 Inputs window in HY-8 software used to build sites and pipe cross sections: Red- Discharge Data; Green- Tailwater Data; Orange- Roadway Data; Blue- Culvert Data; Black- Site Data.

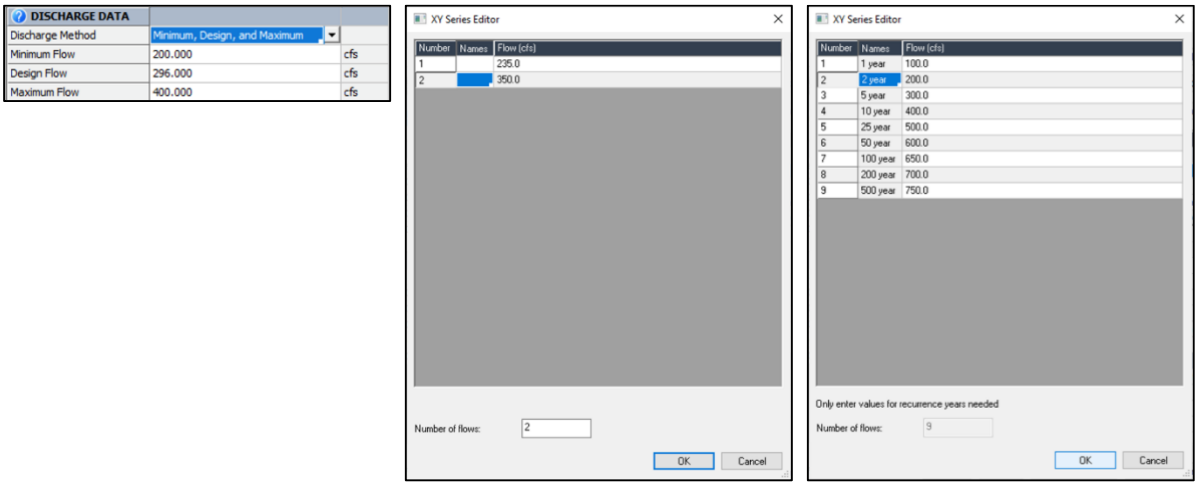

(a) **(b)** **(c)**

Figure 6.10 Discharge Data input windows for HY-8: (a) Minimum, Design, Maximum; (b) User Defined; and (c) Recurrence Interval.

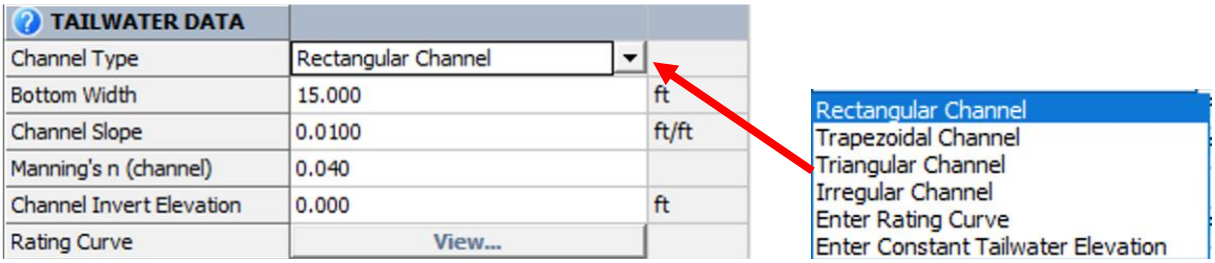

Figure 6.11 Tailwater Data input window where user defines Bottom Width, Channel Slope, Manning's Number, Channel Invert Elevation, and Rating Curve. Additionally to the right, the drop down where user defines channel type.

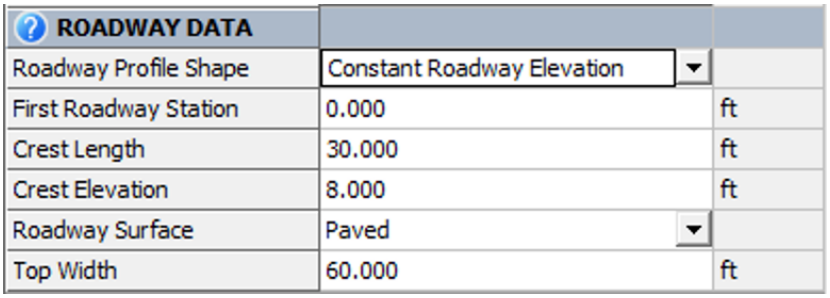

Figure 6.12 Roadway Data input window in HY-8, where user defines roadway elevation data including Crest Length, Crest Elevation and Top Width. Drop down list includes choices for Constant Roadway Elevation and Irregular.

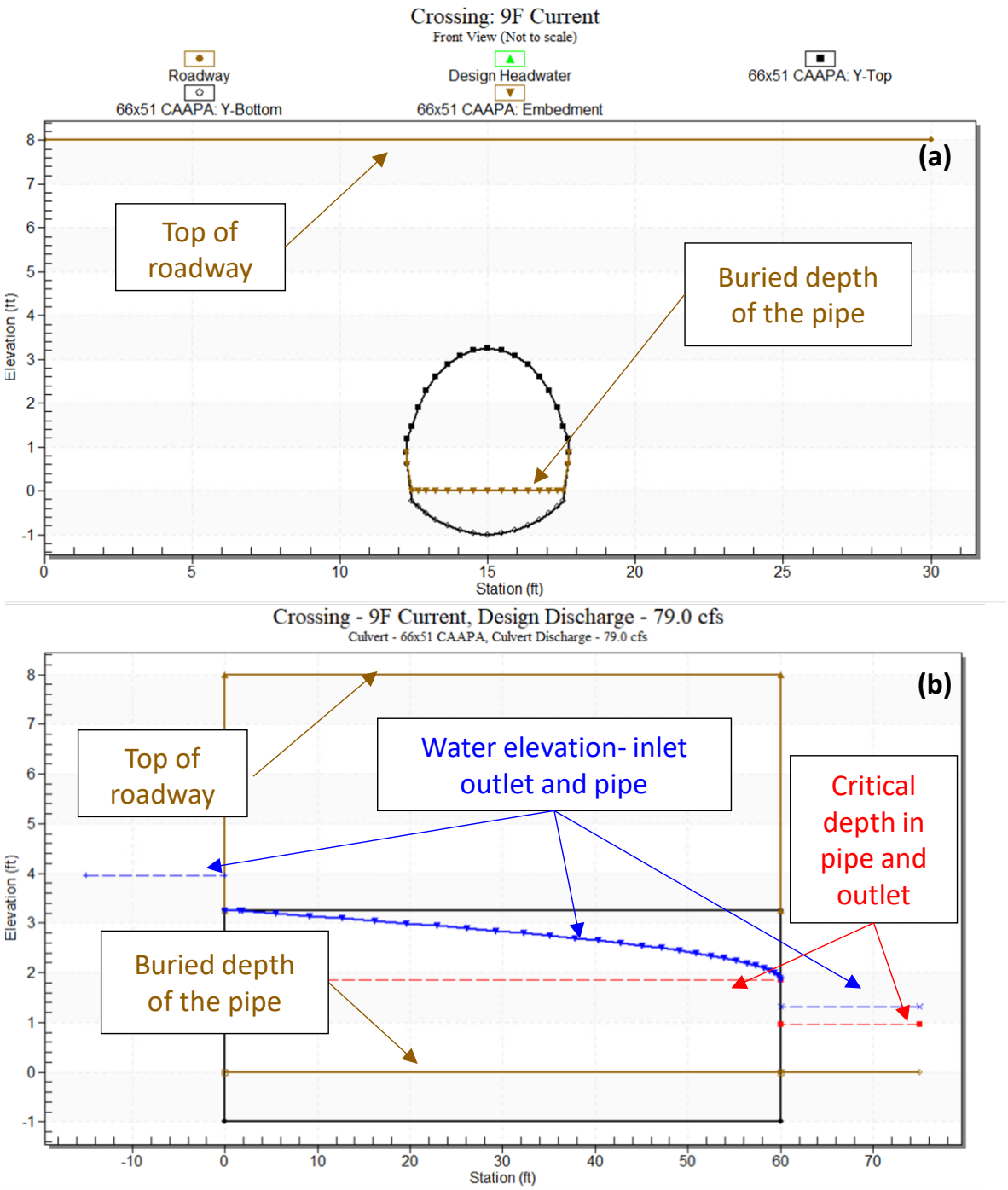

Figure 6.13 Visual of HY-8 software inputs to build cross section along; (a) the roadway direction and (b) along the pipe/flow direction, along with labeled features of analysis and site data.

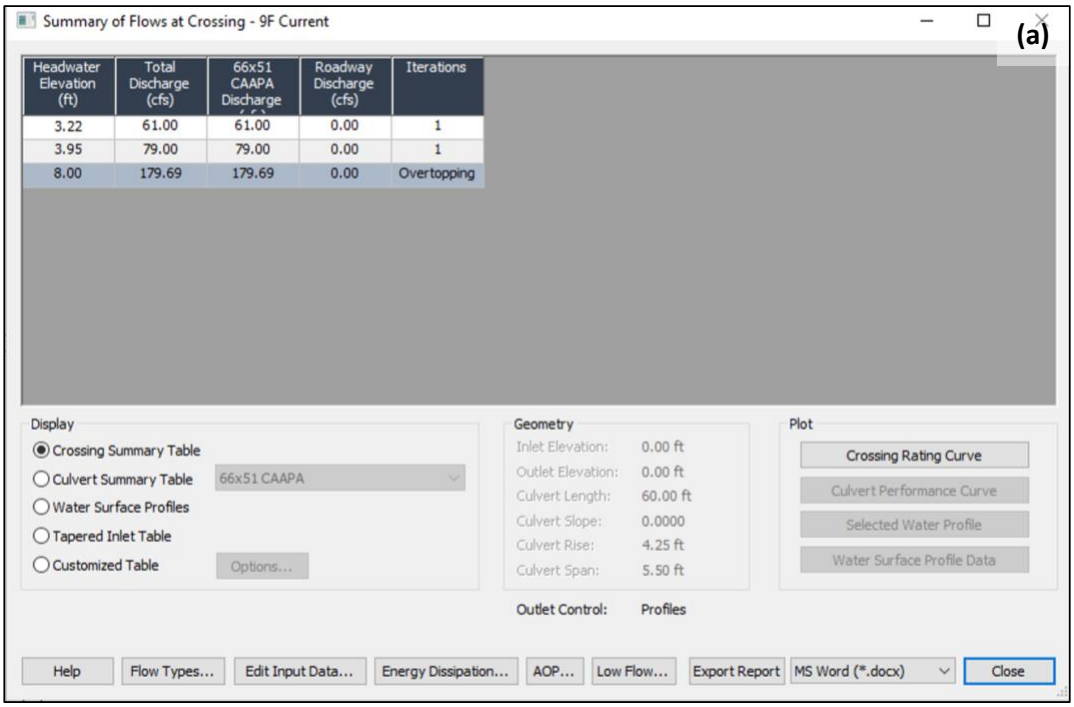

(b)

Total Discharge (cfs)	Culvert Discharge (cfs)	Headwater Elevation (ft)	Inlet Control Depth(ft)	Outlet Control Depth(ft)	Flow Type	Normal Depth (ft)	Critical Depth (ft)	Outlet Depth (ft)	Tailwater Depth (ft)	Outlet Velocity (ft/s)	Tailwater Vel. (ft/s)
61.00	61.00	3.22	2.63	**3.22**	7-H2c	NA	1.56	1.56	1.12	7.32	3.64
79.00	79.00	3.95	3.15	**3.95**	7-H2c	NA	1.85	1.85	1.32	8.12	4.00

Figure 6.14 Outputs of HY-8 Analyze Crossing window showing the results of calculations completed based on inputs previously defined for a given site.

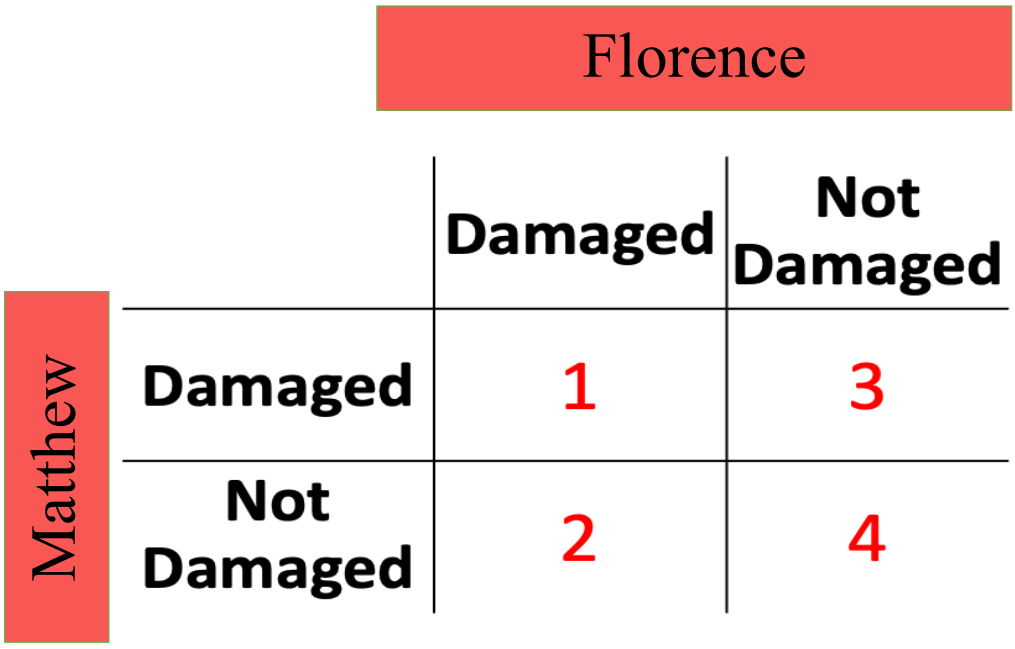

Figure 6.15 Matrix of failure criterion for case study identification.

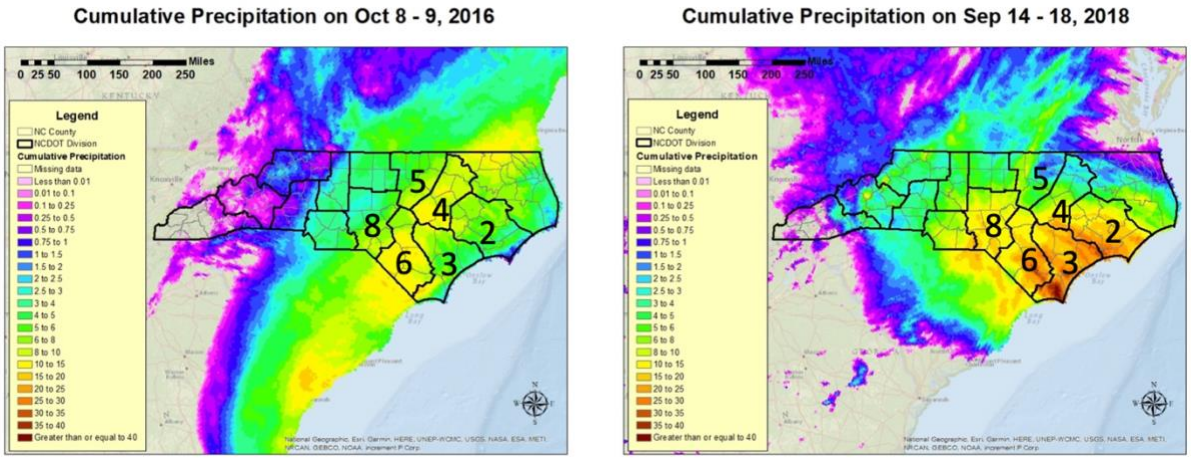

Figure 6.16 Cumulative precipitation for Hurricanes Matthew (a) and Florence (b) for their respective durations. *(Credit to Narges Matini)*

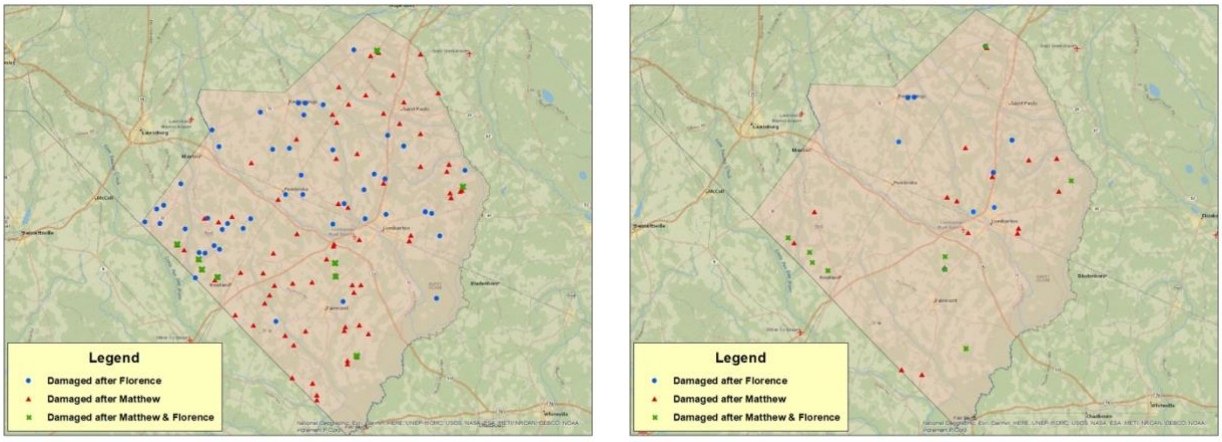

Figure 6.17 Using failure criterion matrix, map of identified a) potential case studies in Robeson County, Division 6, and b) chosen case studies. Blue dots are damaged in only Florence, red triangles are only in Matthew, and Green are damaged in both. *(Credit to Narges Matini)*

Figure 6.18 Timeline of relevant events including examples of damage from storm events.

Chapter 7 Contributions and Future Work

7.1 Contributions

A comprehensive analysis to evaluate the behavior and properties of MICP treated mine tailings materials was completed, and the hydraulic design practices of the NCDOT were investigated. The main contributions in this study are as follows:

- The physical and chemical characteristics of two sets of mine tailings from an iron and gold mine were presented
- MICP treatment methods of ex-situ mixing and bottom-up injection were effective in precipitating calcium carbonate on both Slime and Silt samples
- MICP treatment of the Silt and Slime mine tailings demonstrated increase in shear strength, via FCT and DSS.
- By updating the Hydraulic guidelines in 2016 and phasing out of hydrologic methods that underestimate peak discharges (i.e.- NCDOT 1973 Method), these changes the NCDOT applied should have a large impact on resilience of structures

7.2 Future Work

- Confirm failure envelope of untreated and treated materials with DSS testing completed at varying confining pressures.
- Larger scale bench testing to remove boundary conditions and determine why treatment at higher water contents formed the stiff upper crust that inhibited consolidation and uniform precipitation throughout the samples.
- XRD analysis to confirm that the Silt and Slime materials contain the same base components.

- SEM analyses to examine the fabric differences between Silt 1 and Silt 2 and their slime counterparts which may provide insight into their untreated undrained shear behavior.
- SEM analysis on the treated Silt materials to better understand the differences between the amount and location of calcium carbonate precipitate on each of the tailings materials and how this might correlate to the resultant increase in shear strength.
- Sensitivity analysis into comparing the effects that varying inputs in HY-8 hydraulic design software is necessary to fully understand how the software could be implemented or integrated into NCDOT hydraulic design procedures